


Fall 12-2008

Examination of an Aloe Vera Galacturonate Polysaccharide Capable of In Situ Gelation for the Controlled Release of Protein Therapeutics

Shawn David McConaughy
University of Southern Mississippi

Follow this and additional works at: <https://aquila.usm.edu/dissertations>

 Part of the [Materials Chemistry Commons](#), [Medicinal-Pharmaceutical Chemistry Commons](#), and the [Polymer Chemistry Commons](#)

Recommended Citation

McConaughy, Shawn David, "Examination of an Aloe Vera Galacturonate Polysaccharide Capable of In Situ Gelation for the Controlled Release of Protein Therapeutics" (2008). *Dissertations*. 1153.
<https://aquila.usm.edu/dissertations/1153>

This Dissertation is brought to you for free and open access by The Aquila Digital Community. It has been accepted for inclusion in Dissertations by an authorized administrator of The Aquila Digital Community. For more information, please contact aquilastaff@usm.edu.

The University of Southern Mississippi

EXAMINATION OF AN ALOE VERA GALACTURONATE POLYSACCHARIDE
CAPABLE OF *IN SITU* GELATION FOR THE CONTROLLED RELEASE OF
PROTEIN THERAPEUTICS

by

Shawn David McConaughy

Abstract of a Dissertation
Submitted to the Graduate Studies Office
of The University of Southern Mississippi
in Partial Fulfillment of the Requirements
for the Degree of Doctor of Philosophy

December 2008

COPYRIGHT BY
SHAWN DAVID MCCONAUGHY

2008

The University of Southern Mississippi

EXAMINATION OF AN ALOE VERA GALACTURONATE POLYSACCHARIDE
CAPABLE OF IN SITU GELATION FOR THE CONTROLLED RELEASE OF
PROTEIN THERAPEUTICS

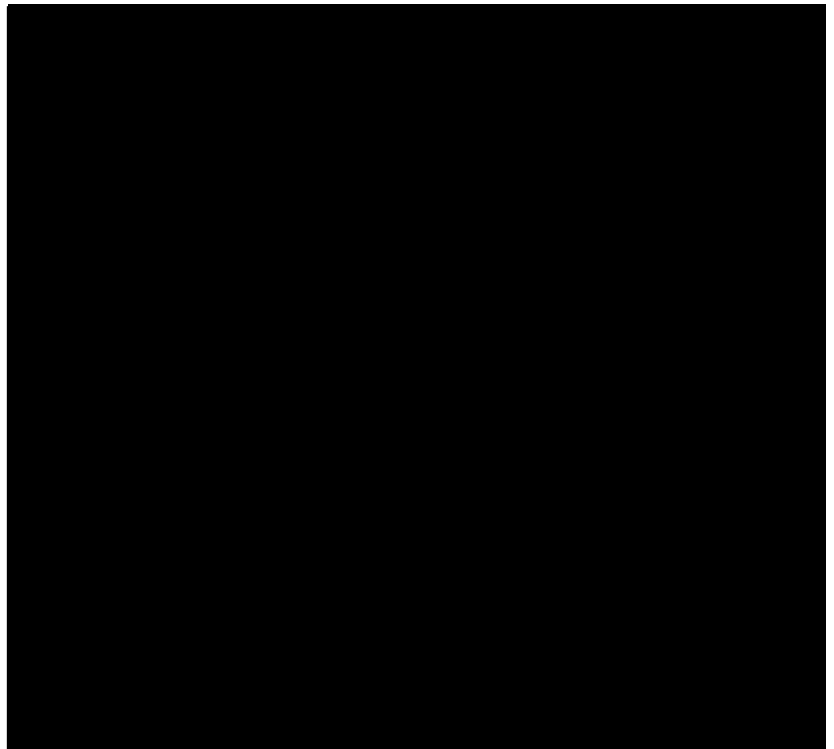
by

Shawn David McConaughy

A Dissertation

Submitted to the Graduate Studies Office
of The University of Southern Mississippi
in Partial Fulfillment of the Requirements
for the Degree of Doctor of Philosophy

Approved:



December 2008

ABSTRACT

EXAMINATION OF AN ALOE VERA GALACTURONATE POLYSACCHARIDE CAPABLE OF *IN SITU* GELATION FOR THE CONTROLLED RELEASE OF PROTEIN THERAPEUTICS

by Shawn David McConaughy

December 2008

A therapeutic delivery platform has been investigated with the ultimate goal of designing a sustained protein release matrix utilizing an *in-situ* gelling, acidic polysaccharide derived from the *Aloe vera* plant. The *Aloe vera* polysaccharide (AvP) has been examined in order to determine how chemical composition, structure, molecular weight and solution behavior affect gelation and protein/peptide delivery. Correlations are drawn between structural characteristics and solution behavior in order to determine the impact of polymer conformation and solvation on gel formation under conditions designed to simulate nasal applications. Steady state and dynamic rheology, classic and dynamic light scattering, zeta potential, pulse field gradient nuclear magnetic resonance and fluorescence spectroscopy have been employed to gain insight into the effects of galacturonic acid content, degree of methylation, entanglement and ionic strength on both solution behavior and the hydrogel state which ultimately governs protein/peptide release.

This dissertation is divided into two sections. In the first section, a series of *Aloe vera* polysaccharides (AvP), from the pectin family have been structurally characterized indicating high galacturonic acid (GalA) content, low degree of methylester substitution (DM), low numbers of rhamnose residues and high molecular weight with respect to pectins extracted from traditional sources. The behavior of AvP was examined utilizing dilute solution, low-shear rheological techniques for specific molecular weight samples at selected conditions of ionic strength. From these dilute aqueous solution studies, the Mark-Houwink-Sakurada (MHS) constants (K and α), persistence length (L_p) and inherent chain stiffness (B parameter) were determined, indicating an expanded random coil in aqueous salt solutions. The critical concentration for transition from dilute to concentrated solution, C_c , was determined by measuring both the zero shear viscosity and fluorescence emission of the probe molecule 1,8-anilino-1-naphthalene sulphonic acid (1,8-ANS) as a function of polymer concentration. Correlations are drawn between viscosity experiments and measurement of zeta potential. Increased degrees of intermolecular interactions are responsible for a shift of C_c to lower polymer concentrations with increasing ionic strength. Additionally, dynamic rheology data are presented highlighting the ability of AvP to form gels at low polymer and calcium ion concentrations, exemplifying the technological potential of this polysaccharide for *in-situ* drug delivery.

In the second section, properties of *Aloe vera* galacturonate hydrogels formed *via* Ca^{2+} crosslinking have been studied in regard to key parameters influencing gel formation including molecular weight, ionic strength and molar ratio of Ca^{2+} to COO^- functionality. Dynamic oscillatory rheology and pulsed field gradient NMR (PFG-NMR)

studies have been conducted on hydrogels formed at specified Ca^{2+} concentrations in the presence and absence of Na^+ and K^+ ions, in order to assess the feasibility of *in situ* gelation for controlled delivery of therapeutics. Aqueous Ca^{2+} concentrations similar to those present in nasal and subcutaneous fluids induce the formation of elastic *Aloe vera* polysaccharide (AvP) hydrogel networks. By altering the ratio of Ca^{2+} to COO^- functionality, networks may be tailored to provide elastic modulus (G') values between 20 and 20,000 Pa. The *Aloe vera* polysaccharide exhibits time dependent phase separation in the presence of monovalent electrolytes. Thus the relative rates of calcium induced gelation and phase separation become major considerations when designing a system for *in situ* delivery applications where both monovalent (Na^+ , K^+) and divalent (Ca^{2+}) ions are present. PFG-NMR and fluorescence microscopy confirm that distinctly different morphologies are present in gels formed in the presence and absence 0.15 M NaCl. Curve fitting of theoretical models to experimental release profiles of fluorescein labeled dextrans indicate diffusion rates are related to hydrogel morphology. These studies suggest that for efficient *in situ* release of therapeutic agents, polymer concentrations should be maintained above the critical entanglement concentration (C_e , 0.60 wt%) when $[\text{Ca}^{2+}]/[\text{COO}^-]$ ratios are less than 1. Additionally, the monovalent electrolyte concentration in AvP solutions should not exceed 0.10 M prior to Ca^{2+} crosslinking.

ACKNOWLEDGEMENTS

I would like to thank Dr. Charles L. McCormick, my research advisor, for his guidance throughout my graduate career. I would also like to thank the members of my graduate committee: Dr. Robert Y. Lochhead, Dr. Andrew B. Lowe, Dr. Kenneth A. Mauritz and Dr. Sarah E. Morgan.

I am grateful to the entire McCormick Research Group, both past and present, for their kind friendship, useful critiques and reviews of both manuscripts and mathematics. Special thanks are reserved for members of DelSite Biotechnologies: Dr. Carlton Turner, Dr. Yawei Ni and Dr. Paul Stroud, for providing advice concerning research and financial support for this project.

I would like to acknowledge past teachers including Phillip Sarver, and Dr. Paul Koch for allowing me to share in their passion for science & technology. My greatest appreciation is given to my first teachers, my mother and father, Jay and Patricia McConaughy. Thank you for reading me books and forcing me to do my homework. To my newest teachers, Funda and Carlos, thank you being a constant source of encouragement and support.

TABLE OF CONTENTS

ABSTRACT.....	ii
ACKNOWLEDGMENTS.....	v
LIST OF ILLUSTRATIONS.....	viii
LIST OF TABLES.....	xiii
CHAPTER	
I. INTRODUCTION.....	1
II. OBJECTIVES AND NEED FOR RESEARCH.....	23
III. EXPERIMENTAL.....	25
Materials and Methods.....	25
Chemical Composition	
Solution Studies	
Hydrogel Studies	
Solution Studies.....	29
Dilute Solutions	
Concentrated Solutions	
Hydrogel Studies.....	32
Mold Design	
Gel Formation	
Dynamic Oscillatory Rheology	
PFG-NMR	
Microscopy	
Release of Model Compounds	

IV. RESULTS AND DISCUSSION.....	37
Structural Characterization and Solution Properties of AvP.....	37
Overview	
Chemical Composition	
Constituent Sugars	
Molecular Weight	
Methylester Substitution	
Dilute Solution Behavior	
Intrinsic Viscosity	
Persistence Length	
Stiffness Factor	
Concentrated Solution Behavior	
Critical Entanglement Concentration	
Hydrophobic Association	
Calcium Induced Gelation of AvP. Network Characterization and Release of Model Compounds.....	60
Overview	
Hydrogel Formation and Characterization	
Viscoelastic Behavior	
Molecular Weight	
Rate of Ca ²⁺ Crosslinking	
Polymer Concentration	
Ca ²⁺ /COO ⁻ Ratio	
Addition of Simple Electrolytes	
Diffusion Studies <i>via</i> PFG-NMR	
Diffusion of Model Compounds	
Release Profiles of Model Compounds	
Application of Theoretical Models	
V. CONCLUSIONS.....	92
VI. RECOMMENDATIONS FOR FUTURE RESEARCH.....	95
APPENDIXES.....	97
REFERENCES.....	134

LIST OF ILLUSTRATIONS

Figure		
I-1.	Molecular structure of carboxymethylcellulose.....	3
I-2.	Molecular structure of hydroxyethylcellulose.....	4
I-3.	Molecular structure of chitosan.....	5
I-4.	Molecular structure of hyaluronic acid.....	6
I-5.	Molecular structure of dextran.....	8
I-6.	Molecular structure of pullulan.....	9
I-7.	Molecular structure of xanthan.....	10
I-8.	Molecular structure of gellan.....	12
I-9.	Molecular structure of carrageenan.....	13
I-10.	Molecular structure of mannuronic and guluronic acid.....	15
I-11.	Molecular structure of alginate.....	15
I-12.	Proposed structure of alginate calcium egg box.....	17
I-13.	Homogalacturonan region of pectin depicting galacturonic acid in the sodium salt form and in the methyl ester form.....	18
I-14.	Rhamnogalacturonan region of pectin with rhamnose sugars incorporated into the polysaccharide backbone <i>via</i> a 1-2 linkage.....	18
I-15.	Linear and branched regions of pectin polysaccharides.....	18
I-16.	Proposed conformation of physical crosslinks formed by complexation of calcium ions with GalA regions from two pectin chains.....	20
I-17.	General structure of pectin.....	21
IV-1.	General structure of AvP.....	38
IV-2.	SEC-MALLS trace of AvP1 including molecular weight and radius of gyration analysis.....	42

IV-3. SEC-MALLS trace of AvP1 depicting radius of gyration as a function of molecular weight.....	43
IV-4. ¹ H NMR spectrum of AvP3.....	44
IV-5. Determination of intrinsic viscosity illustrated for AvP3 in 0.10 M NaCl....	46
IV-6. Determination of MHS parameters α and K.....	48
IV-7. Plot of intrinsic viscosity as a function of the inverse square root of ionic strength.....	52
IV-8. Zeta potential of AvP3 as a function of NaCl and KCl concentration.....	54
IV-9. Determination of the critical entanglement concentration for AvP3 in water and 0.10 M NaCl.....	55
IV-10. The maximum fluorescence emission of 1,8-ANS as a function of polymer concentration depicted for AvP3 in aqueous solution.....	57
IV-11. Evolution of elastic moduli as a function of time for various calcium ion concentrations.....	59
IV-12. Elastic and viscous moduli data as a function of frequency for a series of 0.10 wt% AvP hydrogels formed from AvP samples of molecular weights 523, 435, 200 kDa	63
IV-13. Elastic and viscous moduli as a function of frequency for 0.20 wt% AvP2 hydrogels after introduction of 5 mM CaCl ₂ for 0.5, 1, 2, 6, and 24 hours...	64
IV-14. Hydrogel viscoelastic behavior as indicated by the elastic and viscous moduli of 0.20 and 0.60 wt% AvP2 at specific time intervals after introduction of 5 mM CaCl ₂	65
IV-15. Elastic and viscous moduli as a function of frequency for AvP2 gels at specific polymer concentrations 0.10-0.80 wt% crosslinked by 50 and 3 mM CaCl ₂	67
IV-16. Elastic modulus plotted against AvP2 concentration of hydrogels formed at CaCl ₂ concentrations of 3, 15, 35 and 50 mM.....	68
IV-17. Elastic and viscous moduli as a function of frequency for gels composed of 0.20 and 0.60 wt% AvP2 at CaCl ₂ concentrations of 3, 5, 15, 25, 35, 50 mM.....	70

IV-18. Elastic modulus plotted as a function of the molar ratio $[Ca^{2+}]/[COO^-]$ for AvP2 calcium gels formed at concentrations of 0.10, 0.20, 0.40, 0.60, 0.80 wt% polymer.....	71
IV-19. Example of a non-linear Huggins-Kraemer plots obtained for AvP2 after dissolution in 0.20 M NaCl for 2 and 24 hours, respectively.....	73
IV-20. Turbidity of AvP2 solutions as functions of NaCl and polymer concentration at 2 and 24 hours.....	74
IV-21. Elastic and viscous moduli as a function of frequency for hydrogels formed from 0.20 wt% AvP2 solutions dissolved in 0.05, 0.10, 0.15, 0.20 NaCl for 2 and 24 hours prior to introduction of 35mM $CaCl_2$	75
IV-22. Elastic modulus of 0.20 wt% AvP2 hydrogels formed from aqueous AvP2 solutions at the specified NaCl concentration by crosslinking with 35 mM $CaCl_2$	76
IV-23. Elastic modulus of 0.20 wt% AvP2 hydrogels formed by crosslinking with 5 mM $CaCl_2$ and a simulated nasal fluid containing 5 mM $CaCl_2$, 0.15 M NaCl and 0.04 M KCl.....	77
IV-24. The apparent diffusion coefficient of water plotted against observation time for 0.20 and 0.60 wt% AvP2 gels.....	80
IV-25. Proposed hydrogel morphology of Ca^{2+} crosslinked AvP matrices formed from homogeneous aqueous solutions and solutions containing low concentrations of monovalent ions.....	81
IV-26. Size distribution of 4 and 500 kDa FITC-Dextrans as determined by dynamic light scattering.....	82
IV-27. Cumulative release of 4 kDa and 500 kDa dextran as a function of time from 0.20 wt% and 0.60 wt% hydrogels.....	83
IV-28. Percent of dextran released during the initial study, after EDTA exposure, and after disruption of phase separated polymer regions.....	84
IV-29. Cumulative release of dextran 4 and 500 kDa dextran plotted against the square root of time for 0.20 wt% and 0.60 wt% AvP hydrogels.	87
IV-30. Bright field and fluorescence micrographs of 0.20 wt% AvP2 hydrogels....	91
A-1. SEC-MALLS trace of AvP4 including molecular weight and radius of gyration analysis.....	97

A-2.	SEC-MALLS trace of AvP4 depicting radius of gyration as a function of molecular weight	97
A-3.	¹ H NMR spectrum of AvP1, obtained using HOD suppression techniques	100
A-4.	¹ H NMR spectrum of AvP2, obtained using HOD suppression techniques	100
A-5.	¹ H NMR spectrum of AvP4, obtained using HOD suppression techniques	101
A-6.	¹ H NMR spectrum of AvP5, obtained using HOD suppression techniques	101
A-7.	Huggins-Kraemer plots, illustrated for AvP1, AvP2, AvP3, AvP4, AvP5 in 0.05 M NaCl.....	102
A-8.	Huggins-Kraemer plots, illustrated for AvP1, AvP2, AvP3, AvP4, AvP5 in 0.10 M NaCl.....	103
A-9.	Huggins-Kraemer plots, illustrated for AvP1, AvP2, AvP3, AvP4, AvP5 in 0.15 M NaCl.....	104
A-10.	Huggins-Kraemer plots, illustrated for AvP1, AvP2, AvP3, AvP4, AvP5 in 0.20 M NaCl.....	105
AI-11.	Determination of electrostatic expansion factor and persistence length as a function of the Mark Houwink parameter.....	106
A-12.	Specific viscosity as a function of shear rate for 0.25, 0.50, 0.75, 1.0, 1.25, 1.5, 1.8 wt% AvP3 samples dissolved in aqueous solutions.....	117
A-13.	Specific viscosity as a function of shear rate for 0.15, 0.25, 0.30, 0.40, 0.50, 0.75, 0.90 wt% AvP3 samples dissolved in 0.10 M NaCl.....	118
A-14.	Elastic and viscous modulus as a function of frequency for aqueous AvP solutions.....	118
A-15.	Fluorescence emission of 1,8-ANS.....	119
B-1.	Elastic and viscous moduli as a function of frequency for AvP2 gels crosslinked by 35 and 15 mM CaCl ₂ . Polymer concentrations of 0.10, 0.20, 0.40, 0.60, and 0.80 wt% were utilized for gel formation.....	120
B-2.	Elastic modulus of AvP hydrogels formed at calcium concentrations of 5.0, 15, 35, 50 mM with corresponding fits based on rubber elasticity theory.....	126

C-1.	Specific viscosity of AvP3 dissolved in water, 0.05, 0.10, 0.15 and 0.20 mM NaCl as a function of shear rate.....	128
C-2.	Time dependent scattering intensity of AvP3 dissolved at specified temperature/ionic strength conditions 25°C/0.20 M, 25°C/0.10 M and 15°C/0.20 M NaCl.....	130
C-3.	Time dependent scattering intensity of AvP3 dissolved at specified temperature/ionic strength conditions 10°C/0.20 M, 15°C/0.20 M.....	131
C-4.	Dynamic oscillatory rheology of AvP3 conducted as a function of temperature.....	132
C-5.	Dynamic oscillatory rheology of AvP3 (0.50wt%) conducted as a function of temperature (°C) at a frequency of 6.2 rad/sec and a stress of 0.5 Pa.....	133

LIST OF TABLES

Table		
IV-1.	Chemical composition and physical parameters of <i>Aloe vera</i> polysaccharide (AvP).....	41
IV-2.	Intrinsic viscosity as a function of AvP sample and salt concentration with calculated values of intrinsic viscosity at infinite ionic strength, the flexibility parameter and the persistence length.....	45
IV-3.	Literature values of B the Smidrod Haug stiffness factor.....	53
IV-4.	Experimentally determined elastic and viscous moduli reported at a frequency of AvP hydrogels crosslinked by Ca ²⁺	66
IV-5.	Calculated parameters for release models and goodness of fit indicator based on experimental release profiles of 0.20 and 0.60 wt% AvP2 calcium hydrogels.....	88
A-1.	Integrals of ¹ H NMR peaks and calculated values of degree of methylation	99
B-1.	Absorbance of AvP at 2 and 24 h over a range of polymer (0-2 mg/mL) and NaCl (0-0.20 M) concentrations.....	121

CHAPTER I

INTRODUCTION

Hydrogels

The term hydrogel is generally used to describe three dimensional viscoelastic networks that retain large amounts of water. The network is often formed by a hydrophilic polymer which may be chemically or physically crosslinked. Networks of this nature are considered ideal candidates for drug delivery and have received vast interest.¹ Stimuli responsive hydrogels undergo a reversible phase transition in the presence of stimuli such as pH, temperature, and ionic strength. Stimuli responsive systems can be tailored to provide *in situ* gelation and have been investigated for site specific drug delivery. Several excellent review articles on the subject hydrogels, microgels/nanogels, and *in situ* gelling systems are recommended.²⁻⁵

Hydrogels can be formed from both synthetic and natural polymers. A recent review focusing on hydrogels formed from synthetic block copolymers including; poly(N-substituted acrylamides), poly(vinyl ethers), and polyethylene oxide/polypropylene oxide block copolymers is recommended.⁶ This dissertation focuses on a naturally derived galacturonate polysaccharide hydrogel system. As such the remainder of the introduction pertains to hydrogels formed *via* chemical and physical crosslinking of polysaccharides.

Polysaccharides

Polysaccharides represent a broad class of biological macromolecules that are produced abundantly by both the algal and plant kingdoms and certain strains of microbial bacteria. Due to the diverse range of synthetic pathways present within different plant and bacterial species, polysaccharides display a variety of structural and behavioral characteristics. Over 100 simple sugars and sugar derivatives are included in the monomers available for synthesis. In addition perturbations in covalent linkage position on the sugar ring and chain branching provide added potential for diversity among naturally occurring polysaccharides.⁷

Water soluble polysaccharides have been and continue to be used in many consumer products including application in both the food and personal care industries. Coming from renewable resources, polysaccharides frequently have an economic advantage over synthetic polymers. This results in a distinct advantage within consumer based markets. In other industries such as pharmaceuticals, polysaccharides have received attention due to their non-toxic, biocompatible nature.

Polysaccharides are commonly classified based upon plant or animal source and into groups of similar chemical structure. This introduction will focus on polysaccharides of interest to the pharmaceutical field and is organized in terms of natural source, with a separate section on cellulose derivatives. The order of discussion progresses according to the most common gelation mechanism employed for the individual polysaccharide. Polysaccharide systems which require chemical crosslinking are discussed first,

progressing to those which gel through physical association and finally to those which gel upon exposure to divalent ions.

Cellulose Derivatives

Cellulose serves as the major structural component of plants and is abundant in nature. In order to confer water solubility, cellulose is commonly modified synthetically to produce cellulose ethers. Water soluble cellulose ethers can be prepared by nucleophilic substitution and ring opening mechanisms.⁷ Two of the most widely utilized cellulose derivatives are carboxymethylcellulose and hydroxyethylcellulose.

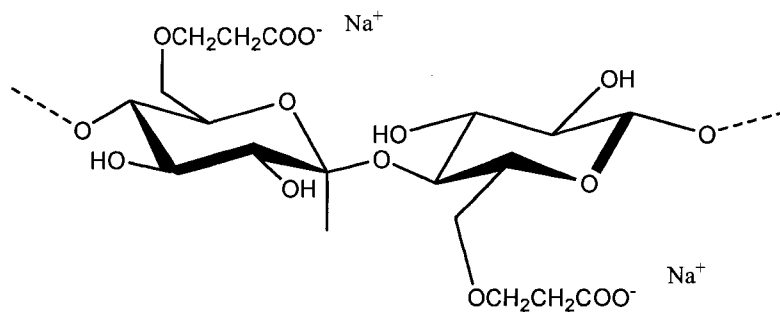


Figure I-1. Molecular Structure of carboxymethylcellulose.

Carboxymethylcellulose. Carboxymethylcellulose (CMC) is usually prepared by the reaction of cellulose with chloroacetic acid in aqueous alkaline organic slurries. The extent of substitution at C-2, C-3, and C-6 is related to the effectiveness of hydrogen bond disruption, steric factors, and reactions conditions.⁷ The acid form of CMC behaves as a polyelectrolyte and exhibits a pK_a of 4. Solutions of sodium CMC are pseudoplastic

for degrees of substitution between 0.9-1.2. Solutions of high molecular weight sodium CMC with a low degree of substitution are thixotropic.

CMC is considered biocompatible and is traditionally utilized as an excipient in pharmaceutical formulations involving oral delivery of tablets. CMC has been used to form interpolymer complexes with chitosan to produce “tablets-in-capsule” oral delivery systems. The approach of these systems is to form a combination of mini-matrices inside a hard gelatin capsule to obtain different drug delivery systems.⁸ Anomalous diffusion of clarithromycin was observed from chitosan/CMC when complexes were formed at a 1:3 ratio. Fickian diffusion was observed when a 3:1 ratio was employed.

Typically CMC hydrogels are prepared by chemical crosslinking or gamma irradiation.^{9, 10} Physically crosslinked hydrogels have been formed utilizing mixtures of CMC and polyvinyl alcohol (PVA).¹¹ A solution containing the two polymers was repeatedly heated and cooled in a freeze-pump-thaw cycle. During the cooling cycle the PVA undergoes crystallization, these crystalline regions then act as junction zones in the resulting hydrogel.

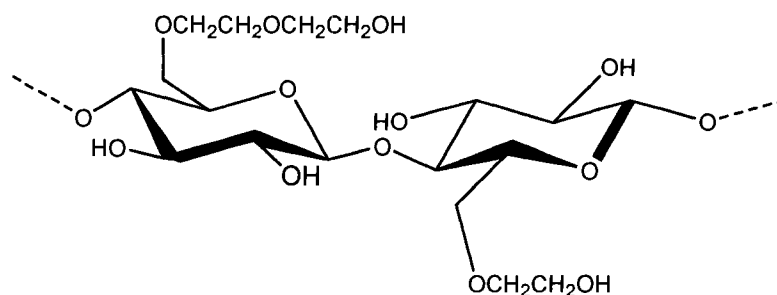


Figure I-2. Molecular Structure of hydroxyethylcellulose.

Hydoxyethylcellulose. Hydroxyethylcellulose (HEC) is prepared by ring opening of ethylene oxide by hydroxyl anions formed on the anhydroglucose ring of cellulose. HEC is a nonionic polymer with little surface activity in solution, making it stable under a wide range of ionic strengths. HEC/chitosan complexes have been studied with specific focus on their mucoadhesive properties.¹² Mucoadhesion studies on HEC solutions alone and HEC/chitosan complexes determined that the presence of chitosan decreases mucoadhesion. However, the presence of chitosan provided improved retention on the mucosal wall. The increased retention time was attributed to an increase in yield stress provide by the HEC/chitosan complex. The yield stress inhibited flow of the sample from the mucosal wall, resulting in an overall higher percent delivery of the target antibacterial agent, metronidazole.

Animal Extracts

Chitin. Chitin is a water-insoluble high molecular weight polysaccharide that is abundant in the skeletal material of invertebrates such as clams, crabs, and lobsters. Chitin may be converted to chitosan (Figure I-3) by partial or complete deacetylation.⁷ In the protonated form the cationic polysaccharide is water soluble. A large focus has been placed on the development of chitosan for nasal drug delivery and many excellent articles have been published by Lisbeth Illum.¹³⁻¹⁸ A recent review article by M. Prabakaran¹⁹ focuses solely on the application of chitosan and chitosan derivatives in controlled drug delivery.

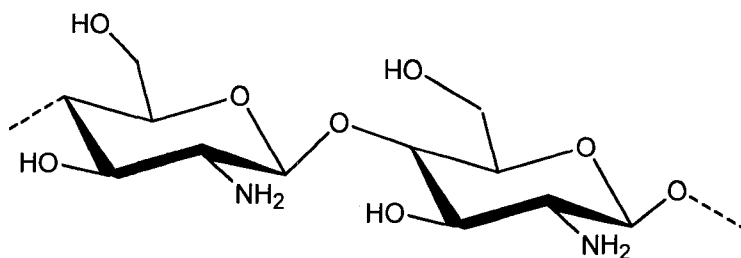


Figure I-3. Molecular Structure of chitosan.

Hyaluronic Acid. While hyaluronic acid is considered a glycosaminoglycan that is present in animal fluids, including human synovial fluid, it is commercially produced from *Streptococci* bacteria. Hyaluronic acid is composed of a repeating disaccharide unit of D-glucuronic acid and N-acetylglucosamine units linked α -(1-4) and β -(1-3), respectively.

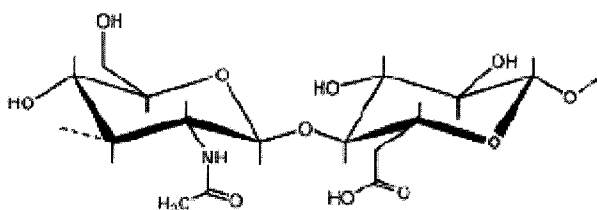


Figure I-4. Molecular structure of hyaluronic acid depicting N-acetylglucosamine and D-glucuronic acid.

Hyaluronic acid is commonly used as a viscoelastic fluid in ophthalmologic surgery and as an injectable solution in joint rehabilitation. Hyaluronic acid hydrogels have received interest as biocompatible and biodegradable materials with applications in drug delivery and tissue engineering. Hyaluronic acid is not a natural gel former and must be chemically modified to produce hydrogels. Typical approaches have relied on chemically crosslinked networks through reactions with; divinylsulfone, glycidyl ether, and gluteraldehyde.²⁰ Additionally, in most hyaluronic acid hydrogel delivery systems

drugs have been covalently attached to the hyaluronic acid backbone, typically via carbodiimide chemistry.²¹ An important problem with these techniques is that they involve small molecule reactants which are not biocompatible and must be removed prior to *in vivo* application.

A more biocompatible crosslinked hyaluronic acid system has been developed.²² The system involved preparation of thiol-modified hyaluronic acid. Dithiobis(propanoic dihydrazide) and dithiobis(butyric dihydrazide) were coupled to hyaluronic acid *via* carbodiimide chemistry. The disulfide bonds of the initial gel were then reduced with dithiothreitol to yield the thiol modified derivatives. In the presence of air, the thiol groups oxidize to form disulfide linkages, yielding a reversible hydrogel system. The system was evaluated for modulated delivery of blue dextran and was shown to release dextran upon reduction of the dithiol linkage.

Bacterial Polysaccharides

Microorganisms produce polysaccharides of three distinct types: extracellular, structural, and storage. Extracellular polysaccharides include those that form a capsule which is integral to the bacteria cell wall and those that are exuded from the bacterial cell wall and diffuse constantly into the surrounding medium.²³ Exuded extracellular polysaccharides have been widely exploited by industry because they can be recovered in large quantities from culture media. Extracellular polysaccharides function to both protect bacteria from the environment and provide a method of cell signaling.

Dextran. Dextrans are high molecular weight homopolysaccharides of α -1-6-D-glucopyranose with varying proportions of α -1-2, α -1-3 and α -1-4 branched linkages. Dextran is produced from sucrose by a number of bacteria from the family *Lactobacillae*. Fractionated commercial dextrans are often used as standards in molecular weight determination of other water soluble polymers *via* size exclusion chromatography. Dextran is utilized in commercial applications as a plasma substitute and anticoagulant.

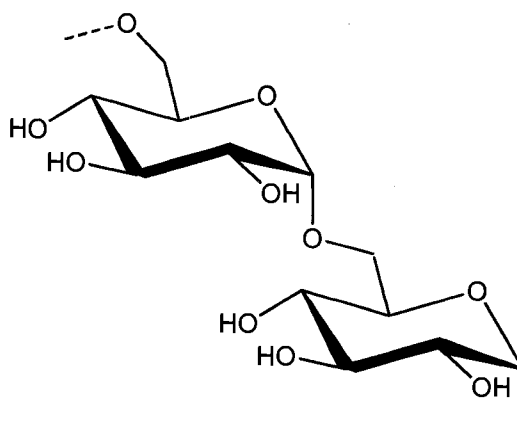


Figure I-5. Dextran molecular structure depicting the 1-6 glucopyranose linkage.

Dextran is commonly modified synthetically; one of the first examples relevant to the pharmaceutical field was the introduction of reactive double bonds *via* functionalization with glycidyl acrylate.²⁴ The acrylate moieties were polymerized utilizing gamma-irradiation, resulting in hydrogels which provide modulated release of drugs upon degradation by dextranase. The cumulative release of model proteins decreased with increasing protein size. Diffusion rates were found to be proportional to the square root of time, indicating that Fickian diffusion was dominant.^{25,26}

Hydroxyethyl methacrylate (HEMA) dextrans have been prepared that are degradable under physiological conditions due to the presence of carbonate esters in the final crosslinked hydrogel.²⁷ The release profiles of interleukin-2, a known mediator of immune response, indicated that increasing crosslink density decreases the release rate. Microgels of HEMA modified dextrans were also investigated for delivery of DNA.²⁸ Further studies involved the encapsulation of Dextran-HEMA microgels with a water permeable lipid membrane. Swelling occurs upon degradation of the dextran-HEMA microgel which ultimately results in rupture of the lipid layer. Using this mechanism the composition of the dextran-HEMA microgel can be altered to modify the degradation rate and provide rupture of the lipid layer at a specific time interval.

Pullulan. Pullulan is a linear bacterial polysaccharide derived from *Aurebasidium pullulans*. The polymer backbone is composed of α -1-6-D-glucopyranose and α -1-4-D-glucopyranose present at a 1:2 ratio. In aqueous solution pullulan appears to behave as an expanded random coil.²⁹

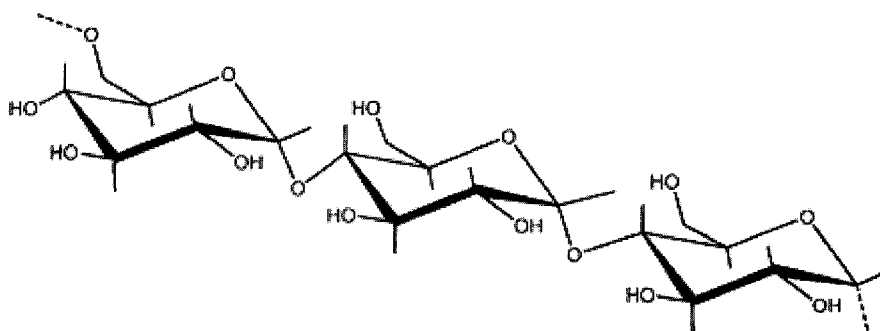


Figure I-6. Pullulan molecular structure depicting α -1-6 and α -1-4 glycosidic linkages.

Pullulan has been used in foods as filler and in pharmaceuticals as a coating agent. Films formed by drying pullulan solutions provide high oxygen permeability and excellent mechanical properties. Pullulan is not a naturally gelling polysaccharide, however as in the case of dextran, synthetic modifications have been shown to provide a gelling mechanism suitable for drug delivery.

Pullulan hydrogels have been examined for drug delivery in the form of micro- or nanogel particles. Hydrophobically modified pullulan has been shown to form nanogels through intramolecular interactions.³⁰⁻³² These interactions are particularly strong when the hydrophobic moiety employed is cholesterol. Cholesterol modified pullulan has been shown to bind both hydrophobic small molecules, such as anticancer drugs, and water soluble proteins.^{33, 34} It has been reported that the size and effective crosslink density of the hydrogel nanoparticles can be altered by varying the degree of cholesterol substitution.³⁰ It has been shown that upon addition of β -cyclodextrin the intramolecular hydrophobic interactions present in the pullulan nanogel are disrupted and the gels expand, leading to the conclusion that pullulan nanogels could be used to deliver therapeutics to hydrophobic environments.³⁴

Xanthan. Xanthan was one of the first commercially available bacterial polysaccharides, it was first put into pilot production by Kelco in 1960.²³ Xanthan gum is a heteropolysaccharide with a cellulosic backbone of β -1-4 linked D-glucose. A side chain of β -D-mannose-(1,4)- β -D-galuronic acid-(1,2)- α -D-mannose is present on alternating glucose sugars along the polymer backbone. The internal mannose unit may be acetylated at C-6, and the terminal mannose unit can be substituted with pyruvate.

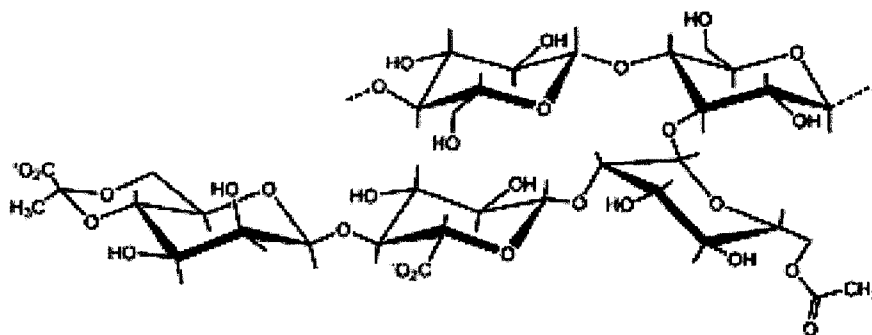


Figure I-7. Xanthan molecular structure depicting β -D-mannose-(1,4)- β -D-guluronic acid-(1,2)- α -D-mannose side chains on the D-glucose backbone.

Xanthan dissolves readily in either hot or cold water to give highly viscous solutions at low concentration. Solutions of xanthan are highly pseudoplastic with the viscosity being nearly independent of temperature and pH. At pH 9 or above, xanthan is gradually deacetylated, however there is a negligible effect on solution properties.²³

Xanthan has been widely used as a tablet excipients to increase the rate of drug delivery, however there are not many studies that have examined xanthan as a drug delivery vehicle. Complexes of xanthan and chitosan form homogeneous hydrogels containing fibrillar structures. These fibrillar gels were used to form channels which permitted transport of polymeric substrates to regions where immobilized enzymes were present, upon exposure of the substrate to the enzyme the desired reaction was achieved and the product was recovered.³⁵

Xanthan has been utilized in the preparation of sponge like *in situ* gelling nasal inserts with the goal of delivering proteins and peptides in the nasal cavity.³⁶ Model drug release relies on the interplay between osmotic forces and electrostatic interactions

between the polymer system and the protein. Extended *in vitro* release was demonstrated over several hours making xanthan a potential candidate for bioadhesive nasal inserts.

Gellan. Gellan is a linear exopolysaccharide commercially prepared by fermentation of *Sphingomonas elodea*. The tetrasaccharide repeat unit is composed of (-4-L-rhamnopyranosyl -(α -1-3)-D-glucopyranosyl -(β -1-4) -D-glucuronopyranosyl-(β -1-). In nature the 1-3 linked glucose unit contains O(2) L-glyceryl and O(6) acetyl substituents.

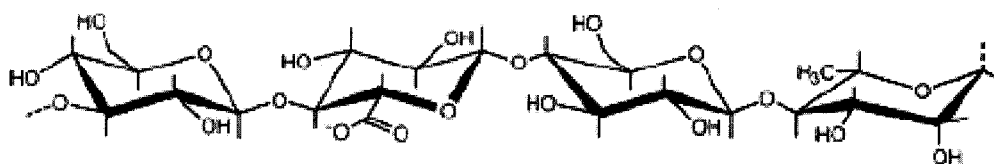


Figure I-8. Gellan molecular structure depicting the tetrasaccharide repeat unit.

Gellan gum forms a 3-fold double helix in solution, with the acetate groups on the periphery, and glyceryl groups stabilizing interchain associations. In order to tailor the mechanical properties of hydrogels formed in the presence of monovalent and divalent counterions gellan gum is often de-esterified prior to use. In the acylated form gellan forms soft, elastic gels, while de-acylation results in transparent, brittle, non-elastic gels.

Gellan hydrogels are thermoreversible transitioning from sol to gel as temperature is reduced below 50°C. The transition temperature is increased in the presence of cations that stabilize the gel. Gellan has been widely investigated in ophthalmic drug delivery formulations due to its ability to gel in the presence of cations contained within tear fluid.³⁷ *In vivo* experiments determined that appreciable amounts of ocular bioavailability

were obtain only when the gel strength was within set limits. Gellan has been tested *in vivo* in rats for delivery of model fluorescein dextran compounds and was shown to exhibit retention times relevant to nasal delivery (1-2 hr).³⁸ Parallel *in vitro* studies determined that strong gels were formed in the presence of 0.9% NaCl. The presence of divalent calcium ions further increased the gel strength.

Algal Extracts

Carrageenan. Carrageenan is a seaweed that was originally harvested along the south coast of Ireland by shore residents of the County Carrageen approximately 600 years ago.²³ It was brought to the coast of North America by Irish settlers and was recognized as a component of local flora of the coast of Massachusetts in the 1700's. Carrageenan is composed of a linear disaccharide repeat unit composed of β -D-galactose and 3,6-anhydro- α -D-galactose. In general three different types of carrageenan exist, which are classified based on the degree of sulfation (ranges from 15 to 45%).

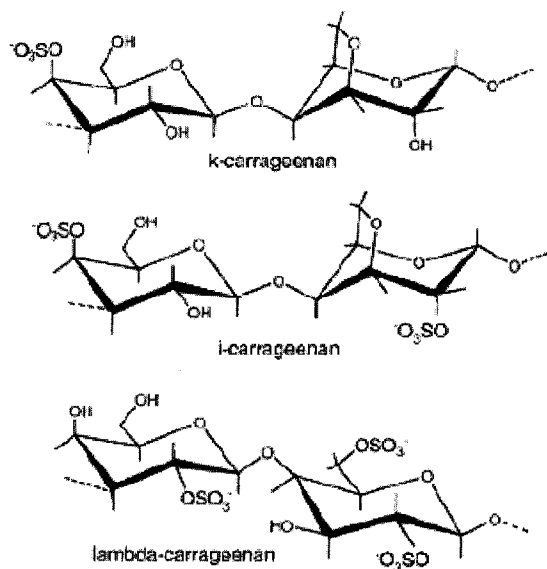


Figure I-9. Molecular structures of kappa, iota, and lambda-carrageenan.

Kappa and iota carrageenans exist as right handed threefold helices that have been shown to form reversible double helices in solution.²³ Physically crosslinked hydrogels are formed by kappa and iota carrageen upon exposure to monovalent ions, specifically potassium. Junctions in kappa-carrageenan hydrogels are thought to involve intermolecular association of double helix segments.^{39, 40} The properties of hydrogels can vary from hard and brittle to soft and elastic. The properties of the gel are directly dependent on the chemical nature of the carrageenan, the type of counter ion present and the presence of other non-gelling polysaccharides.

Carrageenans are often utilized to form interpenetrating hydrogel networks with agar and gelatin. Release of model compounds was found to rely heavily on the network structure of the original polysaccharide constituents. This suggests that the networks were not truly interpenetrating.⁴¹

A comparison of gels formed from *k*-carrageenan on crosslinking with mono, di and trivalent ions revealed that trivalent ions are less effective at forming hydrogels for drug delivery applications. Microscopy revealed that large channels were present within the network.⁴²

Alginates. Alginates are a class of polysaccharides which contribute to the structural components of marine algae.²⁹ Alginates are known for their ability to retain water and for their gelling and viscosifying properties. Alginates are unique in that they exhibit an almost temperature-independent gelation behavior in the presence of multivalent cations, making them suitable materials for the immobilization of living cells.

Alginates are composed of (1-4) linked β -D-mannuronic acid and α -L-guluronic acid residues (Figure I-10) found in a wide variety of compositions and sequences. Haug and Smidsrod reported that alginate structure contains three primary regions; two of these regions contain almost homopolymeric sequences of mannuronic and guluronic acid residues. The third region consists of alternating sequences of mannuronic and guluronic residues, as depicted in Figure I-11.⁴³

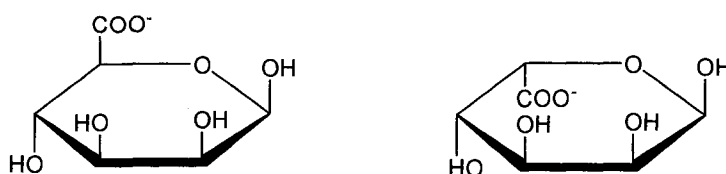


Figure I-10. β -D-Mannuronic Acid (left) and α -L-Guluronic Acid (right)

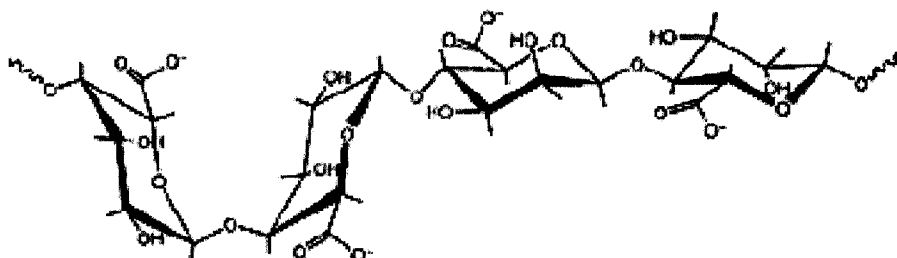


Figure I-11. General structure of alginates depicting mannuronic and guluronic repeat units.

Gelation of alginates requires dissolution followed by changes in pH and/or ion type and concentration with almost no dependence on temperature. Potentiometric measurements by Haug revealed that an abrupt decrease in pH below the pK_a of the

alginate causes precipitation, whereas a metered addition of acid created an “alginic acid gel”.⁴³ The pH range of gelation was found to be dependent upon molecular weight and the chemical composition and sequence of the alginate; for example, alginates containing more alternating blocks of mannuronic and guluronic acid precipitate at lower pH values than those with more homogeneous block structures. Alginates with homogeneous block structures promote the growth of crystalline regions, enhancing the formation of a hydrogen bonded gel.

Alginates exhibit specific ion binding characteristics; for example, equilibrium dialysis experiments have shown selective binding to alkaline earth metals such as calcium.⁴⁴ The prevalence of specific ion binding was found to increase with increasing content of α -L-guluronate residues. This indicates that chelation is caused by some structural feature of the α -L-guluronate residues. A widely accepted theory by Grant *et al.*⁴⁵ proposes “egg-box structures” (Figure I-12), based on the linkage structures of the guluronate residues. NMR studies by Kvam and Steginsky have suggested similar binding sites for calcium ions.⁴⁶

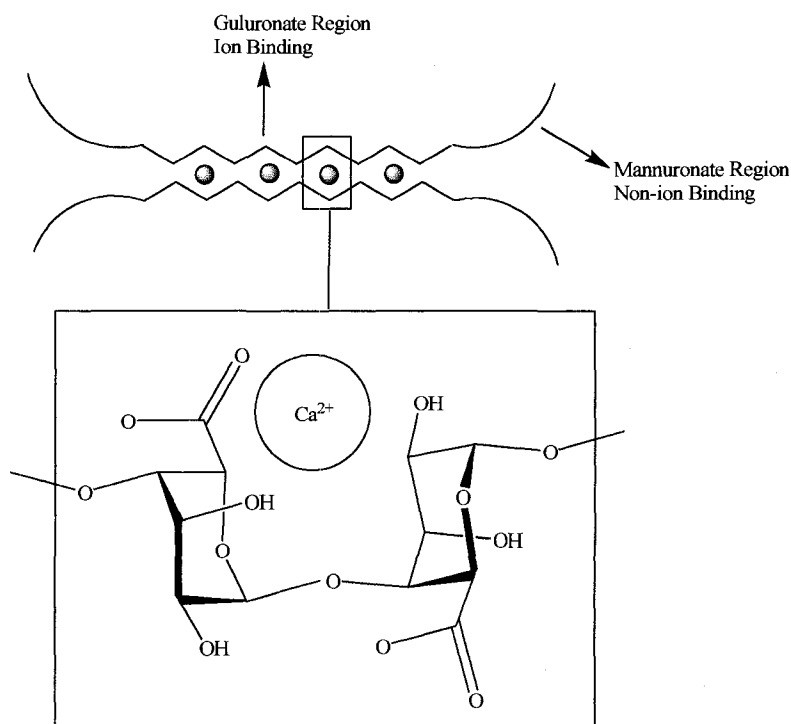


Figure I-12. Alginate Egg Box Structure

Plant Extracts

Traditional Glacturonate Polysaccharides: Pectins. Pectins are a broad class of complex plant polysaccharides which are present in the primary cell walls and intercellular regions of plants. Pectins are commonly extracted from citrus sources such as grapes, apples, and oranges and have been heavily utilized in the food industry.²³ Pectins present in plant cell walls are responsible for the controlled permeation of water and structural integrity of the cell.²⁹ This class of polysaccharides is characterized structurally by a heterogeneous composition of partially methyl-esterified galacturonic acid, rhamnose, and neutral sugars. Pectins are primarily composed of an α -(1-4)-linked D-galacturonic acid polymer backbone, commonly referred to as “smooth” or linear homogalacturonic regions (Figure I-1). Regions containing intermittent (1-2)-linked

rhamnopyranosyl units (Figure I-2) are also present along the polymer backbone. These regions, referred to as “hairy” or branched rhamnogalacturonic regions, are branch sites for neutral sugars such as glucose, mannose, galactose, fucose, and xylose.

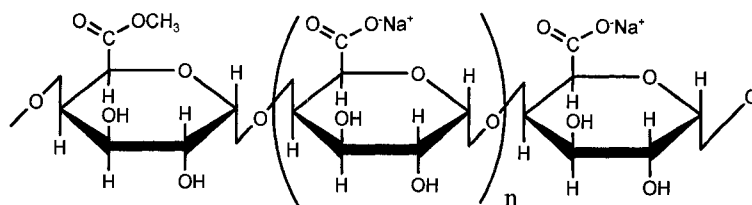


Figure I-13. Homogalacturonan region of pectin depicting galacturonic acid in the sodium salt form and in the methyl ester form.

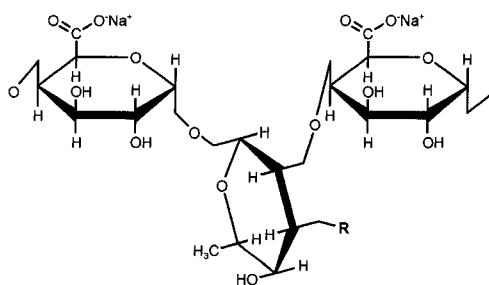


Figure I-14. Rhamnogalacturonan region of pectin with rhamnose sugars incorporated into the polysaccharide backbone *via* a 1-2 linkage.

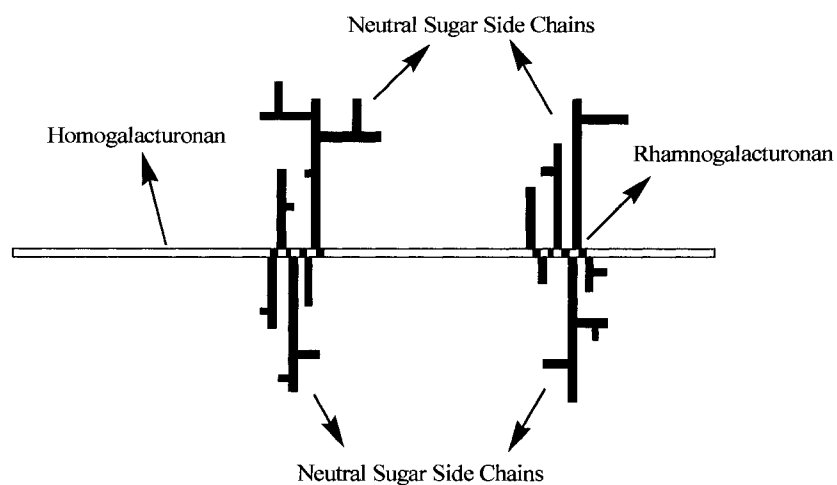


Figure I-15. Linear and branched regions of pectin polysaccharides

In nature the carboxylic acid located at C-6 of the galacturonic acid unit may be esterified with methanol. Pectins are further divided in classification based upon the percentage of methyl-esters naturally present on the galacturonic acid polymer backbone. Pectins with degrees of methylation higher than 50% are termed high-methoxy pectins⁴⁷ (HM) and those below 50% are low-methoxy pectins (LM). Natural pectins, such as those from apple, citrus, and grape are often highly methylated.^{23, 29}

LM pectins are generally obtained by controlled, acidic de-esterification, but may also be obtained using acidic microbial pectin methylsterases (PME).⁴⁸ These procedures tend to lead to LM pectins with a random distribution of free carboxyl groups. Thibault and Rinaudo⁴⁸ demonstrated that alkaline PME may be used to create pectins with blockwise arrangement of free carboxyl groups. In separate studies it was shown that the distribution of free carboxyl groups has a marked effect on the gelation properties of pectins.^{49, 50} Measurements of the calcium transport parameter and calcium activity coefficient as a function of degree of methylation (DM) for a series of alkali, acid, fungal PME, and plant PME de-esterified pectins showed that a blockwise arrangement of free carboxyl groups leads to stronger calcium binding.^{49, 51} Recent studies involving side chain modifying enzymes revealed that removal of neutral sugar side chains results in significantly lower solution viscosity.⁵² The reduction in viscosity was attributed to loss of neutral sugar-driven associations in solution and was shown to correlate to an order of magnitude reduction in hydrogel mechanical properties. These studies exemplify the large impact of chemical structure and solution behavior on the gelation of pectins.

Gelation of pectins can occur under a variety of conditions, including changes in solution pH,⁵³ ionic strength,^{54, 55} and temperature.^{56, 57} However, the primary

requirement for efficient gelation is that the pectin be initially soluble. Pectin solubility in aqueous media is favored by the dissociation of carboxyl groups, which creates Coulombic repulsion between polymer chains enhancing polymer-solvent interactions. Once the pectin is solubilized, it may gel through inter-chain associations. The hydroxyl groups at C-2 and C-3 on galacturonic acid units may readily elicit hydrogen bonding^{58, 59} with the free, methylated, or amidated carboxyl functions located at C-6. In addition, hydrophobic interactions between aliphatic regions of the polysaccharide may result in further polymer-polymer interactions.⁶⁰ The combination of these conditions gives rise to rigid non-reversible gels.

LM pectins also gel in the presence of divalent cations such as calcium, exhibiting an increased propensity towards gelation as the DM decreases. Furthermore, LM pectins with a blockwise arrangement of carboxyl groups exhibit high sensitivity to calcium ions.^{49, 58, 61} Many rheological studies have been conducted on pectin hydrogels formed in the presence of Ca^{2+} and cosolutes, such as sugars⁶²⁻⁶⁴ and polysaccharides,⁶⁵⁻⁷⁰ due to the vast number of applications in food and personal care products. The addition of calcium to LM pectins has been shown to create pectin dimers *via* physical crosslinking of carboxyl functional units. Physical crosslinking is shown to occur in the “smooth” homogalacturonic regions. The proposed structure of the pectin calcium ion physical crosslink is depicted in Figure I-4 with crosslinked areas being referred to as junction zones.^{58, 71}

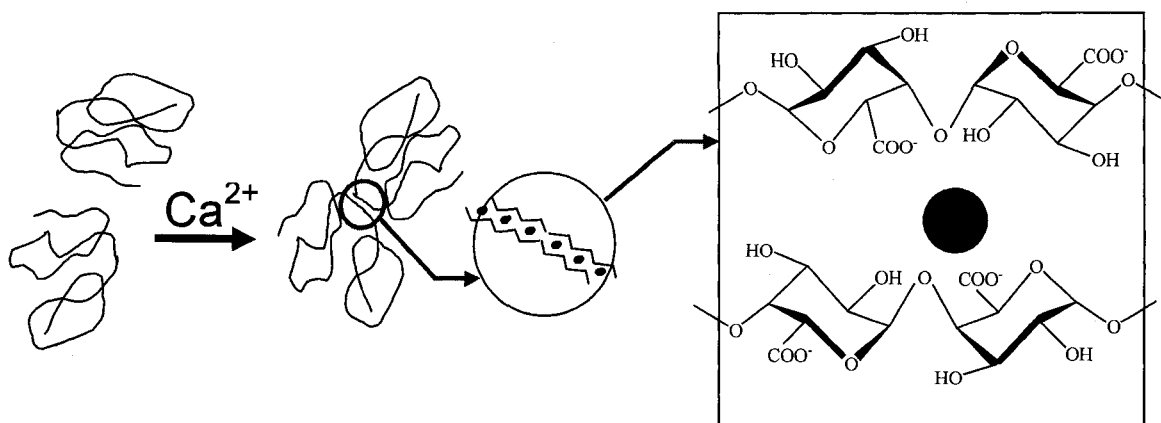


Figure I-16 Proposed conformation of physical crosslinks formed by complexation of calcium ions with GalA regions from two pectin chains.

The specific binding of Ca^{2+} to polysaccharides was first examined for alginates, a family of polysaccharides closely related to pectins. The general alginate structure is principally composed of (1-4) linked β -D-mannuronic acid and α -L-galuronic acid residues found in a wide variety of compositions and sequences.¹ Where the galuronic acid units of alginate and the galacturonic acid units of pectin differ only in the position of C-3 hydroxyl group. The Ca^{2+} binding phenomena of alginates and pectins have been studied by techniques including activity coefficient measurements,^{48, 50} circular dichroism,^{59, 71-74} light scattering,^{50, 75} fast field cycling relaxometry,⁷⁶ FT-IR,⁷⁷ ^{13}C NMR,⁷⁸ and ^{23}Na NMR.⁷⁹ The “egg box” model of binding was originally proposed for both alginates and pectins, and was postulated to occur through a two stage process, where the formation of strong dimer associations is followed by the formation of weaker interdimer aggregates.⁵⁸ Recent isothermal calorimetry studies have confirmed a gradual two stage process for pectin Ca^{2+} association.⁸⁰ Additional studies involving theoretical modeling have recently questioned the applicability of the “egg box” model to both systems, suggesting instead a “shifted egg box” model for pectins.⁸¹ While the exact

nature of pectin junctions zones may still be under debate, some established relationships between pectin chemical composition and hydrogel properties have presented in several texts^{23, 82, 83} and a recent review article.⁸⁴

In an effort to build on current knowledge regarding traditional pectins, we initiated the study of a newly discovered *Aloe vera* polysaccharide (Figure I-5). The *Aloe vera* polysaccharide (AvP) is readily isolated as a high molecular weight species (300-500 kDa) composed of greater than 90% galacturonic acid. AvP molecular weight is approximately twice the average M_w of traditional pectins, and the fraction of GalA units in the acid form (as apposed to the methyl ester form) is extremely high. This provides a large number of carboxyl functional groups which provides unique solution behavior and hydrogel properties. In the first section of this thesis, the chemical composition of AvP has been elucidated and related to fundamental solution behavior. The second section focuses on Ca^{2+} -induced hydrogel formation and matrix properties at conditions relevant to nasal and subcutaneous delivery.

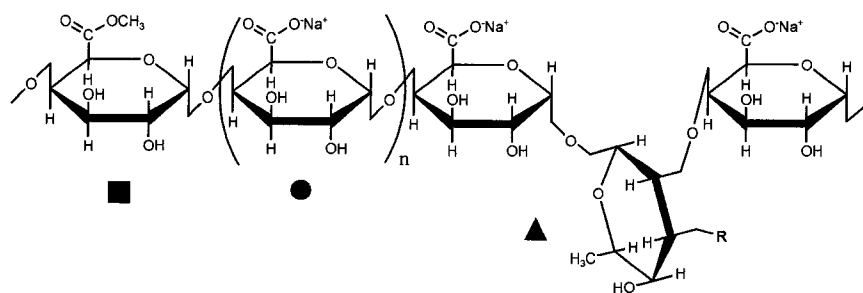


Figure I-17. General structure of pectin including galacturonic acid units with methyl esters (■), galacturonic acid sodium salt form (●), rhamnose (▲), and neutral sugar branches (R).

CHAPTER II

OBJECTIVES AND NEED FOR RESEARCH

The efficient, controlled delivery of protein therapeutics is a necessary feature in both current and future drug delivery formulations. Since synthetic insulin was introduced over 26 years ago, approximately 130 protein therapeutics designed to treat illnesses ranging from osteoporosis to chemotherapy-induced neutropenia have received approval; however, their role in treatment of illness is still limited.⁸⁵ Clinical application of protein therapeutics remains challenging due to large molecular size, short circulatory half life, and moderate stability. Since the efficacy of protein drugs typically relies on a cascade of events, precise timing of delivery at specific concentrations is required.⁸⁶ Hydrogel systems comprised of both synthetic^{6, 87} and natural polymers^{86, 88-90} have been studied, with emphasis being placed on polysaccharide-based systems due to their natural abundance, biocompatibility, and, in some cases, stimuli-responsive behavior.^{86, 91}

Galacturonates, commonly termed pectins, are naturally occurring polyelectrolytes with characteristics especially amenable to controlled delivery applications. To date limited research has been conducted on the *Aloe vera* polysaccharide. Initial studies indicate that the polysaccharide extracted from the *Aloe vera* plant possesses characteristics superior to other polysaccharides currently utilized in the pharmaceutical industry. Additionally, the GRAS (generally regarded as safe) status given to the *Aloe vera* polysaccharide presents an advantage from a regulatory point of view. In this research, a detailed examination of AvP chemical composition, solution behavior, and hydrogel characteristics has been conducted with the *overall goal* of

structuring Ca^{2+} crosslinked AvP matrices for use in nasal and subcutaneous protein delivery applications. Specific *objectives* are outlined below.

- Determine AvP chemical composition including; GalA, rhamnose, neutral sugar content and the percentage of GalA units present in the methyl-ester form
- Characterize the polymer molecular weight and polydispersity.
- Examine steady state rheological properties in both the dilute and concentrated regimes as a function of controlled environmental conditions including the ionic strength of the medium
- Elucidate polymer size, conformation, solvent/polymer, and polymer/polymer, interactions using dilute solution rheology and existing theories of polymer solution behavior
- Synthesize AvP hydrogel matrices *via* Ca^{2+} crosslinking
- Determine effects of solvent ionic strength, AvP molecular weight and concentration, and the ratio of Ca^{2+} to COO^- functionality in the system on the viscoelastic behavior of Ca^{2+} crosslinked hydrogels
- Determine hydrogel morphology through the study of the viscoelastic behavior and diffusion of water within Ca^{2+} crosslinked hydrogels under specific conditions of ionic strength
- Examine controlled release profiles of model macromolecular compounds from polysaccharide delivery platforms in physiologically simulated solutions
- Recommend polysaccharide system conditions necessary for successful protein therapeutic delivery based on relationships between solution properties, hydrogel morphology, and release mechanisms

CHAPTER III

EXPERIMENTAL

Materials and Methods

The *Aloe vera* polysaccharide (AvP) (Figure I-5) trademarked as GelSite[®] polymer was kindly donated by DelSite Biotechnologies (Irving, TX). The pectin was isolated by extraction with EDTA from the rind of *Aloe vera L.*, clarified by 0.2 μm filtration, and purified by difiltration. Deionized water (DI H₂O) was obtained from a Barnstead NANO-Pure reverse osmosis/filtration unit (resistivity: 18 M Ω).

Chemical Composition

The chemical composition of the *Aloe vera* Polysaccharide was determined utilizing established techniques for polysaccharide analysis. In a typically experiment the polysaccharide is degraded by either chemical or enzymatic methods and the tri, di, and monosaccharides obtained are analyzed by a combination of liquid chromatography and mass spectroscopy (LC-MS). The LC-MS work was conducted by collaborators at DelSite Biotechnologies. In order to validate data obtained by LC-MS techniques, ¹H NMR studies were conducted by researchers at The University of Southern Mississippi.

Galacturonic Acid Analysis. Analysis of Galacturonic acid (GalA) was performed by digestion of AvP using commercially available pectinase (Sigma, EC 3.2.1.15). In a 25 mL volumetric flask the following were combined: 20 mL of a 2 mg/mL AvP solution in deionized (DI) water, 50 μL of glacial acetic acid and 40 μL of

pectinase. DI water was then added to bring the total volume to 25 mL. The sample was heated with stirring at 40 °C for 4 hrs. Analysis was performed on a Waters 2690 Separations Module equipped with a Waters 2487 Dual Absorbance UV detector at 215 nm and a Phenomenex Rezex RHM-Monosaccharide column (8 μ m, 300 \times 7.8 mm) at 55 °C. The mobile phase was 6.4 mN H₂SO₄ maintained at a flow rate of 0.6 mL/min. The injection volume was 20 μ L. GalA was observed as a single peak at a retention time of 9.2 min and quantitated by comparing against a commercially available GalA sodium salt standard (Fluka).

Neutral Sugar Analysis. To 5 mL of a 5 mg/mL aqueous solution of AvP, 1 mL of 12 M HCl was added. The reaction mixture was heated to 80 °C for approximately 6 hr and then passed through a filter with a 0.2 μ m pore size. To 200 μ L of the hydrolyzed AvP, 800 μ L of 0.5 M triethylamine in acetonitrile was added. Analysis was performed on an Agilent 1100 series LC/MSD using a Phenomenex Phenosphere Amino column (5 μ m, 250 \times 4.6 mm). The mobile phase was 20% water, 79% acetonitrile, and 1% chloroform (present for adduct formation) at 40 °C, with a flow rate of 1 mL/min and an injection volume of 50 μ L. Detection was in atmospheric pressure chemical ionization negative mode with drying gas set to 300 °C, the vaporizer set to 350 °C, and fragmentor set to 20 V. Sugars were detected as chloride adducts (M+Cl⁻) and quantitated by comparing against commercially available standards, rhamnose and arabinose from United States Biochemical Corporation, and glucose, mannose, galactose, fucose, xylose from Sigma-Aldrich.

Determination of Methylester Substitution. The determination of methylesters substitution (commonly referred to as degree of methylesterification or DM) present on C-6 of GalA by LC-MS techniques is known to be inaccurate when the DM value in question is less than 10%. Due to the inherently low DM of AvP both LC-MS and ^1H NMR were employed in the determination of DM.

Utilizing LC-MS techniques the degree of methylesters was determined by the method of Wood & Siddiqui adapted to base-hydrolyzed pectin. Samples were prepared by dissolving 10 mg of AvP in 10 mL of 0.5 M LiOH followed by heating to 80 °C for 3 h in a sealed vial. The sample (0.75 ml) was then neutralized by adding 0.25 mL of 5.5 N H_2SO_4 . Solutions of commercially available methanol in 1 N H_2SO_4 were used as standards. Methanol oxidation to formaldehyde with KMnO_4 and further derivatization steps were performed as described by Wood & Siddiqui. The final sample was passed through a syringe filter with a 0.45 μm pore size and analyzed by LC/MS. The mobile phase consisted of solvent A (0.1% acetic acid in water and solvent B (0.1% acetic acid in methanol) with a gradient of 50% B to 100% B in 4 min. Detection of the M^{+1} ion of the methanol derivative 3,5-diacetyl-1,4-dihydro-2,6-dimethylpyridine was by ES positive mode with drying gas set to 200 °C and fragmentor set to 70 V.

AvP samples utilized in ^1H NMR techniques were stored under reduced pressure for 5 days prior to dissolution in D_2O at a concentration of 0.20 wt%. In an effort to reduce the HOD signal the D_2O was evaporated at 130°C. The sample was then re-dissolved in D_2O and centrifuged, with ^1H NMR being run on the supernatant. All spectra were acquired on a Varian Unity Inova spectrometer operating at a frequency of 499.8 MHz for protons and using a 5 mm three-channel HCN probe. The WET suppression

sequence was used to remove the H₂O resonance.⁹² A 90° flip angle (7.2 ms) was applied after the selective pulses/gradients, and an acquisition time of 2 seconds was used. The spectral width was 8 kHz, the FID composed of 32k data points, and an exponential line broadening of 1 Hz was applied prior to Fourier transformation. The recycle time between scans was 10 seconds. Chemical shifts were determined using the chemical shift of the HOD peak as a reference which is known to be a function of temperature.⁹³

Molecular Weight. The weight average molecular weight (M_w) and radius of gyration (R_g) were determined utilizing multiple-angle laser-light scattering coupled to size-exclusion chromatography (SEC). Samples of AvP were prepared in purified water at a concentration of 1 mg/ml and were allowed to shake at 250 rpm on an orbital shaker for 2 hours at room temperature. The AvP samples (50 μ l injections) were separated by four SEC columns in series using a Shodex OHPak SB-G guard column (50 x 6 mm), Shodex OH pak SB-806HQ (300 x 8 mm) Shodex OHPak SB-805HQ (300 x 8 mm,) and Shodex OHPak SB-804HQ (300 x 8 mm), with 0.10 ammonium acetate (NH₄OAc) and 200 ppm sodium azide as the mobile phase with a flow rate of 0.50 mL/min. An inline 25 mm Millipore filtration device (Millipore Corporation, Bedford, MA) was installed between the pump and injector equipped with a Millipore 0.10 μ m 25 mm Durapore[®] membrane filter. Data were collected by the Wyatt Technology Corporation Dawn Enhanced Optical System (DAWN-EOS) (Santa Barbara, CA) and the Waters 2410 refractive index detector (Milford, MA) directly after the SEC column. The DAWN-EOS ($\lambda = 690$ nm) was calibrated by the manufacturer and normalized with bovine serum albumin monomer (Sigma #A1900, St. Louis, MO, A1900) in 0.10 M ammonium acetate

with 200 ppm sodium azide. The Waters RI detector was calibrated using the RICAL v.5.90 software package (Wyatt Technology Corporation) with known concentrations (0.10-1 mg/ml) of NaCl in water using the specific refractive index increment (dn/dc) value of 0.172 ml/g. Data collection and processing were performed by the Astra v.4.90 software package (Wyatt Technology Corporation) utilizing the Zimm math fit analysis.

The dn/dc value of purified AvP was measured with a Wyatt Technology Corporation Optilab DSP interferometric refractometer which was calibrated by the manufacturer. A series of AvP solutions (0.10-1 mg/ml) in 0.10 M ammonium acetate with 200 ppm sodium azide were passed through the Optilab DSP flow cell with a Razel Model A-99 syringe pump (Razel Scientific Instruments, Inc., Stamford, CT) at a flow rate of 0.5 ml/min. The DNDC software package v.5.90 (Wyatt Technology Corporation) was used to process the data and to determine a dn/dc value of 0.149 ± 0.001 ml/g.

Solution Studies

Dilute solution properties have been studied in order to determine the inherent stiffness of the polysaccharide chain under a range of aqueous salt conditions. Relationships between intrinsic viscosity, zeta potential, turbidity and salt conditions are used to determine the extent of intra- and intermolecular interactions in solution. Information concerning intermolecular interactions within concentrated solutions has been obtained by examining zero shear viscosity, steady state fluorescence and dynamic oscillatory rheology.

Dilute Solutions. AvP solutions were prepared for rheological studies by dissolving the polymer sample in DI water overnight to prepare stock aqueous solutions. Stock solutions for intrinsic viscosity studies were made in DI water at a concentration of 1 mg/mL with dilutions ranging from 0.01 mg/mL to 0.80 mg/mL being tested. In the case of studies involving salts, stock polymer solutions were made at 2 mg/mL in DI water and adjusted to the final polymer and salt concentrations via dilution with stock salt solutions. Samples were placed on an orbital shaker at low rpm for at least 1 hr prior to measurement. A pKa value of 3.7 for AvP3 in aqueous solution was determined via potentiometric titration. The pH values of all test solutions were 6.4 to 7.0 resulting in a maximum degree of ionization for the polymers.

Apparent viscosities were determined for dilute solutions (0.01 - 0.80 mg/mL) using a Contraves LS-30 low shear rheometer at a shear rate of 5.91 sec^{-1} , fitted with bob and cup geometry. Reduced and inherent viscosities were calculated for each polymer concentration. Extrapolation to zero polymer concentration provided a value of intrinsic viscosity.

Zeta potential was measured using Malvern Instruments Zetasizer Nano Series equipped with an autotitrator in zeta cells purchased from Malvern Instruments. Starting polymer concentrations were 1.0 mg/ml, which is within the dilute regime of the polymer. Stock salt solutions of 1.0 M were used as titrants in order to minimize the change in polymer concentration as a function of added titrant. Solution pH was maintained at approximately 6.4 throughout the tests.

In order to determine the stability of AvP in aqueous solutions containing monovalent salts, turbidity was monitored *via* measurement of absorbance at 410 nm, and

phase diagrams were constructed. Stock polymer (4 mg/mL) and NaCl (0.40 M) solutions were dissolved overnight in deionized water containing 5 ppm sodium azide. Samples were prepared at appropriate polymer/ionic strength combinations in a 96 well plate using a Biomek FX liquid handler system. High throughput analysis was conducted using a Tecan Sapphire dual fluorescence and UV-vis detector. Turbidity at 25°C was measured at 1 h time intervals. Phase diagrams were constructed from approximately 96 data points utilizing the mesh feature of DPlot software version 2.1.3.8. Results were confirmed *via* visual monitoring of separate solutions prepared in 15 mL scintillation vials.

Concentrated Solutions. Steady state stress sweeps (0.01 - 100.0 Pa) were conducted using a Rheometrics SR-5000 controlled stress rheometer equipped with 40 mm cone and plate geometry (cone angle 2.25°) with a 0.05 mm gap setting, on semi-dilute and concentrated samples (1.0 - 20.0 mg/mL).

Fluorescence emission (400-620 nm) of 1,8-Anilino-1-naphthalene sulphonic acid (1,8-ANS) was monitored at an excitation wavelength of 360 nm on a Photon Technology International spectrometer. A 20 mg/mL aqueous polymer solution was used to prepare samples ranging from 0.10 to 15 mg/mL. An 8 mM stock solution of 1,8-Anilino-1-naphthalene sulphonic acid (1,8-ANS) was prepared in phosphate buffer (pH 7.1) and added to the samples to provide a final 1,8-ANS concentration of 0.20 μ M. The samples were placed on an orbital shaker 24 hrs prior to measurement.

Hydrogel Studies

The nature of AvP gelation in the presence of calcium ions has been examined in order to determine relationships between hydrogel characteristics and the release of protein therapeutics. Experiments have been design to simulate *in situ* gelation of AvP upon contact with physiological solutions, which will be important to the delivery of proteins in nasal and subcutaneous environments. Dynamic rheology, pulse field gradient nuclear magnetic resonance and optical microscopy have utilized to probe the nature of both the polymer rich network and aqueous pores within the hydrogel.

Mold Design & Gel Formation. Several mold designs were utilized to form hydrogels upon exposure to an external calcium ion source. The first mold utilized three stainless steel plates, containing four 45mm thru holes. Cellulose membranes (M_w cutoff 6-8 kDa) were sandwiched between the first and second plates as well as the second and third plates; this created a cavity in which AvP solutions could be held and exposed to Ca^{2+} via submersion in an aqueous $CaCl_2$ bath. While this mold provided formation of very uniform gels, due to the size of the mold it was necessary to utilize large volumes of $CaCl_2$ solution making the examination of hydrogel properties at specified Ca^{2+} to COO^- ratios difficult.

A second iteration allowed for lower volumes of $CaCl_2$ solution to be employed for gelation. The mold consisted of an upper and lower reservoir, in which 5 mL of AvP solution (1-8 mg/mL) was placed in the lower reservoir. This reservoir was then covered with 6-80 kDa M_w cutoff dialysis tubing (Spectra/Por), and 5 mL of the desired $CaCl_2$ solution (3-50mM) was gently pipetted into the latter. Diffusion of Ca^{2+} from the upper to

lower reservoir initiated hydrogel formation. Experiments were conducted to determine the CaCl_2 exposure time necessary to reach equilibrium gel strength and unless otherwise stated hydrogels presented within this dissertation were given 24 h to ensure that equilibrium conditions were reached.

Dynamic Oscillatory Rheology. Oscillatory dynamic rheological experiments were conducted using an Ares-G2 stress controlled rheometer equipped with a 40 mm crosshatched parallel plate and a Rheometrics SR-5000 equipped with a 45 mm serrated parallel plate. Experiments utilized a stress of 0.50 Pa at a frequency of 1 Hz, which was determined to be within the linear viscoelastic regime of AvP hydrogels. All gels were tested at 25°C after compression to a normal force of 0.30 N and a 1 minute equilibrium time, during which stress relaxation occurred and the measured normal force was approximately zero.

Pulse Field Gradient Nuclear Magnetic Resonance. AvP hydrogels were prepared directly in NMR tubes. 30 μL of AvP solution (0.20 or 0.60 wt%) was placed in a 5mm NMR tube, to which 30 μL of the appropriate CaCl_2 solution was added. Gels were given 24 h to reach equilibrium prior to NMR analysis. Sample volumes were kept at 60 μL in order to optimize signal to noise ratios during the pulsed field gradient (PFG) experiments. All spectra were obtained with a Varian Unity Inova 500 MHz spectrometer using a standard 5 mm 2 channel probe equipped with gradients. The standard Stejskal-Tanner sequence (acquisition time of 0.5 s, a recycle delay of 5 s, and gradient pulses of 0.8-1.0 ms) was utilized in the PFG-NMR experiments to determine the time-dependent

diffusion coefficient of water (D_{app}). The self-diffusion coefficient of water was determined from the negative slope of a log-attenuation plot ($\log \psi$ versus $\gamma^2 g^2 \delta^2 (\Delta - \delta/3)$), where ψ is the echo attenuation, γ is the proton gyromagnetic ratio, δ is the width of the gradient pulse, g is the magnitude of the applied field gradient, and Δ is the total diffusion time. The total diffusion time was varied from 20 to 500 ms and the gradient amplitude ranged from 20 to 80 G/cm to ensure the signal was attenuated $\sim 80\%$. The spectral width was 50 kHz and the number of scans for each spectrum ranged from 8-32. Exponential line broadening was applied prior to Fourier transformation of the FIDs. Gradient calibration was performed using a deionized water standard prior to data collection.

Microscopy. Bright field and fluorescence images were obtained on a Nikon Eclipse 80i microscope and images were processed utilizing NIS-elements *f* software. Thin hydrogel samples were prepared directly on cleaned glass slides in the following manner; 60 μ L of AvP solution was pipetted onto a slide and spread into a thin film ($\sim 15 \mu$ m) utilizing a doctor blade. The edge of the AvP film was exposed to CaCl_2 solution and subsequent diffusion of Ca^{2+} initiated gelation. Samples were stained with 0.10 wt% ruthenium red which has been shown to effectively stain pectins.⁶⁵

Release Studies. Fluorescein labeled 4 and 500 kDa M_w dextrans (Dex4, Dex500) were purchased from Sigma-Aldrich and utilized as model compounds in controlled release experiments. In order to minimize photo-bleaching, release experiments involving fluorescein labeled dextrans were performed in a dark room under red light. Stock AvP and FITC-dextran solutions were dissolved overnight and combined to yield 4 stock

solutions at AvP concentrations of 6 and 2 mg/mL and a FITC-dextran concentration of 0.10 mg/mL (6AvP-Dex4, 6AvP-Dex500, 2AvP-Dex4, 2AvP-Dex500). All AvP/FITC-dextran solutions included 0.05 M NaCl. All experiments were conducted in triplicate (standard deviations averaged 5% and were used to create error bars). Samples were prepared in 1.5 mL microcentrifuge tubes and contained 0.5 mL of AvP-Dex solution. In order to create a consistent interface between the AvP-dextran solution and the release medium, a Teflon® grid with a macroscopic grid opening (1 mm x 0.635mm) (McMaster-Carr) was placed on top of the AvP-Dex solution. Next, 1 mL of a simulated nasal fluid (SNF); 10 mM Tris, 0.15 M NaCl, 0.04 M KCl and 5 mM CaCl₂ was added. Subsequent diffusion of Ca²⁺ into the AvP/FITC-dextran solution initiated crosslinking, and release of the FITC-dextran into the SNF solution was monitored. 500 µL aliquots were taken at various time intervals and replaced with fresh SNF.

The fluorescence emission (510-600 nm) of FITC-dextran present in aliquots was measured at an excitation wavelength of 495 nm on a Photon Technology International spectrometer. After 4 days the release experiment was halted. In order to determine the amount of free dextran remaining in the gels, gels were suspended in fresh SNF within 1.5 mL microcentrifuge tubes and centrifuged for 2 min at 1000 rpm. The solutions were collected and fluorescence emission was measured. To determine if FITC-dextran was permanently entrapped within the calcium hydrogels, the gels were dissolved in a 0.5 M EDTA solution overnight, and fluorescence of the resulting solutions was measured. Calibration curves were constructed for both FITC-dextran as well as FITC-dextran/polymer solutions and separate experiments were conducted in order to ensure

that the concentration gradient present in the system maintained a sufficient driving force for diffusion into the release medium throughout the experiment.

Curve fitting was performed using the non-linear curve fitting tool from Origin software (version 7.0383). Additional analysis of the squared sum of residuals (SSR) between experimental data and theoretical data was conducted in order to determine the goodness of fit for each diffusion model. SSR values were substituted into the Akaike Information Criterion (AIC) defined as;

$$AIC = N(\ln SSR) + 2p \quad (1)$$

where N accounts for the number of data points being compared and p represents the number of variables used in model fitting. The best fit is represented by the lowest value of AIC.⁹⁴

CHAPTER IV

RESULTS AND DISCUSSION

STRUCTURAL CHARACTERIZATION AND SOLUTION PROPERTIES OF A
GALACTURONATE POLSACCHARIDE DERIVED FROM *ALOE VERA* CAPABLE
OF *IN SITU* GELATION

Overview

A growing understanding of human biochemistry along with the implementation of combinatorial methods has led to an expanding library of peptides and proteins that possess therapeutic benefits. However, limitations including stability throughout storage, degradation upon administration *in-vivo*, and post administration efficacy have limited the application of protein therapeutics.¹⁵ These issues are not only related to the inherent stability and efficacy of the therapeutic agent but are also related to the delivery route and delivery system utilized for treatment. For instance, only 0.1% of orally dosed insulin reaches the bloodstream intact, making administration of the protein through injections a current necessity. Injections are often painful and lead to poor patient compliance.⁹⁵ Additionally, it has been found that effective intramuscular injection of a developmental H5N1 vaccine requires dose serum antibody levels 12 times that of seasonal flu vaccines, a level which would strain current antibody production.⁹⁶

Nasal administration routes offer many advantages, including ease of administration and activation of an additional mucosal immune response within the nasal cavity, which has been shown to increase the efficacy of antibodies.¹⁴ However, challenges must be addressed within nasal administration routes. Of primary concern is

adhesion to the mucosal lining within the nasal cavity. Current formulations involved in nasal delivery yield a clearance half life of only 15 minutes when administered onto human epithelium.⁹⁷ Natural polysaccharides including hyaluronic acid⁹⁸ and chitosan¹⁶ have been incorporated into protein therapeutic formulations in order to improve the efficacy of delivery. In addition to the aforementioned biopolymers, pectins are receiving renewed attention in the drug delivery field.⁸⁴ Discussed in this manuscript is a galacturonate polysaccharide derived from *Aloe vera* that possess the requisite properties amenable to nasal drug delivery.

Pectins are a class of anionic polysaccharides that have been widely studied for use as food additives^{82, 99}, and in pharmaceuticals as tablet binders for oral and colonic drug delivery.⁸⁹ Pectins are comprised primarily of (1→4) α -D-galacturonic acid (GalA) repeat units with intermittently (1→2) linked rhamnose residues acting as branch points for neutral sugar side chains (Figure IV-1). The GalA units may be present in the acid form or may exist as methylesters with the degree of methylester substitution (DM) affecting the extent of gel formation in the presence of multivalent ions such as calcium.⁵⁷

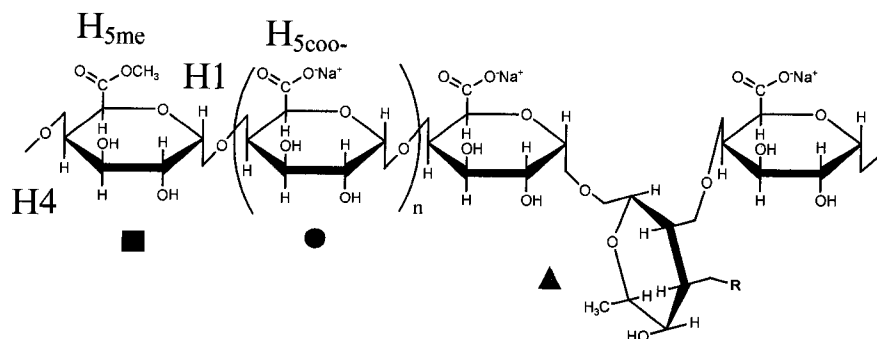


Figure IV-1. General structure of AvP including galacturonic acid units with methyl esters (■), galacturonic acid sodium salt form (●), rhamnose (▲), and neutral sugar

branches (R) with proton designations H1,H4, H5_{me}, and H5_{coo-} used to label H¹ NMR spectra.

There are a variety of intrinsic and extrinsic parameters which have been reported to affect the solution properties and subsequent gelation of pectins with low DM values; from these studies many conclusions, some of them contradictory, have been drawn.^{66-70, 100-109} However, the consensus is that key intrinsic parameters include molecular weight, the respective GalA, rhamnose and neutral sugar composition, as well as the DM. Pectins with a low DM value contain large numbers of “free” GalA carboxylate units which are responsible for gelation upon addition of divalent cations. Although it is still the subject of some debate,^{78, 110} the gelation mechanism of low DM pectins has been shown to involve the formation of “egg box” junction zones between carboxylate GalA units and divalent cations.^{71, 75} It has been further shown that formation of elastically active junction zones within pectin gels requires a minimum of ~ 7 adjacent GalA units and that the sensitivity of pectins to calcium ions increases as the DM decreases.^{59, 111}

Considering the importance of fundamental understanding in the development of effective delivery systems and the potential incorporation of pectins into protein and vaccine delivery formulations we have undertaken a thorough examination of an *Aloe vera* pectin. In this study we report the chemical composition, solution properties in dilute and concentrated regimes, and calcium ion sensitivity of a newly discovered *Aloe vera* polysaccharide (AvP) extracted from the *Aloe vera* plant. The percent composition of GalA units, the DM, and rhamnose/neutral sugar content have been determined along with relevant molecular parameters such as molecular weight. Dilute solution properties have been studied in order to determine the inherent stiffness of the polysaccharide chain under a range of aqueous salt conditions. Information regarding intra and intermolecular

interactions has been obtained by examining zero shear viscosity and steady state fluorescence as a function of polymer concentration and determining the zeta potential at various salt concentrations. Finally, the dynamic moduli of gels formed at low polymer and calcium ion concentrations have been examined. The solution and rheological properties intrinsic to AvP, which have not been previously reported in the literature, indicate the potential utility of this polysaccharide in drug delivery applications.

Chemical Composition

The chemical compositions of five *Aloe vera* pectin (AvP) samples are shown in Table IV-1. Samples AvP1 - AvP4 represent separate extractions and subsequent purifications from the rinds of the *Aloe vera* plant. AvP5 is a hydrolyzed version of AvP3. Samples are listed in order of descending molecular weight ranging from 523 kDa to 200kDa.

Table IV-1. Chemical composition and physical parameters of *Aloe vera* polysaccharide (AvP).

Pectin	Mw ^a (kDa)	PDI ^a	Rg ^a (nm)	GalA ^b	Rha ^b	Man ^b	Gla ^b	Ara ^b	Glu ^b	Fuc ^b	Xyl ^b	DM ^c	DM ^d
AvP1	523	1.62	115	95.8	0.46	2.02	1.04	0.31	0.19	0.16	0.06	6	5.3
AvP2	435	1.58	103	94.5	0.49	2.4	1.39	0.53	0.41	0.17	0.12	3	5.3
AvP3	405	1.53	96.8	96.9	0.54	1.23	0.48	0.43	0.11	0.16	0.1	4.7	2
AvP4	330	1.51	86.7	98	0.52	0.32	0.46	0.39	0.06	0.18	0.12	4.5	5.8
AvP5 ^e	200	ND ^f	ND ^f	97.1	0.33	1.37	0.69	0.15	0.16	0.14	0.08	ND ^f	4.7

a) Obtained from SEC-MALLS

b) Listed as percent of total carbohydrates

c) Listed as mole percent of GalA

d) Listed as mole percent of GalA as determined by ¹H NMR

e) Sample prepared from AvP3 via hydrolysis

f) Not determined

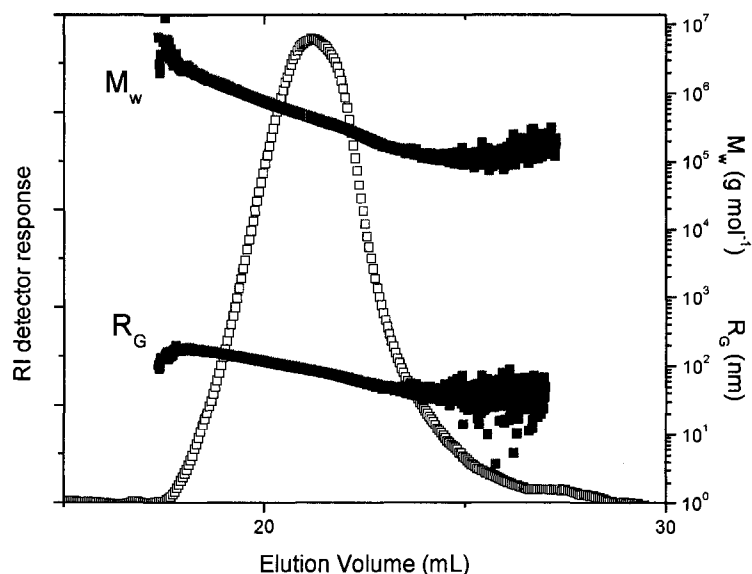


Figure IV-2. SEC-MALLS trace of AvP1 including molecular weight (M_w) and radius of gyration (R_g) analysis.

The molecular weight (M_w) and R_g were determined by aqueous SEC using multi-angled laser light scattering (MALLS) and refractive index detection. An example chromatogram (Figure IV-2) depicts the RI trace versus elution volume and the values of M_w and R_g that correspond to each slice of the chromatogram (Further Figures are included in Appendix A). For a series of alginates the profile of M_w and R_g vs. elution volume has been shown to be related to the state of aggregation within the sample where a non-linear profile was obtained when aggregation was evident.¹¹² The M_w and R_g relationships for AvP are linear as a function of elution volume, indicating that the pectins chains are well dispersed under the SEC conditions employed. The SEC-MALLS data provides facile analysis of the R_g/M_w relationship (Equ. 1).

$$R_g = kM^p \quad (1)$$

Using the data shown in Figure IV-2 for AvP1 plotted as R_g vs. M_w (Figure IV-3),

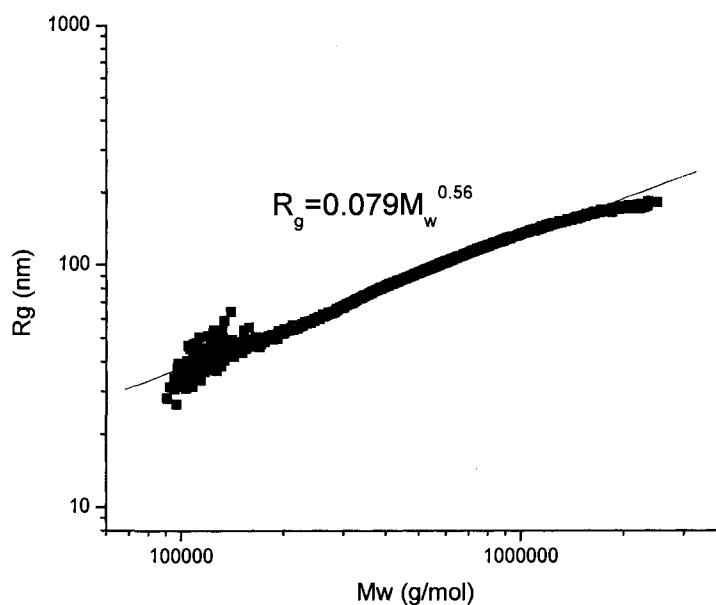


Figure IV-3. SEC-MALLS trace of AvP1 depicting radius of gyration (R_g) as a function of molecular weight (M_w).

the R_g/M_w relationship is linear and has been found to fit the following equation;

$$R_g = 0.079M_w^{0.56} \quad (2)$$

Similar k and ρ values, 0.033 and 0.61 respectively, are calculated when the individual M_w and R_g values obtained for AvP1-AvP5 (Table IV-1) are used to examine the M_w/R_g relationship. The agreement between ρ values calculated via these two methods suggests that the polydispersity of the AvP samples does not significantly affect the analysis of R_g .

It is important to note that the M_w values are 2 to 10 times higher than typical values reported in literature for LM pectins (low degrees of methyl esterification).^{57, 106, 109} In addition to being a high molecular weight pectin, AvP contains a very high percentage of GalA residues. On average 95% of the total carbohydrate content of AvP is galacturonic acid. LM pectins extracted from traditional plant sources (citrus, apple and

sunflower) have GalA contents ranging from 60 to 85%,^{14, 57} with the remainder of the carbohydrate content being reported as short branches of neutral sugars such as arabinose, galactose, and mannose whose branch points originate at rhamnose. AvP has less than 1% rhamnose and a total of 5% neutral sugars suggesting a structure primarily composed of long GalA blocks with very few neutral sugar branches. Of the GalA units present in previously reported pectins, 30 to 40% typically exist as methylesters,^{53, 66, 106, 113} with chemical de-esterification methods often resulting in undesired reductions in molecular weight.⁵⁷ As determined through GPC-Mass spec techniques, 3 to 5% of the GalA units in AvP exist as methyl esters.⁵⁹

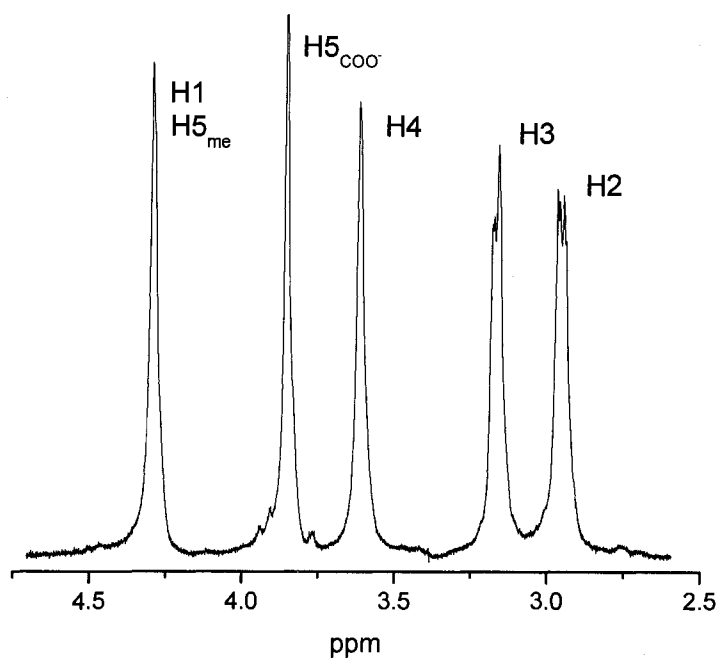


Figure IV-4. ¹H NMR spectrum of AvP3, obtained using HOD suppression techniques on a 500 MHz NMR spectrometer.

Utilizing ^1H NMR techniques, the ratio of protons at C5 adjacent to methyl esters ($H5_{me}$) and those adjacent to carboxylic acids ($H5_{COO^-}$) may be determined.¹¹⁴⁻¹¹⁷ Integrating the spectrum obtained for each sample (Figure IV-4 and Appendix A) and utilizing Equation 3 results in DM values ranging from 2-5.8%, which are in reasonable agreement with the results from GPC-Mass spectrometry.

$$DM = \frac{\int (H1 + H5_{me}) - \int H5_{COO^-}}{\int (H1 + H5_{me}) + \int H5_{COO^-}} \quad (3)$$

Physical Characteristics in Dilute Solution

Using the Huggins and Kraemer relationships, the intrinsic viscosity of each AvP sample was determined (Table IV-2).

Table IV-2. Intrinsic viscosity (η) as a function of AvP sample and salt concentration with calculated values of intrinsic viscosity at infinite ionic strength (η_{inf}), the flexibility parameter B and the persistence length (L_p) at 0.10 M NaCl and infinite ionic strength. Additional L_p values calculated using Bohdanecky method are provided for each M_w/η relationship at the specified ionic strength.

	Intrinsic Viscosity, η (dL/g) at specified NaCl Concentration (M)				η_{inf} (dL/g)	$B_{0.10}$	$L_{p0.10}^a$ (nm)	$L_{p,inf}^a$ (nm)
	0.05	0.10	0.15	0.2				
AvP1	19.8	18.0	17.0	15.9	12.5	0.043	16	11
AvP2	16.9	15.2	14.5	14.0	11.1	0.041	15	12
AvP3	16.2	15.0	14.0	14.2	11.8	0.032	16	12
AvP4	13.1	11.6	11.4	11.2	9.1	0.039	15	11
AvP5	9.4	9.0	8.2	8.0	6.6	0.040	17	12
L_p^b (nm)	14	11	12	8.8				

a) Obtained from Yamakawa-Fuji analysis

b) Obtained from Bohdanecky analysis

A representative Huggins-Kraemer plot is illustrated in Figure IV-5, (plots for each sample are found in Appendix A) where the linear fits represent the well known Huggins and Kraemer equations respectively. It can be seen that there is no significant curvature in the plot, suggesting that AvP aggregation is not occurring as a function of polymer or salt concentration over the time scale of these measurements. Huggins constants (k') vary from 0.36 - 0.48 in 0.05 M NaCl to 0.54 - 0.74 in 0.20 M NaCl.

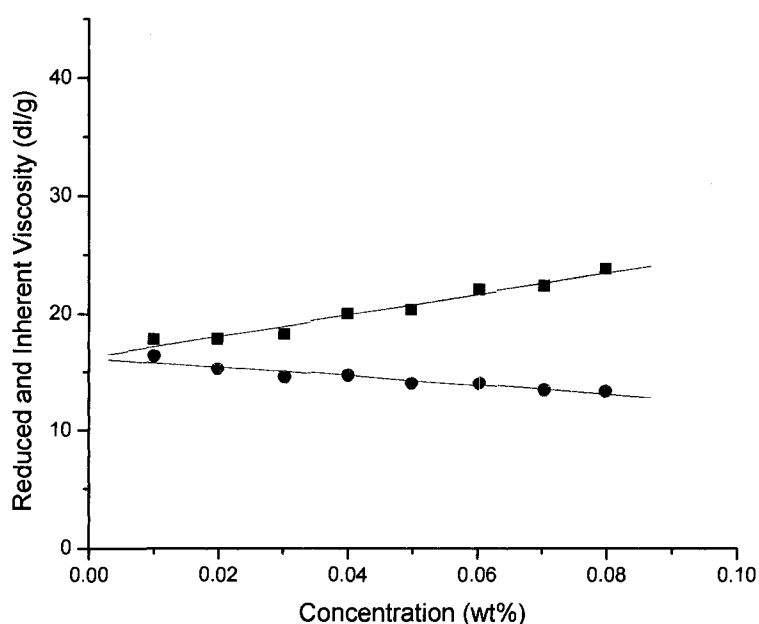


Figure IV-5. Determination of intrinsic viscosity from Huggins (■) and Kraemer (●) plots, illustrated for AvP3 in 0.10 M NaCl.

It is worth noting that at NaCl concentrations of 0.20 M, AvP solutions are not stable indefinitely and coagulates begin forming within a 24 hr time period. Huggins-Kraemer plots of AvP solutions aged for 24 hr (Appendix A) exhibit significant curvature and result in Huggins constants ranging between 4.5 and 5.9. This behavior has been often reported for colloidal systems.¹¹⁸⁻¹²⁰ Our results are further supported by the zeta potential values reported later in Figure IV-8, which suggest the likelihood of coagulation

at extended times. From these experiments and observations of initial solubility, followed by coagulation, it may be hypothesized that AvP dissolved in 0.20 M NaCl solution is in a regime of phase separation controlled by spinodal decomposition, similar to that observed for the phase separation of thermo-associative polymers.¹²¹

Utilizing Equation 4, experimentally determined values of intrinsic viscosity may be plotted versus molecular weight obtained from SEC-MALLS (Figure IV-2), resulting in the Mark-Houwink-Sakurada (MHS) plot shown in Figure IV-6.

$$\eta = KM^a \quad (4)$$

Determination of the MHS parameters K and a provides information regarding the conformation of the polysaccharide in solution. Pectins from various plant sources exhibit a wide range of a values including those that suggest rigid coils, worm-like chains and rod-like chains.^{57, 82, 99, 101-103, 109} The values of a determined for AvP at NaCl concentrations from 0.05 to 0.20 [M] range from 0.72 to 0.77 suggesting that AvP exists in solution as an expanded random coil. K values ranged from 1.0-1.15 further supporting the presence of an expanded conformation.

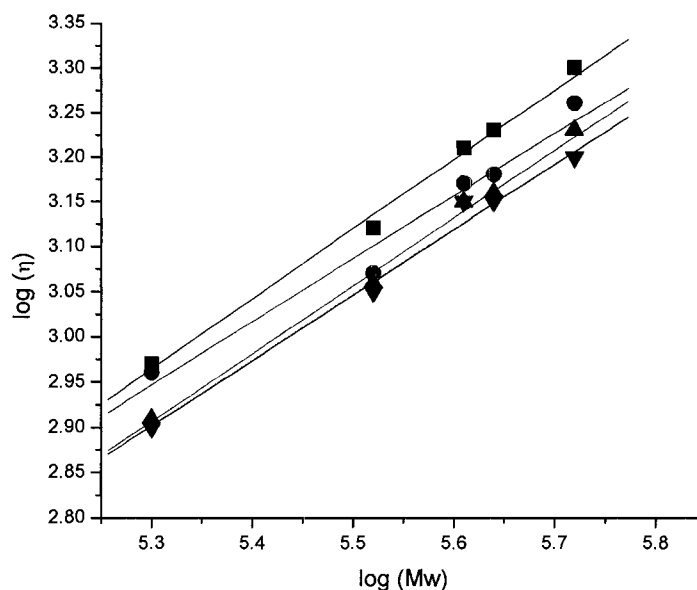


Figure IV-6. Determination of MHS parameters α and K from a double logarithmic plot of intrinsic viscosity and molecular weight at various NaCl concentrations 0.05 (■), 0.10 (●), 0.15(▲), 0.20 (▼).

The values of ρ (0.56-0.61) and a (0.72-0.77), from the R_g/M_w and $[\eta]/M_w$ relationships are related by the following equation,^{122, 123}

$$a = (3 \times \rho) - 1 \quad (5)$$

Using this equation it can be seen that the a values determined by intrinsic viscosity are in good agreement with the ρ values obtained from SEC-MALLS.

Additionally, the a values are consistent with those reported in literature for other high molecular weight polysaccharides, where it has been found that the $[\eta]/M_w$ relationship is not linear over a broad range of molecular weights.¹⁰⁴ This can be further understood by examining the calculated persistence lengths (L_p) of a wormlike pectin chain. Applying the Yamakawa-Fujii iterative method of calculating the Flory parameter (Φ) and the persistence length (Eq. 6), the persistence length of AvP specimens were obtained.¹²⁴

$$[\eta] = \frac{\Phi_{\infty} L^{3/2}}{M} \frac{1}{1 - \sum_{i=1}^4 C_i L^{-i/2}} \quad (6)$$

The coefficient C_i is stated to be independent of the length of the monomeric repeat unit (l_0) and dependent on the diameter of the chain (d). Solutions for the four values of C_i are determined by the method of least squares and are included in the original work of Yamakawa and Fujii. Values of d and l_0 were taken from previous literature regarding pectins and used in our analysis. X-ray diffraction studies have revealed d values between 6 and 8 Å and reported 4.35 Å for the value of l_0 .¹¹⁸ Additionally, the molecular weight of the GalA repeat unit without methyl esters in the sodium salt form (198 g/mol) was used. Obtaining results for the persistence length via the original Yamakawa-Fuji analysis, requires iteration of Φ and L_p , the final values of the Flory parameter were approximately 1.30×10^{23} and L_p values for each AvP sample are listed in Table IV-2.

Values obtained via the original Yamakawa-Fuji analysis for AvP samples in 0.10 M NaCl range from 15 to 17 nm. These values are slightly larger than those obtained in previous literature, for related polysaccharides (5.9-12.6 nm).^{102, 104, 105, 125-130} The persistence lengths determined for AvP may be larger due to variations in the method of calculating L_p , various calculation methods may be applied and each has certain limitations as is discussed throughout literature.¹²⁷⁻¹³⁰ Specific limitations of the Yamakawa-Fuji approach include the assumption that excluded volume is negligible and the reliance on Φ which is molecular weight dependent. For comparison L_p was also calculated using the modified Yamakawa-Fuji method as proposed by Bohdanecky¹²⁹ and outlined in the work of Mendichi *et. al.*¹³⁰. In the original work of Bohdanecky excluded volume is again neglected, however, it has been shown that an expansion factor α_{η} may

be utilized. Using a value of $0.71 \text{ cm}^3/\text{g}$ for v for pectic acid in salt¹³¹ and setting $M_L = M_w/L$ where L is contour length, values of L_p , M_L and α_η the expansion factor for intrinsic viscosity were determined for AvP at ionic strengths ranging from 0.05 to 0.20 M (Table IV-2). As the ionic strength increases the calculated L_p values decrease from 14 to 8.8 nm. Further details concerning the Mathcad programs written to perform L_p calculations are included in Appendix A.

The large L_p values are most likely related to AvP's high percentage of non-esterified GalA units which provide an inherent high charge density, causing electrostatic repulsion and a rigid conformation. This is supported by the L_p values of 20-25 and 67 Å determined by Hourdet and Muller for pectins with low GalA content and homogalacturonan, respectively¹⁰⁵, and the calculated value of $300 \pm 50 \text{ Å}$ predicted by Monte Carlo simulations for a fully charged polygalacturonic acid chain in water.^{132, 133}

The electrostatic contribution to persistence length may be estimated using a variety of theoretical models^{127-130, 133}. Additionally, the electrostatic contribution may be taken into account by utilizing the intrinsic viscosity at infinite ionic strength ($[\eta_{\text{inf}}]$).¹¹² In this method $[\eta_{\text{inf}}]$ replaces $[\eta]$ in Yamakawa-Fuji L_p calculations in order to arrive at the intrinsic persistence length, or the persistence length in the absence of electrostatic effects. When $[\eta_{\text{inf}}]$ is substituted into the Yamakawa-Fuji analysis the calculated values of L_p ranged from 11-13 nm (Table IV-2), which are in good agreement with the Bohdanecky values obtained at higher ionic strength (0.10- 0.20 M).

The persistence length is determined by the inherent properties of a monomeric repeat unit and is defined as the end-to-end distance of a polymer segment (composed of n monomers) in which monomers M_n and M_{n+1} are located at related points in space, e.g.

the monomers in the segment possess persistence.¹³⁴ Alternatively, L_p can be defined as the segment length at which the orientation of two successive polymer segments no longer exhibit correlation.^{123, 135} With this definition, a wormlike chain may be assumed to behave as an ideal coil of a bond length $2L_p$.¹³⁶ For example, AvP in 0.05 M NaCl has a persistence length of 15 nm and a Kuhn length ($2L_p$) of 30 nm, equivalent to approximately 70 GalA repeat units. While the polymer may be rigid at the length scale of the persistence length, if the number of repeat units in the AvP1 chain is greater than 70 (corresponding to an M_w of approximately 14,000 g/mol) the behavior of the chain in solution will resemble that of a random coil. This is observed upon examination of intrinsic viscosity behavior as a function of molecular weight; the number of repeat units in each of the AvP samples corresponds to a molar mass much greater than 14,000 g/mol, resulting in MHK a values indicative of expanded random coil behavior in solution.

Physical Characteristics as a Function of External Stimuli. In order to further probe the effects of electrostatic repulsion on the conformation of AvP in solution, the intrinsic viscosity was studied as a function of salt concentration. Figure 6, depicts the respective intrinsic viscosity values obtained for AvP samples in NaCl solutions. The data show a clear reduction in viscosity as the ionic strength of the medium is increased, suggesting a reduction in hydrodynamic volume of the polymer as the electrostatic repulsions between GalA units are screened. The extent of polyelectrolyte contraction from an extended conformation, where charge repulsion is an important contributor, to the random coil conformation of an equivalent uncharged polymer is dependent upon the inherent stiffness of the polymer. The parameter B has been established by Smidsrød and

Haug as a simple means of describing the relative stiffness of a polyelectrolyte based on the reduction in intrinsic viscosity as a function of ionic strength.¹³⁷

By constructing a plot wherein the intrinsic viscosity is extrapolated to infinite ionic strength ($[\eta]_{\infty}$), and utilizing the value of intrinsic viscosity at a given ionic strength (0.10 M, $[\eta]_{0.10}$) a linear relationship (Eq. 7) can be found in which the slope of the line (S) relates to the inherent stiffness of the polymer (B).

$$[\eta]_I = [\eta]_{\infty} + B[\eta]_{0.10}^{\nu} (I^{-1/2}) \quad (7)$$

Polymers with greater flexibility exhibit a greater reduction in hydrodynamic volume; hence larger slopes are obtained.

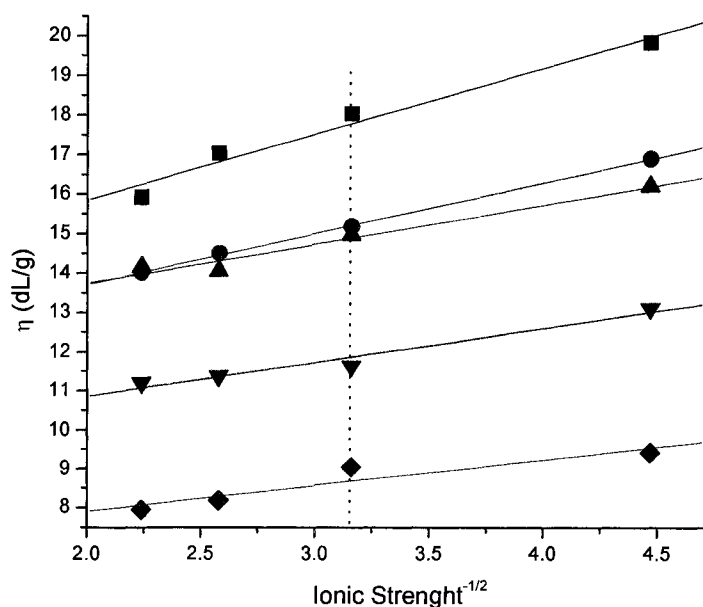


Figure IV-7. Plot of intrinsic viscosity (η) as a function of the inverse square root of ionic strength depicted for AvP1 (■), AvP2 (●), AvP3 (▲), AvP4 (▼) and AvP5 (◆) dissolved in various NaCl solutions. The vertical dashed line indicates $[\eta]_{0.10}$ the value used in determination of the flexibility parameter B .

Inserting the slopes (S) determined from Figure IV-7 and the intrinsic viscosity measured in 0.10 M NaCl concentration into Equation (8) yields the stiffness parameter B which is reported in Table IV-2 for each AvP sample.

$$B = \frac{S}{([\eta]_{0.10})^\nu} \quad (8)$$

In the above relationships ν is the slope from a double logarithmic plot of S vs $[\eta]_{0.10}$ for a series of polyelectrolytes with varying molecular weight. As shown by Smidsrød, Haug and others, the parameter ν exhibits a small amount of variation as a function of polyelectrolyte species and a value of 1.3 is thus commonly employed when sufficient samples of various M_w are not available.⁶⁸ However, since samples of various M_w were available and a value of ν for pectins is not available from literature, ν was determined experimentally. A value of 1.27 was obtained. The values of B listed in Table IV-2 were calculated using the experimentally determined value of 1.27 for ν and are in agreement with the values obtained by Simdsrod and Haug for a series of pectins with various DM, indicating that AvP has an inherently stiff polymer backbone.

Table IV-3. Values of B reported in literature¹³⁷ representing polymers with inherently flexible (polyacrylate) and rigid (DNA) chain structures.

Polymer	Stiffness Value (B) at 0.10 M NaCl
Polyacrylate	0.47
Dextran Sulfate	0.23
Carboxymethylamylose	0.20
Gum Arabic	0.10
Hyaluronate	0.065
Alginate	0.04
Citrus Pectin	0.04
<i>Aloe vera</i> Pectin	0.032-0.043
DNA	0.0055

In addition to monitoring the screening of charges on a polyelectrolyte by assessing viscosity, one may measure the zeta potential of a charged molecule in solution. The zeta potential is defined as the electrical potential which exists at the hydrodynamic plane of shear surrounding a charged particle, and is essentially the potential at the point in space where low molecular weight ions cease to move with the particle and remain within the surrounding solvent. In cases where steric stabilization is not sufficient, electrostatic forces may help prevent intermolecular interactions from occurring. It has been found that particles with zeta potential values of magnitude greater than 30 mV result in stable aqueous solutions.¹³⁸ The relationship between zeta potential and salt concentration for AvP is depicted in Figure IV-8.

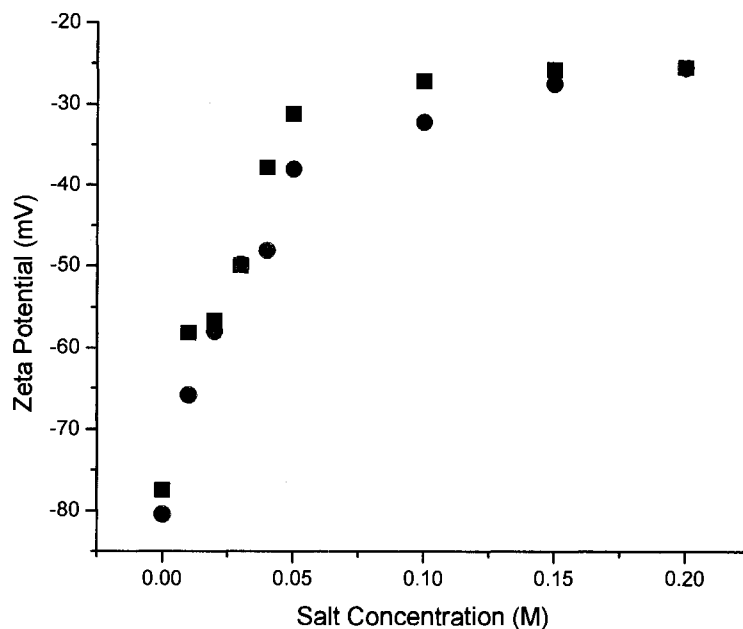


Figure IV-8. Zeta potential (mV) of AvP as a function of NaCl (■) and KCl (●) concentration (M), illustrated for AvP3 at 0.10 wt%.

It can be seen that at low ionic strength, the magnitude of the zeta potential is high (-80 mV) and as the ionic strength is increased, the magnitude of the potential decreases. At approximately 0.10 M salt concentration, the zeta potential reaches the point where intermolecular interactions may no longer be inhibited by electrostatic forces. This is further supported by observations of aggregation over time at ionic strengths greater than 0.10 M, as is discussed further in section B of the results and discussion (Phase Diagrams, Figure IV-20).

Transition from the Dilute to Concentrated Regime. In order to further investigate the transition from dilute solution, where intrapolymer interactions dominate, to the concentrated regime where interpolymer interactions occur, the zero shear viscosity was monitored as a function of AvP concentration in water and aqueous 0.10 M NaCl solutions (Figure IV-9). Zero shear viscosities were obtained from plots of specific viscosity as a function of shear rate and are included in Appendix A.

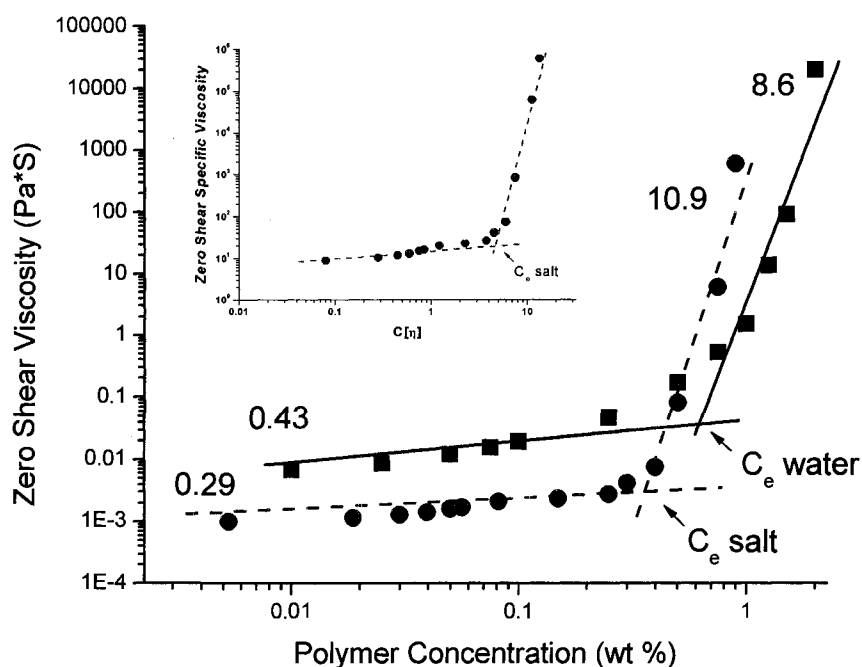


Figure IV-9. Determination of the critical entanglement concentration (C_e) for AvP3 in water (■), 0.60 wt% and 0.10 M NaCl (●), 0.37 wt% from a plot of zero shear viscosity vs. polymer concentration. Inset depicts zero shear specific viscosity vs. $C[\eta]$, for the 0.10 M NaCl series.

The critical entanglement concentration (C_e) for AvP in water is ~ 0.60 wt% while in salt it shifts to ~ 0.37 wt%. The shift in C_e agrees with the zeta potential measurements which suggest significant charge screening at a 0.10 M salt concentration, allowing the onset of intermolecular interactions.

The exponent in the dilute regime (0.43) of AvP in water is consistent with the theoretically predicted value (0.5) for polyelectrolytes above the critical overlap concentration C^* and below C_e . The exponent in the concentrated regime (8.6) is much higher than the value of 4.0 predicted by polyelectrolyte scaling theory. Scaling theory predicts polyelectrolyte behavior above C_e based on a model of electrostatic blob interactions in which the polymer behaves as a neutral, randomly coiled entity in the

entangled regime.¹³⁹ It is further noted that the values obtained for AvP are higher than reported values determined for hydrophobically modified polyelectrolytes,^{140, 141} although in some cases values as high as 9 have been observed.¹⁴² The inset depicts $\eta_{o,sp}$ vs. $C[\eta]$ for the 0.10 M NaCl series only, $[\eta]$ for a polyelectrolyte in water may be determined via a Fuoss approximation, and has been calculated as 59 dL/g for AvP. It is seen that the C_e transition occurs when $C[\eta]$ is much greater than unity.

In order to further investigate the nature of these abnormally high exponents, fluorescence emission of the fluorescent probe 1,8-ANS, which has been shown to be sensitive to hydrophobic microenvironments¹⁴³⁻¹⁴⁵, was monitored as a function of polymer concentration (Figure IV-10).

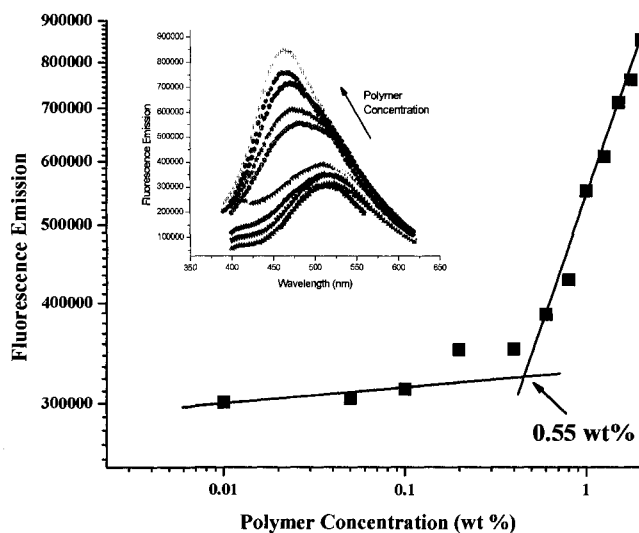


Figure IV-10. The maximum fluorescence emission of 1,8-ANS as a function of polymer concentration depicted for AvP3 in aqueous solution. Raw fluorescence data is depicted in the inset. A change in the slope is noted at 0.55 wt %, which corresponds to the C_e (0.60 wt%) of AvP3 in water shown in Figure IV-9.

A sharp rise in the fluorescence emission is noted at an AvP concentration of 0.55 wt% which corresponds to the C_e determined in aqueous solution. The high exponents noted in the concentrated regime and the increase in fluorescence intensity suggest that AvP may be involved in hydrophobic aggregation, possibly forming rod-like bundles or worm-like micelles at high concentrations in both water and salt solutions.¹⁴⁶

Hydrogel Studies

Initial dynamic rheology experiments have shown that AvP can gel in the presence of Ca^{2+} ions at concentrations as low as 0.89 mM. With gelation occurring at Ca^{2+} concentrations this low, sufficient calcium exists in bodily fluids to allow for *in-situ* gelling, an important characteristic in potential pharmaceutical applications. Attempts to study the gelation of AvP following literature procedures¹⁴⁶⁻¹⁴⁹ for traditional pectins have been unsuccessful. In previous literature, the pectin solution and the Ca^{2+} solution are prepared separately, heated at 70°C, mixed on a heated rheometer plate and cooled below the sol-gel transition to the desired test temperature. However, the sol-gel transition for AvP is above 90°C for all calcium concentrations studied. Therefore, to measure the evolution of moduli, a method was developed in our labs wherein AvP solutions are placed in the confines of the rheometer geometry and a small volume of $CaCl_2$ solution is introduced to a reservoir surrounding the sample while rheological measurements are made (see experimental section). A plot of the elastic modulus (G') measured in this manner is shown in Figure IV-11.

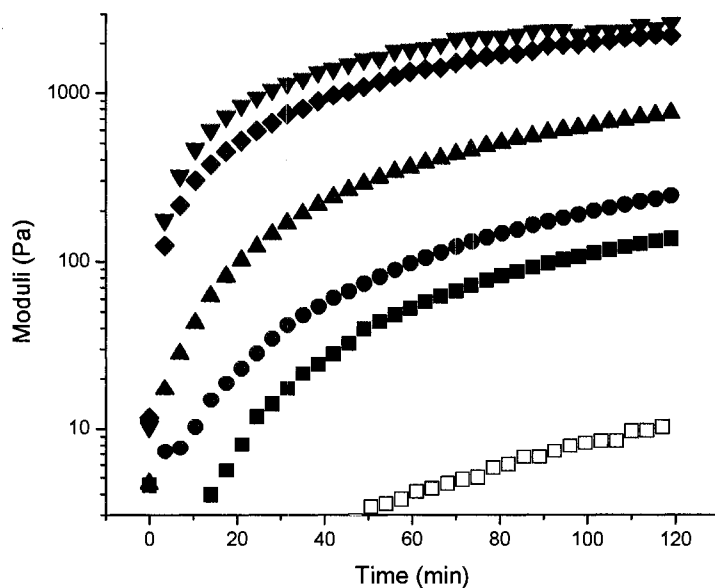


Figure IV-11. Evolution of elastic modulus (Pa) as a function of time for various calcium ion concentrations 0.87 (■), 1.75 (●), 2.79(▲), 5.59 (◆) and 8.38 (▼) mM and viscous modulus (Pa) for 0.87 (□) mM Ca^{2+} . Illustrated for AvP2 at 0.20 wt%.

For all Ca^{2+} concentrations studied, the viscous modulus (G'') is much less than the elastic modulus (G'), indicating that strong gels are formed. In order to confirm the *in-situ* results, additional experiments have been conducted on gels formed within a mold under 24 hr exposure to 0.80 and 8.0 mM CaCl_2 which display linear G' values as a function of frequency, G' equaled 300 and 1000 Pa, respectively. It is interesting to note that the elastic modulus values obtained for AvP (0.20 wt%, 2000 Pa) are approximately the same as those obtained for citrus pectins ($G' \sim 3000$ Pa) tested at higher polymer (2.0 wt%) and calcium concentrations (10 mM).^{56, 67, 150, 151}

TAILORING THE NETWORK PROPERTIES OF Ca^{2+} CROSSLINKED *ALOE VERA* POLYSACCHARIDE HYDROGELS FOR *IN SITU* RELEASE OF THERAPEUTIC AGENTS

Overview

Galacturonates, commonly termed pectins, are naturally occurring polyelectrolytes with characteristics especially amenable to controlled release applications.⁸⁴ These polysaccharides have also been widely used in the food industry^{62, 64} and are composed primarily of (1→4) α -D-galacturonic acid (GalA) repeat units and contain regions that include (1→2) linked rhamnose residues which act as branch points for neutral sugars. The carboxyl units along the backbone provide salt responsiveness and allow formation of hydrogel networks when divalent ions such as Ca^{2+} are introduced (Figure IV-1).^{59, 71, 72, 152} The oral delivery of small molecules including colon-specific drugs^{153, 154} from pectin hydrogels formed by Ca^{2+} crosslinking have been extensively studied and excellent reviews of the subject are available in the literature.^{53, 84, 89, 149} However, effective methods by which networks may be tailored for controlled delivery of macromolecular species such as protein therapeutics remain undeveloped.^{85, 86, 91} For example, oral delivery of proteins requires efficient transportation across the gastrointestinal (GI) tract membrane and limiting enzymatic and hydrolytic protein degradation.⁸⁹

Alternative routes that circumvent some of the aforementioned issues involve protein delivery *via* subcutaneous injection or introduction through the nasal cavity by adsorption of proteins at the epithelial surface.¹³⁻¹⁵ The latter route results in direct entry of the therapeutic agent into systemic circulation.^{13, 86} The presence of Ca^{2+} in mucosal

and subcutaneous fluids provides a natural source for *in situ* gelation of carboxylated polymers. Given the low concentrations (3-5 mM) of Ca^{2+} present in mucosal¹⁵⁵ and subcutaneous fluids¹⁵⁶, suitable macromolecules must have a large number of carboxyl functional groups available for crosslinking. Previous research in our laboratories¹⁵⁷ has shown that a polysaccharide extracted from the *Aloe vera* plant has a high galacturonic acid content and low degree of methyl ester substitution that allows for facile gel formation in the presence of Ca^{2+} at relatively low concentrations. Interestingly, the *Aloe vera* polysaccharide exhibits phase separation over time at ionic strengths similar to those of biological fluids. Thus, the relative rates of calcium induced gelation and phase separation become major considerations when designing a system for *in situ* delivery applications where both monovalent (Na^+ , K^+) and divalent (Ca^{2+}) ions are present.

In this research we report the gelation behavior and matrix characteristics of Ca^{2+} crosslinked AvP hydrogels. Additionally, we investigate the effects of inducing phase separation by addition of monovalent electrolytes prior to Ca^{2+} -induced gelation. The matrix characteristics of AvP hydrogels formed in solutions at the ionic strengths and molar $[\text{Ca}^{2+}]/[\text{COO}^-]$ ratios of physiological fluids have been determined based on viscoelastic behavior and PFG-NMR studies of water diffusion. In order to establish relationships between AvP network properties and the diffusion behavior of macromolecules through the gel, the release profiles of fluorescein labeled dextrans have been measured as a model for therapeutic proteins. The results of this study serve as a basis for establishing guidelines for monovalent salt and polymer concentrations, as well as $[\text{Ca}^{2+}]/[\text{COO}^-]$ ratios, appropriate for *in situ* AvP crosslinking and the controlled release of therapeutic agents in nasal or subcutaneous environments.

Hydrogel Preparation and Characterization

In order to determine network characteristics, hydrogels were prepared as detailed in the experimental section by introducing calcium chloride solutions of desired concentration into a reservoir containing AvP solutions. A membrane was placed on top of the AvP solution to ensure uniform diffusion as Ca^{2+} -induced gelation occurred. This procedure not only allows experimental control of reaction parameters including polymer concentration, ionic strength, and $[\text{Ca}^{2+}]/[\text{COO}^-]$ ratios but also mimics in a practical manner *in situ* gelation for therapeutic delivery applications. Dynamic oscillatory rheology was conducted, and the viscoelastic behavior of AvP networks were characterized in terms of Ca^{2+} crosslinking conditions as discussed in subsequent sections.

Molecular Weight and Chemical Composition. AvP samples with molecular weights of 200, 435, and 500 kDa were dissolved at 0.10 wt% and crosslinked *via* introduction of 5 mM CaCl_2 . After allowing a 24 h reaction time, AvP solutions formed clear hydrogels that were easily transferred from the mold and studied by dynamic rheometry. As shown in Figure IV-12, the elastic moduli (G') of all samples were much greater than the viscous moduli (G'') and were essentially linear as a function of frequency.

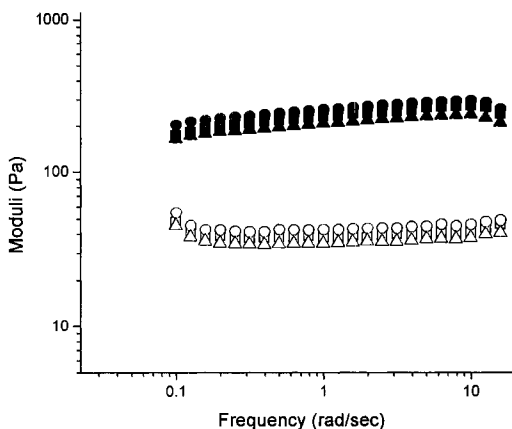


Figure IV-12. Elastic modulus (closed symbols) and viscous modulus (open symbols) data as a function of frequency a series of 0.10 wt% AvP hydrogels formed from AvP samples of molecular weights 523 (■), 435 (●), 200 (▲) kDa 24 h after introduction of 5 mM CaCl₂.

The variation in chemical composition between AvP samples (Table IV-1) is small and does not significantly affect G' values after Ca²⁺ crosslinking. Additionally, G' appears to be independent of AvP molecular weight over the 200-500 kDa range studied here. It should be noted that this is not the case for low molecular weight pectins. In studies utilizing 6, 22, and 66 kDa pectins Durand *et. al.*¹⁵⁰ have shown that low molecular weight species are less effective at forming elastically active networks. Apparently, their existence as rigid rods in solution hinders the formation of elastically active junctions in the hydrogels. Since the molecular weights of all AvP samples studied in our work are well above the rod limit,¹⁵⁷ no variation in hydrogel elastic modulus is evident. Given the structural regularity of the AvP polymers and molecular weight independence of gel properties, AvP2 was chosen for the remainder of the studies reported here.

Rate of Ca²⁺ Crosslinking. Dynamic oscillatory measurements conducted over a 0.5-200 1/rad frequency range illustrate the expected increase in values of G' and G'' with increasing gelation time for AvP2 at concentrations of 0.20 and 0.60 wt% in 5 mM CaCl₂. G' is much greater than G'' and both are linear as a function of frequency, as illustrated for 0.20 wt% hydrogels in Figure IV-13.

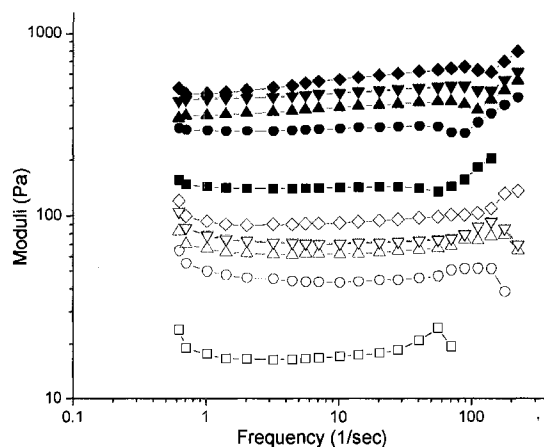


Figure IV-13. Elastic (closed symbols) and viscous moduli (open symbols) as a function of frequency for 0.20 wt% AvP2 hydrogels after introduction of 5 mM CaCl₂ for 0.5 (■), 1 (●), 2 (▲), 6 (▼), and 24 (◆) hours. In the interest of clarity the 12 and 18 hr samples are omitted.

Examination of the values of G' and G'' as a function of time reveals that under these conditions, most gelation occurs within the first six hours after which asymptotic values of G' and G'' are reached (Figure IV-14). These results are in agreement with studies conducted by Silva *et. al.*¹⁵⁸ In order to ensure the degree of crosslinking had reached equilibrium oscillatory rheology studies were conducted on gels 24 h after introduction of Ca²⁺.

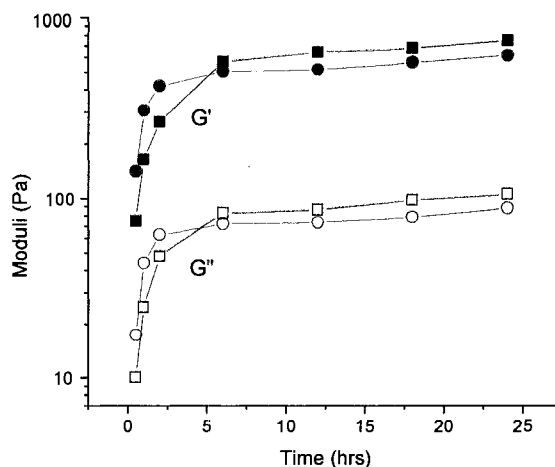


Figure IV-14. Hydrogel viscoelastic behavior as indicated by the elastic (filled symbols) and viscous (open symbols) moduli of 0.20 (●) and 0.60 (■) wt% AvP2 at specific time intervals after introduction of 5 mM CaCl₂.

Polymer Concentration. The network characteristics of biopolymer gels are often heavily dependent on the concentration of polymer present in the system.¹⁵⁹⁻¹⁶¹ In the case of pectin hydrogels, polymer concentration has been shown to be a key factor affecting the final pectin network characteristics.^{162, 163} AvP2 solutions at concentrations ranging from 0.10 to 0.80 wt% were crosslinked with 3, 5, 15, 35 and 50 mM CaCl₂. Oscillatory rheology conducted as a function of frequency provides values of G' , G'' and $\tan \delta$ (Table IV-4) that can be utilized as a diagnostic of gel rigidity.¹⁶⁴

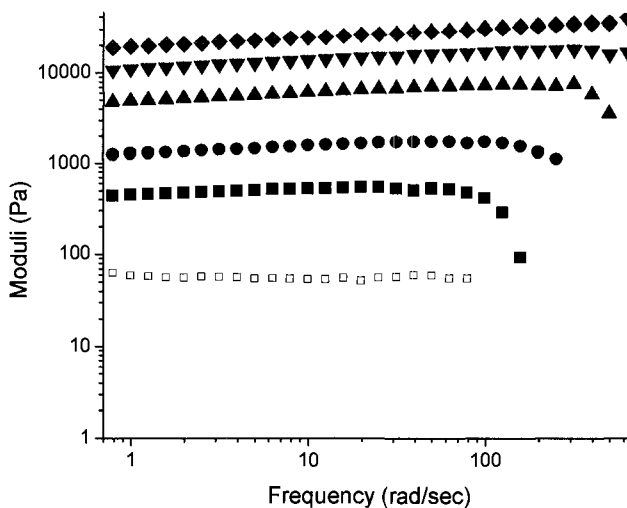
Table IV-4. Experimentally determined elastic (G') and viscous (G'') moduli reported at a frequency of 6.2 rad/sec for AvP hydrogels crosslinked by Ca^{2+} .

[Ca ²⁺] (mM)	0.10 wt% AvP					0.20 wt% AvP				
	$\frac{[\text{Ca}^{2+}]}{[\text{COO}]}$	G' (Pa)	G'' (Pa)	Tan δ	G'/G'' Crossover (rad/sec)	$\frac{[\text{Ca}^{2+}]}{[\text{COO}]}$	G' (Pa)	G'' (Pa)	Tan δ	G'/G'' Crossover (rad/sec)
3	0.62	29	24	1.09	2.1	0.31	17	11	0.80	3.9
5	1.03	189	22	0.11	NA*	0.52	496	54	0.11	1.1
15	3.08	461	45	0.10	NA	1.54	1516	192	0.13	NA
25	5.14	541	58	0.11	NA	2.35	1478	197	0.13	NA
35	7.19	488	57	0.12	NA	3.60	1579	209	0.13	NA
50	10.27	550	64	0.12	NA	5.14	1747	239	0.14	NA

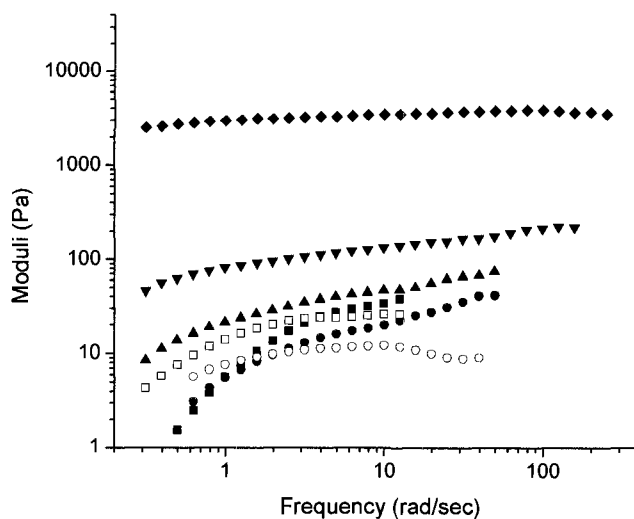
[Ca ²⁺] (mM)	0.60 wt% AvP					0.80 wt% AvP				
	$\frac{[\text{Ca}^{2+}]}{[\text{COO}]}$	G' (Pa)	G'' (Pa)	Tan δ	G'/G'' Crossover (rad/sec)	$\frac{[\text{Ca}^{2+}]}{[\text{COO}]}$	G' (Pa)	G'' (Pa)	Tan δ	G'/G'' Crossover (rad/sec)
3	0.10	123	21	0.17	NA	0.08	1254	439	0.34	NA
5	0.17	562	88	0.16	NA	0.13	2361	572	0.28	NA
15	0.34	2460	371	0.15	NA	0.39	5237	1334	0.24	NA
25	0.52	8534	1290	0.15	NA	0.64	15690	2815	0.18	NA
35	0.86	9783	1328	0.14	NA	0.90	24150	4091	0.17	NA
50	1.71	12260	1626	0.13	NA	1.28	26370	3529	0.13	NA

* NA - Not applicable, G' and G'' were linear as a function of frequency and no crossover was observed.

AvP hydrogels exhibit strong gel behavior ($\tan \delta < 1$, G' & G'' independent of frequency) at all polymer concentrations studied when crosslinked with 15, 35, and 50 mM Ca^{2+} , see for example Figure IV-15a. Dilute AvP2 samples (≤ 0.20 wt%) crosslinked at 3 mM Ca^{2+} exhibit frequency-dependent elastic and viscous moduli (Figure IV-15b) indicative of weak gel behavior.^{65, 164}



a)



b)

Figure IV-15. Elastic (open symbols) and viscous (closed symbols) moduli as a function of frequency for AvP2 gels at equilibrium conditions (a) 50 and (b) 3 mM CaCl_2 . Polymer concentrations of 0.10 (■), 0.20 (●), 0.40 (▲), 0.60 (▼), and 0.80 (◆) wt% were utilized for gel formation.

For a given series of hydrogels crosslinked at a specific Ca^{2+} concentration, a marked increase in G' is observed as the polymer concentration is increased from 0.10 wt% to 0.80 wt%. The data can be fitted to power law relationships when AvP solutions are crosslinked at Ca^{2+} concentrations above 35 mM (Figure IV-16). Power law behavior

has been previously reported for biopolymer gels and is typically observed when pectins are crosslinked in the presence of excess calcium ions.^{67, 165} Hydrogels prepared at lower Ca^{2+} levels show little increase in G' up to a critical AvP concentration of 0.60 wt%, beyond which a dramatic increase in G' occurs (Figure IV-16 Inset). This polymer concentration corresponds to the entanglement concentration of AvP in aqueous solutions¹⁵⁷ and likely indicates the onset of intermolecular crosslinking. Similar studies on synthetic polyacrylamide hydrogel systems have also found that dramatic increases in mechanical properties occur when gels are formed in the concentrated solution regime.¹⁶⁶

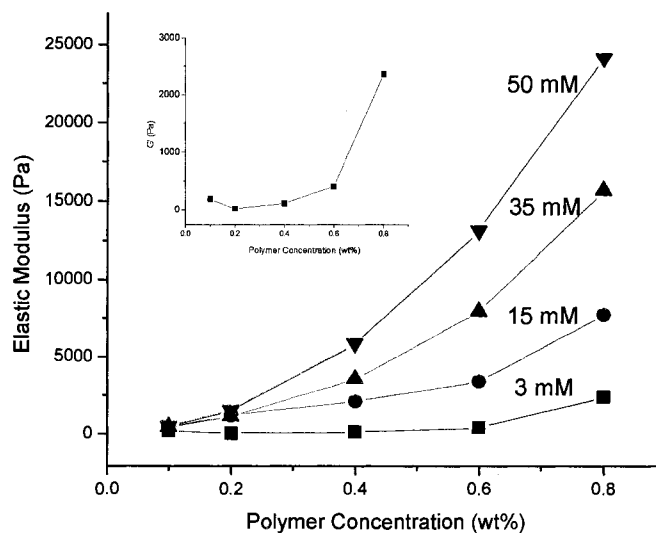
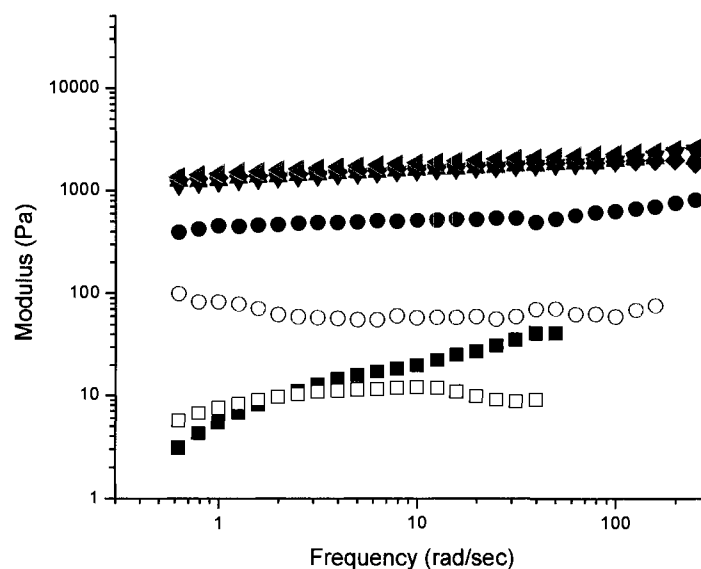


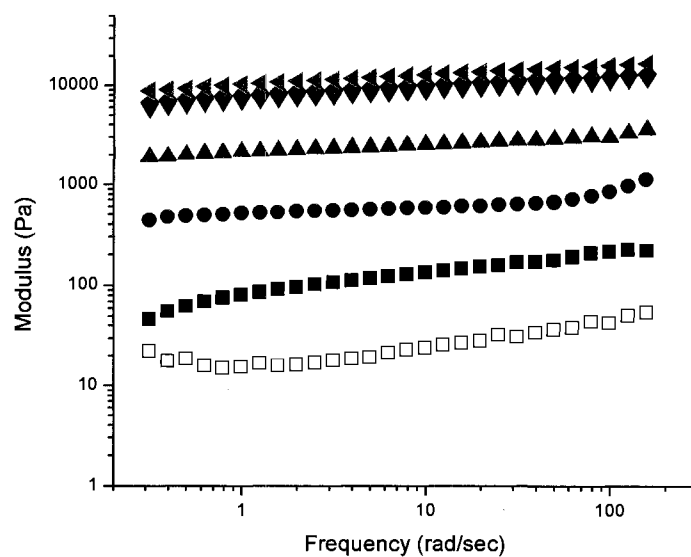
Figure IV-16. Elastic modulus plotted against AvP2 concentration of hydrogels formed at CaCl_2 concentrations of 3 (■), 15 (●), 35 (▲) and 50 (▼) mM. The y-axis of the inset is scaled to depict the 3 mM CaCl_2 series only and draw attention to the dramatic increase in G' evident for hydrogels formed from concentrated solutions (>0.60 wt%).

Elastic modulus data, such as that presented in Figure IV-16 can be plotted according to rubber elasticity theory¹⁶⁷⁻¹⁶⁹ in order to provide an approximate value of the molecular weight between crosslinks (M_c). While the application of rubber elasticity theory to physically crosslinked polysaccharide networks has many limitations, it is often utilized as the foundation of current theory^{159, 163, 165, 170} and may be easily applied in order to obtain a first approximation of M_c .¹⁷¹ From the elastic modulus values of AvP hydrogels crosslinked with 5 mM CaCl_2 , an M_c value of 10,000 g/mol can be calculated. Utilizing the M_w of the monomer unit (174 g/mol) and the reported length of a GalA unit as determined by x-ray diffraction (4.35 \AA)⁵⁷, a crosslink spacing of approximately 25 nm is obtained. As will be shown later, this value correlates well with data from diffusion studies.

Ca²⁺/COO⁻ Ratio. The stoichiometric ratio of Ca^{2+} cations to carboxylate anions present in the system affects pectin hydrogel formation.^{48, 111} As previously described, AvP2 solutions (0.10 to 0.80 wt%) were crosslinked *via* introduction of CaCl_2 (3.0-50 mM). The profiles of G' and G'' as a function of frequency are depicted for 0.20 and 0.60 wt% hydrogels in the Figures IV-17a and 17b) and indicate that $G' \gg G''$ for all samples except the 0.20 wt% hydrogel crosslinked by 3 mM CaCl_2 .



a)



b)

Figure IV-17. Elastic (filled symbols) and viscous (open symbols) moduli as a function of frequency for gels composed of (a) 0.20 and (b) 0.60 wt% AvP2 at CaCl_2 concentrations of 3 (■), 5 (●), 15 (▲), 25 (▼), 35 (◆), 50 (◄) mM.

In binding studies involving a traditional citrus pectin and Mn^{2+} conducted by Williams *et. al.*, G' exhibited a maximum at a stoichiometric ratio of 0.40.¹⁵¹ In contrast, for a series of AvP hydrogels prepared at a fixed polymer concentration, elastic moduli

increase dramatically as experimental values of $[Ca^{2+}]/[COO^-]$ increase (Figure IV-18). As the ratio of $[Ca^{2+}]/[COO^-]$ becomes greater than 1, G' reaches an asymptotic value for each polymer concentration.

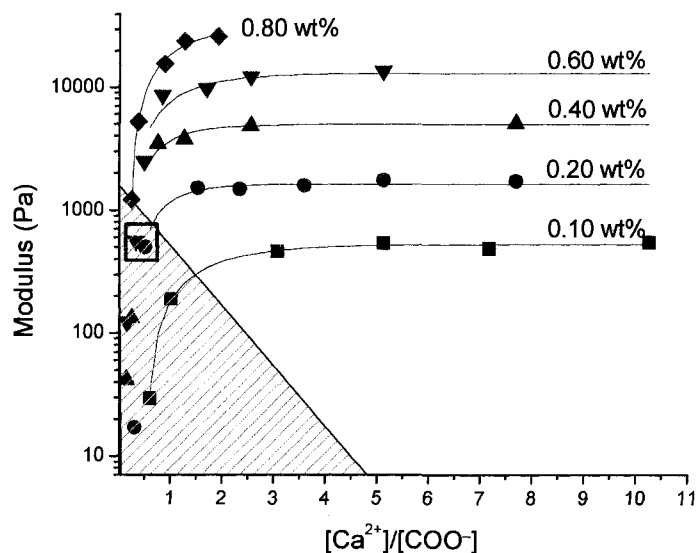


Figure IV-18. Elastic modulus (Pa) plotted as a function of the molar ratio $[Ca^{2+}]/[COO^-]$ for AvP2 calcium gels formed at concentrations of 0.10 (■), 0.20 (●), 0.40 (▲), 0.60 (▼), 0.80 (◆) wt% polymer. Shaded area corresponds to Ca^{2+} concentrations found in nasal fluids. The boxed area indicates the region from which hydrogels were evaluated in release studies described in section 3.3 of the discussion.

The extensive rheological data presented above clearly indicate the facility by which calcium ions diffusing into AvP2 solutions elicit hydrogel network formation and the fact that crosslink density (indicated by G' values) can be tailored by adjusting the fundamental parameters of polymer concentration and $[Ca^{2+}]/[COO^-]$ ratios. However, *in situ* gelation, yielding hydrogel matrix characteristics necessary for efficient delivery of therapeutics directly in the nasal cavity, requires consideration of additional key issues such as the limited calcium concentration available in physiological fluids and the effects of low molecular weight electrolytes on polymer conformation and solubility.

In Figure IV-18, the domain of theoretically accessible networks (shown in the shaded area) is limited by the Ca^{2+} content in nasal and subcutaneous fluids, which is approximately 5 mM. Two samples (highlighted data points in Figure IV-18) having sufficiently high moduli for hydrogel integrity were chosen for the diffusion and controlled release studies addressed in subsequent sections of this manuscript. It is important to note that, although prepared at substantially different polymer concentrations (0.20 vs. 0.60 wt%), the experimentally measured values of G' are similar (~ 500 Pa) for $[\text{Ca}^{2+}]/[\text{COO}^-]$ ratios of 0.5 and 0.2, respectively.

Addition of Simple Electrolytes. Electrolyte addition to anionic polysaccharides lowers hydrodynamic volume in aqueous solution by effective charge screening and by reduction of polymer solvent interactions. Although the conformationally stiff AvP is less prone to viscosity loss when compared to flexible polyelectrolytes such as poly(sodium acrylate), addition of electrolytes such as NaCl reduces hydrodynamic volume. For AvP2, a 17% decrease in intrinsic viscosity was observed as NaCl concentration was increased from 0.05 M to 0.20 M.¹⁵⁷ These experimentally determined effects on conformation and solvation are expected to be manifested in properties of the crosslinked gel matrices as well.

Another critical issue arising from changes in solvation from added electrolytes is the possibility of phase separation and aggregation. While conducting previous intrinsic viscosity studies on AvPs, we observed phase separation in dilute solutions at ionic strengths above 0.15 M.¹⁵⁷ A closer examination reveals gradual association of AvP chains that becomes noticeable at extended time. For example, initially linear

Huggins/Kraemer plots (2 h) become non-linear after 24 hours (Figure IV-19). Further evidence was obtained from zeta potential and dynamic light scattering studies. At low ionic strength, the zeta potential is -80 mV and the solutions are stable, however as the ionic strength is increased to 0.10 M, the zeta potential approaches -30 mV.¹⁵⁷

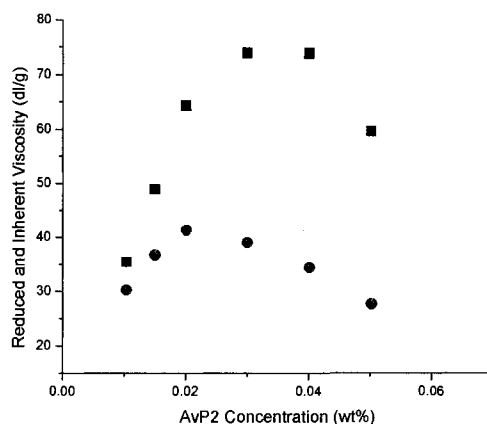


Figure IV-19. Example of a non-linear Huggins (■) Kraemer (●) plots obtained for AvP2 after dissolution in 0.20 M NaCl for 2 and 24 hours, respectively.

Turbidimetric experiments were conducted on AvP2 solutions for a wide range of polymer concentrations and ionic strengths as detailed in the experimental section. Polymer concentrations were chosen between 0 and 0.20 wt% and the ionic strength was assumed to be that of the NaCl solution. Turbidity measurements, specifically the three dimensional plots shown in Figures IV-20a and 20b, confirm that the extent of phase separation is time-dependent and related to polymer concentration and ionic strength. After two hours, the extent of phase separation observed in solutions containing greater than 0.10 wt% AvP at ionic strengths greater than 0.15 M is moderate. However, Figure 20b shows that phase separation is more prevalent after 24 hours. It should be pointed out that, though phase separation can occur in the presence of NaCl, the time dependency for this process is slow relative to the rate of Ca^{2+} -induced gelation (Figure IV-14).

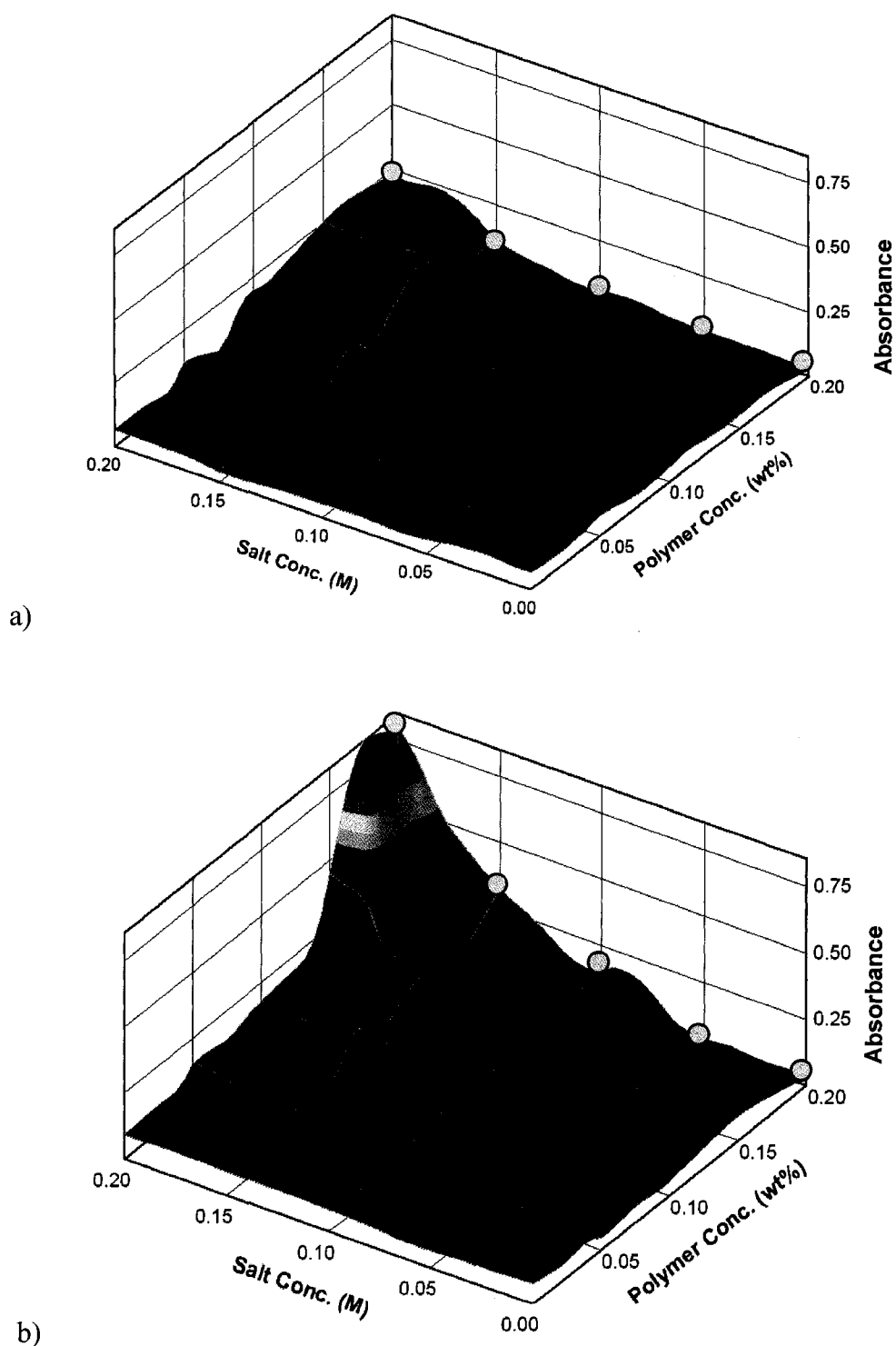


Figure IV-20. Turbidity of AvP2 solutions as functions of NaCl (M) and polymer (wt%) concentration at 2 (a) and 24 (b) hours. Select combinations of salt and polymer concentration (●) were used in Ca^{2+} induced gel formation studies in order to determine the effect of phase behavior on hydrogel elastic modulus (Figure IV-22).

Based on our studies and previous reports regarding the kinetic competition between phase separation and gelation,^{54, 57, 172} we anticipated that sample history would affect network properties and therefore prepared hydrogels from two series of 0.20 wt% AvP2 solutions with 0, 0.05, 0.10, 0.15, and 0.20 M NaCl aged for 2 and 24 hours, respectively. These compositions are indicated by the open circles in Figures IV-20a and 20b and include; homogeneous solutions (lowest turbidity), microphase separated solutions (moderate turbidity) and phase separated colloidal dispersions (highest turbidity). Elastic and viscous modulus profiles as a function of frequency are recorded in Figure IV-21.

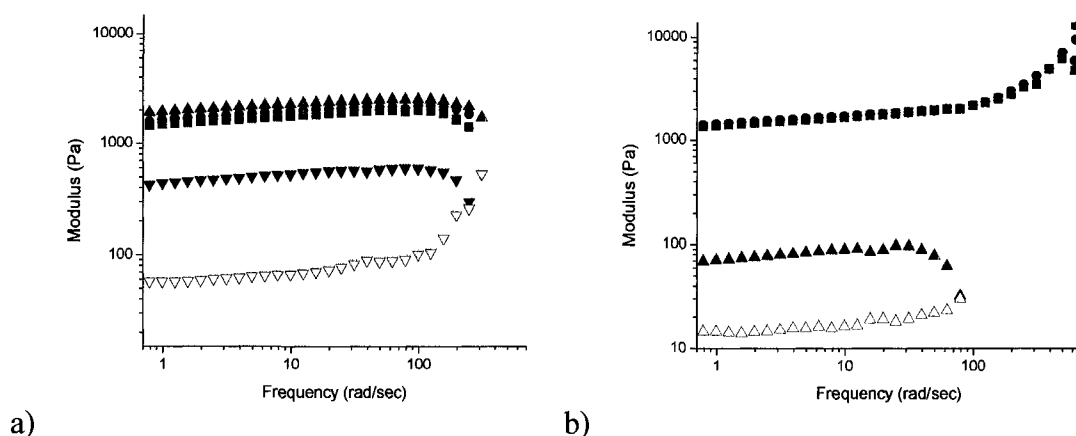


Figure IV-21. Elastic (filled symbols) and viscous (open symbols) moduli as a function of frequency for hydrogels formed from 0.20 wt% AvP2 solutions dissolved in 0.05 (■), 0.10 (●), 0.15 (▲), 0.20 (▼) NaCl for (a) 2 and (b) 24 hours prior to introduction of 35mM CaCl_2 .

Both the effects of ionic strength (NaCl concentration) of the AvP2 solutions and aging time prior to crosslinking can be ascertained by examination of Figure IV-22. The single reference point on the left side of the plot represents the hydrogel modulus value of 1500 Pa after Ca^{2+} (35mM) crosslinking of a 0.20 wt% solution of AvP2 in the absence of

NaCl (0.00 M). Increases in experimentally measured G' values are observed reaching 2300 Pa at 0.15 M NaCl before falling abruptly at higher ionic strength to ~ 600 Pa in the samples aged for 2 hours prior to crosslinking. Smaller but discernable increases in G' are observed for AvP2 samples aged for 24 hours prior to crosslinking that contained 0.05 and 0.10 M NaCl. Since the modulus (Figure IV-22) and turbidity (Figures IV-20a and 20b, data points indicated by circles) measurements are on the same samples, it appears that low concentrations of NaCl induce associations which are helpful to network formation. Higher levels of association which occur with increased aging and/or NaCl concentration result in total phase separation and incomplete gelation.

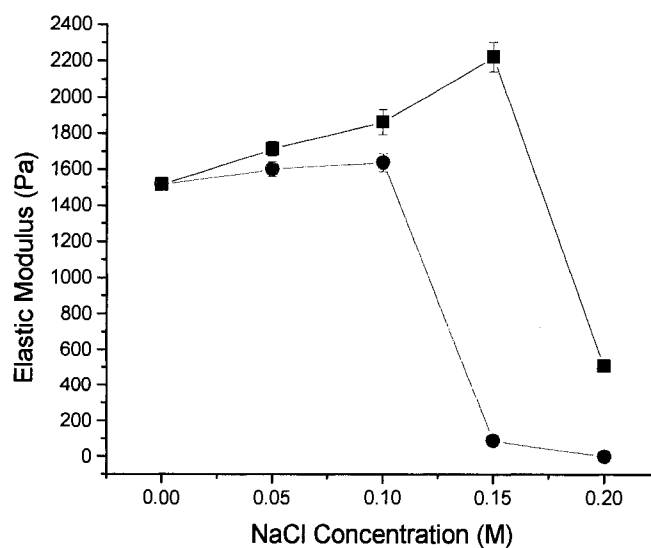


Figure IV-22. Elastic modulus of 0.20 wt% AvP2 hydrogels formed by crosslinking with 35 mM CaCl_2 . Aqueous AvP2 solutions at the specified NaCl concentration shown along the abscissa were aged for 2 (■) and 24 (●) hours prior to addition of CaCl_2 solutions.

In order to simulate Ca^{2+} crosslinking at the ionic strength of a nasal fluid, homogeneous aqueous solutions of 0.20 wt% AvP were crosslinked *via* introduction of a solution containing 5 mM CaCl_2 , 0.15 M NaCl and 0.04 M KCl.¹⁵⁵ When crosslinked under these conditions, aqueous AvP solutions form hydrogels with an elastic modulus value of 1200 Pa, representing a significant increase over the 500 Pa value obtained when AvP solutions are crosslinked by 5 mM CaCl_2 alone (Figure IV-23). The formation of a strong hydrogel is consistent with the absence of large scale phase separation, further supporting the conclusion that the rate of Ca^{2+} crosslinking is fast relative to the rate of phase separation. However, when simulated nasal fluids (SNF) are employed in the crosslinking reaction, an increase in G' occurs (Figure IV-23) which is similar to that observed for moderate NaCl concentrations (Figure IV-22).

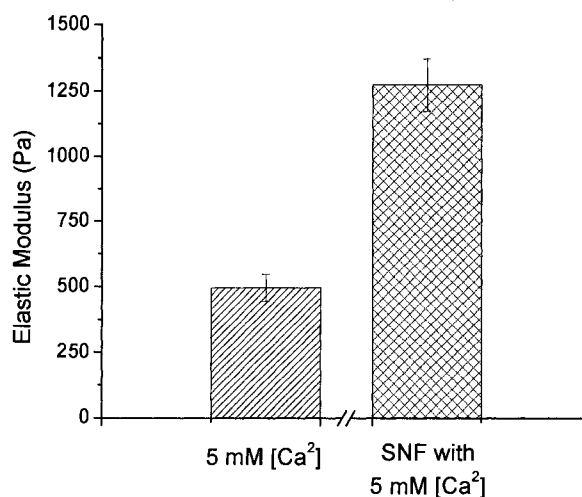


Figure IV-23. Elastic modulus of 0.20 wt% AvP2 hydrogels formed by crosslinking with 5 mM CaCl_2 and a simulated nasal fluid (SNF) containing 5 mM CaCl_2 , 0.15 M NaCl and 0.04 M KCl.

Diffusion Studies via PFG-NMR. Information regarding pores within the viscoelastic hydrogel matrix can be gained from diffusion studies utilizing pulsed field gradient NMR (PFG-NMR). In PFG-NMR experiments, the apparent diffusion coefficient of water (D_{app}) is monitored as a function of total diffusion time (Δ). In restricted geometries (such as hydrogel matrixes) D_{app} is unhindered at short diffusion times and equals the diffusion coefficient of bulk water (D_{free}). However, as Δ increases, an increasing fraction of the water molecules encounter network boundaries, thereby restricting diffusion and lowering D_{app} to values less than D_{free} . At long Δ , all water molecules experience boundaries, resulting in a limiting value of D_{app} that may be correlated to the root mean square (RMS) end-to-end distance of the pore space in the hydrogel matrix *via* Equation 2, in which r is the RMS end-to-end distance and t_d is the value of Δ which approaches the limiting value of D_{app} .¹⁷³

$$D_{app} = (1/6)t_d^{-1}r^2 \quad (2)$$

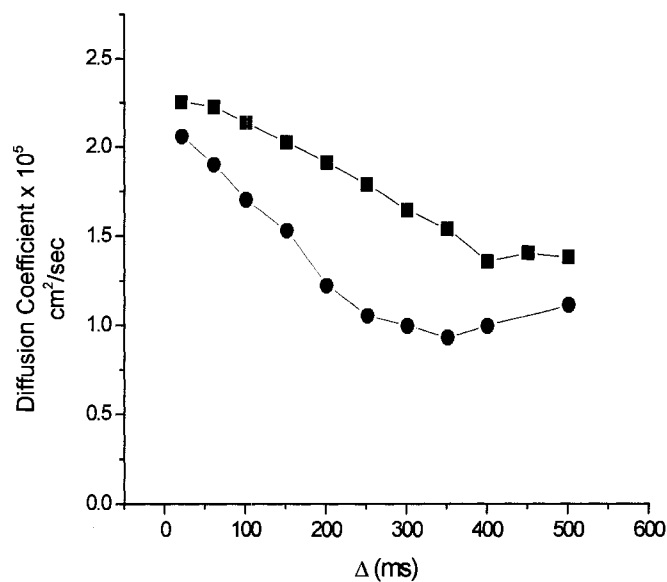
Additional information can be obtained through further examination of the D_{app} vs Δ profile. The slope of the initial decay in D_{app} yields information concerning the surface area to pore volume ratio (S/V_p), and the magnitude of D_{app} at the long time plateau is indicative of the tortuosity of the medium in which diffusion is occurring. A rapid decay of D_{app} in the short time regime indicates a larger S/V_p and lower values of D_{app} at long times indicate greater tortuosity.¹⁷⁴ For example, PFG-NMR experiments conducted on idealized systems containing hard spheres provide quantitative values of S/V_p in agreement with the known values for the beads.^{175, 176} Although quantitative analysis of S/V_p for fractal geometries including hydrogel matrices is currently debated,¹⁷⁷ qualitative comparisons have been made for hydrogel systems.¹⁷⁸

PFG-NMR experiments were first conducted on hydrogels prepared by crosslinking 0.20 and 0.60 wt% AvP solutions with 5 mM CaCl_2 , resulting in the diffusion profiles shown in Figure IV-24a. RMS values of 14 and 13 μm were calculated utilizing the individual D_{app} and t_d values of the 0.20 and 0.60 wt% crosslinked systems, respectively. While the calculated pore sizes of the two systems are similar, the diffusion profiles suggest subtle differences in hydrogel morphology. In comparison to 0.20 wt% hydrogels, the 0.60 wt% systems exhibit a sharper transition as a function of Δ and lower values of D_{app} at long Δ , indicating greater surface area and tortuosity.

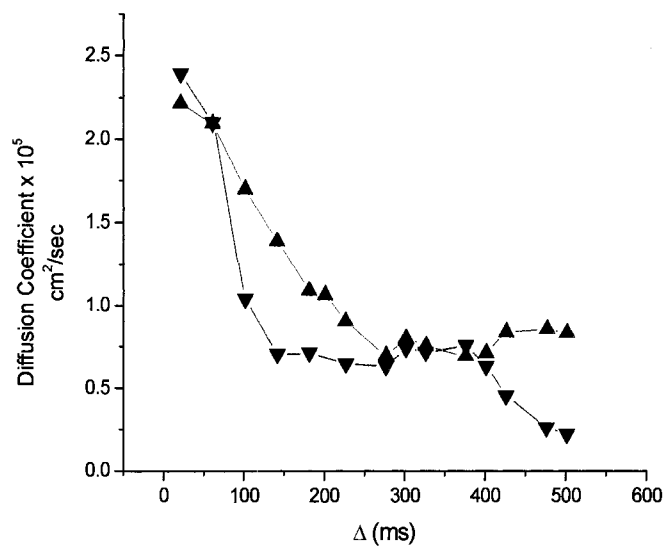
Additional PFG-NMR experiments (Figure IV-24b) conducted on hydrogels prepared from solutions of moderate ionic strength (0.20 wt% AvP aged in 0.15 M NaCl solutions for 2 and 24 h prior to Ca^{2+} crosslinking) indicate pores with RMS values of 8 μm . A rapid decay in D_{app} as a function of Δ is observed for both samples, suggesting that high S/V_p ratios are present. Similar magnitudes of D_{app} are obtained at long Δ , suggesting that tortuosity remains relatively constant in the two systems. Interestingly, the 24 h sample exhibits a second D_{app} plateau at long Δ , suggesting the presence of additional heterogeneities within the hydrogel network.

Large differences in PFG-NMR diffusion profiles between hydrogels formed from homogeneous aqueous solutions and solutions containing 0.15 M NaCl are experimentally observed (Figures IV-24a and 24b). Changes in both polymer conformation and solubility may account for the 40% reduction in RMS pore size noted for hydrogels formed in the latter case. The PFG-NMR diffusion profiles also suggest that hydrogels formed in the presence of NaCl contain greater surface-to-volume ratios

(sharper transition in D_{app}) and higher levels of tortuosity (lower value of D_{app} at long Δ) in comparison to the corresponding aqueous systems.



a)



b)

Figure IV-24. a) The apparent diffusion coefficient (D_{app}) of water plotted against observation time for 0.20 (■) and 0.60 (●) wt% AvP2 gels crosslinked by introduction of 5 mM CaCl_2 . b) Profile of D_{app} for 0.20 wt% hydrogels formed from solutions containing 0.15 M NaCl equilibrated for 2 (▲) and 24 (▼) h prior to introduction of 5 mM CaCl_2 .

Hydrogel Morphology. A model of AvP2 hydrogel morphology consistent with both elastic modulus data and the PFG-NMR studies is depicted in Figure IV-25. The model contains microscopic aqueous voids surrounded by a polymer rich gel network. Clear aqueous AvP solutions crosslinked by Ca^{2+} form homogeneous hydrogel networks with a large amount of connectivity between pores. Na^+ and K^+ ions present in nasal fluid have an additional effect on hydrogel morphology. Experimental evidence has shown that monovalent ions increase AvP association in solution, which at incrementally higher concentration, eventually cause phase separation. Upon crosslinking, AvP solutions containing moderate NaCl concentration (<0.15) result in AvP hydrogels with increased elastic modulus, suggesting that interchain associations are present in the hydrogel network. The sharp transition and magnitude of D_{app} observed in PFG-NMR studies suggest that polymer associations increase surface area-to-pore volume ratios and tortuosity within hydrogels.

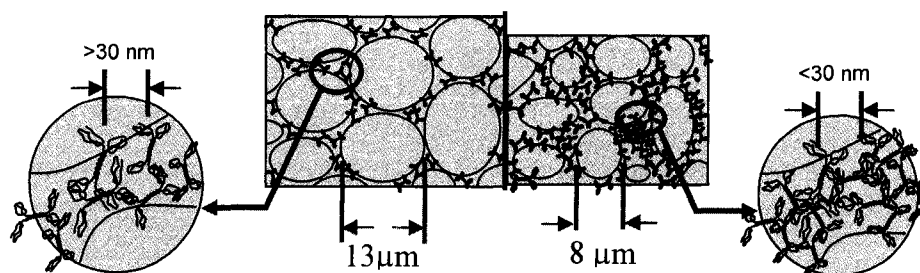


Figure IV-25. Proposed hydrogel morphology of Ca^{2+} crosslinked AvP matrices formed from homogeneous aqueous solutions (left) and solutions containing low concentrations of monovalent ions (right) depicting microscopic pores as defined by the AvP network. Smaller pore sizes and increased tortuosity in the presence of moderate concentration of NaCl are responsible for slower release rates of fluorescently modeled dextran according to the proposed model.

Release Profiles of Macromolecular Model Compounds

The major objective of this study is to control the diffusion characteristics of crosslinked AvP in order to elicit sustained release of therapeutic agents. In previous sections we have shown that controlling AvP concentration, $[\text{Ca}^{2+}]/[\text{COO}^-]$ ratio, and ionic strength prior to or during the cross-linking process results in dramatic changes in physical properties, in particular viscoelastic behavior and water diffusion. In this section we compare the relative rates and extents of release of fluorescein labeled 4 kDa ($d_h=3\text{nm}$) and 500 kDa ($d_h=27\text{nm}$) dextran model compounds from Ca^{2+} crosslinked gels prepared at low (0.20 wt%) or high (0.60 wt%) concentrations of AvP2. The Ca^{2+} concentration for crosslinking was maintained at 5 mM in each case, a value near that in physiological fluids. It should be noted that the labeled model compounds Dex4 and Dex500 (Figures IV-26a and 26b) were chosen as macromolecular model compounds because of their stability in solution, comparable size to proteins, known effect on pectin gelation,⁷⁰ and successful use in similar studies.^{179, 180}

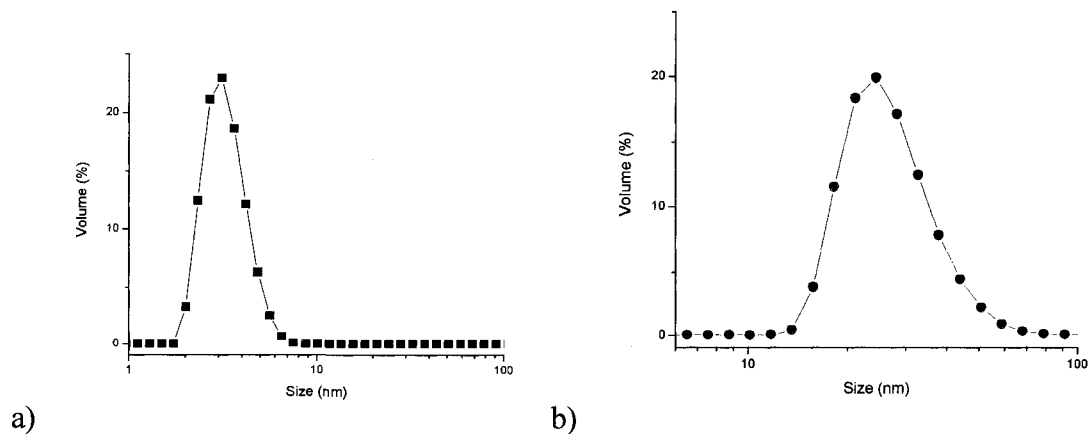


Figure IV-26. Size distribution of 4 and 500 kDa FITC-Dextrans as determined by dynamic light scattering. a) 4 kDa dextran (■) and b) 500 kDa dextran (●) dissolved in SNF containing 5 mM CaCl_2 .

Figure IV-27 illustrates the release profiles of the labeled dextrans from AvP hydrogel matrices as compared to the freely diffusing controls, C1 and C2. Curves 1 and 2 demonstrate the rapid release of Dex4 and Dex500 respectively in matrices formed from 0.20 wt% (dilute) AvP in the presence of Ca^{2+} only. Cumulative release approaches 100% in 30 hours. For curves 3 and 4, again from 0.20 wt% AvP hydrogels, but crosslinked in a solution with the Ca^{2+} , Na^+ , and K^+ content of simulated nasal fluid (SNF), release is slower and only reaches 75-80% after 96 h, with Dex4 showing only a slightly greater rate and extent of release than the larger Dex500. The effects of increasing AvP2 concentration to (0.60 wt%) and size of the dextran on release are seen in the final two profiles 5 and 6, again crosslinked under SNF conditions. Here the larger dextran, Dex500, exhibits a significantly reduced rate and extent of release as compared to Dex4.

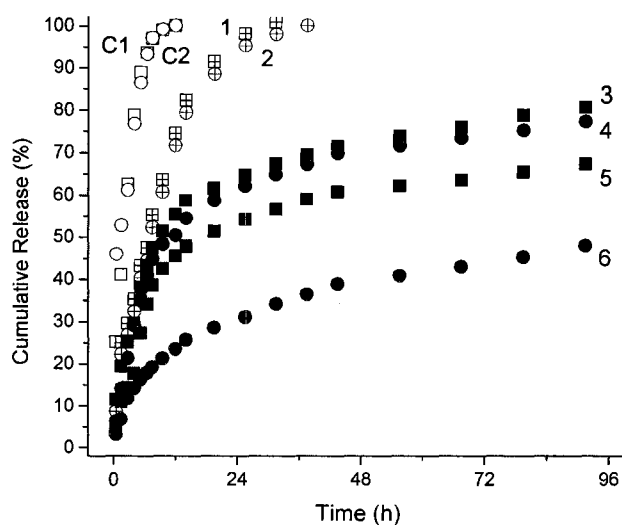


Figure IV-27. Cumulative release (%) of 4 kDa (squares) and 500 kDa (circles) dextran as a function of time (h) from 0.20 wt% (black & red symbols) and 0.60 wt% (blue and green symbols) hydrogels. In the presence of Na and K only, no gel forms and free diffusion is observed (Curves C1 & C2), while a Ca^{2+} -induced AvP matrix reduces the diffusion rate (Curves 1 & 2). When gelled by SNF, diffusion rates are further reduced and dependent on dextran size and AvP concentration (Curves 3-6).

In an additional experiment we determined the amount of retained dextran that could be released by treating the respective hydrogel networks with EDTA, and then further disrupting the remaining network utilizing mechanical force and mild hydrolysis (Figure IV-28). For example, 5-8% of the dextran is entrapped within crosslinked domains that are disrupted by extraction of Ca^{2+} with EDTA, in both 0.20 (Curves 3 and 4) and 0.60 (Curves 5 and 6) wt% hydrogels. However, in curves 5 and 6, an additional 3% of Dex4 and 5% of Dex500 is entrapped within domains which remain intact after EDTA exposure.

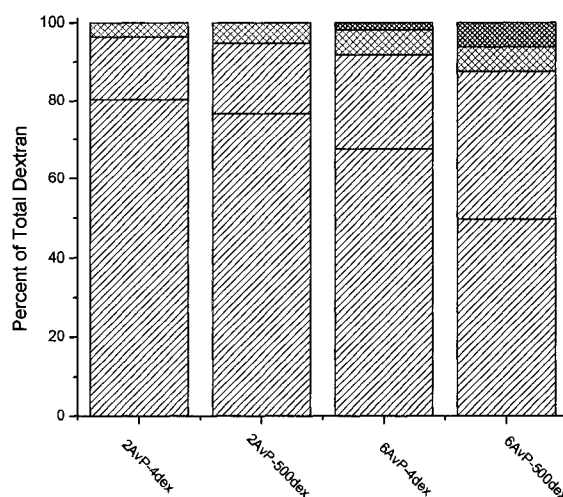


Figure IV-28. Population depicted in black represents dextran available for release. Percent of dextran released during the initial study (black line), after EDTA exposure (green crosshatch), and after disruption of phase separated polymer regions (blue crosshatch).

Theoretical Diffusion Models. In order to elucidate the diffusion mechanism occurring in AvP hydrogels, the experimental release profiles have been fitted to 3 existing models.¹⁸¹⁻¹⁸³ These models have been previously applied to similar hydrogel systems including alginates and pectins.^{154, 184} Agreement between our experimental data

and the 3 diffusion models outlined below provides a diagnostic measure of the relative contributions of Fickian diffusion and Case II diffusion occurring in Ca^{2+} crosslinked AvP hydrogels.

The first model describes Fickian diffusion based on the Higuchi equation (Eq 3).¹⁸⁵

$$\frac{M_t}{M_\infty} = k_H t^{1/2} \quad (3)$$

where M_t / M_∞ represents the fraction of release, t is the release time, and k_H is the rate coefficient. A fit of experimental data to the Higuchi model indicates diffusion driven release in the absence of matrix relaxation effects. The characteristic shape of the experimental M_t / M_∞ vs. $t^{1/2}$ curve is related to the dominant release mechanism, where a sigmoidal departure from linearity is indicative of Case II diffusion.¹⁸⁶

The second model considered was the Ritger-Peppas equation (Eq. 4) where the exponent n is related to the drug transport mechanism and the shape of the object from which diffusion occurs.¹⁸² In the case of diffusion from a slab, when $n=0.5$ equations 3 and 4 are equal and Fickian diffusion dominates. When $n=1$, equation 4 leads to a description of zero-order release, termed Case II diffusion. Case II diffusion is prevalent when macromolecular chain relaxations within the hydrogel matrix alter the diffusion rate of the analyte.⁹⁴ When n is between 0.5 and 1, anomalous or heterogeneous diffusion is suggested.

$$\frac{M_t}{M_\infty} = k_1 t^n \quad (4)$$

The third model, the Peppas-Sahlin equation (Eq. 5) employs a 3 parameter fit which is utilized to describe anomalous release, wherein release profiles are coupled to

contributions from both Fickian and Case II diffusion. In Eq. 5, k_1 and k_2 represent the contribution of Fickian diffusion and Case II transport, respectively. In practicality, this model is difficult to analyze due to the implicit co-dependence of k_1 and k_2 , however reliable solutions for n can be obtained.¹⁵⁴

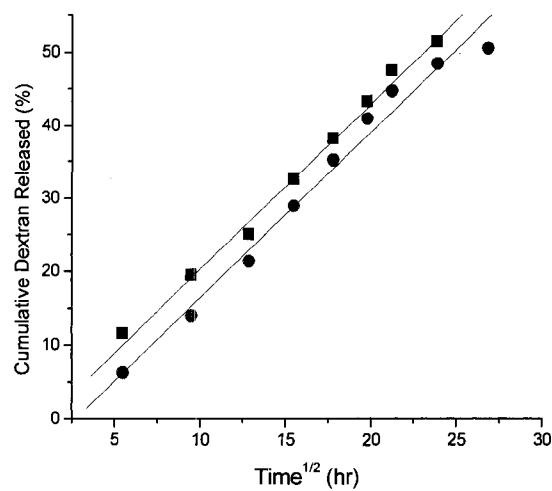
$$\frac{M_t}{M_\infty} = k_1 t^n + k_2 t^{2n} \quad (5)$$

To simplify the model, the case where $n=0.5$ has been examined from which k_1 and k_2 can be easily determined.⁹⁴

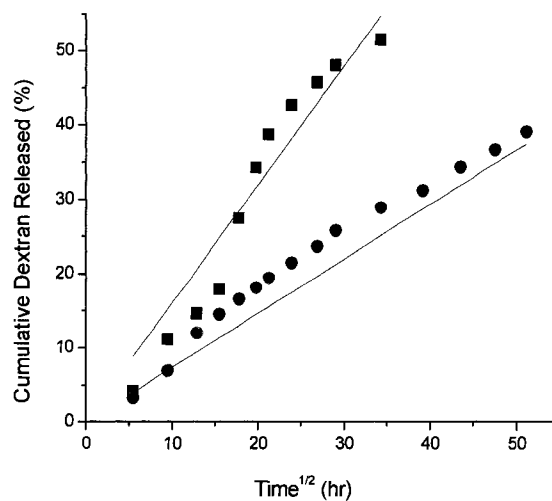
$$\frac{M_t}{M_\infty} = k_1 t^{1/2} + k_2 t \quad (6)$$

Application of Theoretical Models. Evaluation of experimental data relative to the above release models suggests that an increase in dextran size results in a change in diffusion mechanism. Of the three models examined, the Higuchi equation provides the best fit to the release profile for curves 1 & 2, suggesting pure Fickian diffusion within hydrogel systems crosslinked by Ca^{2+} only. When hydrogels crosslinked under SNF conditions are examined (Table IV-5), it is found that the Higuchi equation still provides the best fit for the release of Dex4 from 0.20 wt% hydrogels (Curve 3). With the larger dextran sample curve 4, diffusion is best described by the Ritger-Peppas equation. For this system $n=0.63$, suggesting that both Fickian and Case II diffusion mechanisms are present. Additionally, the Higuchi plot of curve 4 displays sigmoidal curvature, supporting the conclusion that matrix interactions are involved in the diffusion mechanism (Figure IV-29). Analysis of 0.60 wt% samples in terms of theoretical models reveals that the release profiles for both Dex4 and Dex500 (Curves 5 & 6) are best

described by the Ritger-Peppas model (Table IV-5). The values of n suggest that anomalous diffusion is present in both systems, with the contribution of matrix relaxations becoming more significant as the size of the dextran species increases.



a)



b)

Figure IV-29. Cumulative release of dextran 4Dex (■) and 500Dex (●) plotted against the square root of time for a) 0.20 wt% b) 0.60 wt% AvP hydrogels. Sigmoidal departure from linearity indicates that matrix relaxations affect diffusion.

Table IV-5. Calculated parameters for release models and goodness of fit indicator (AIC) based on experimental release profiles of 0.20 and 0.60 wt% AvP2 calcium hydrogels.

(3) 2AvP-4Dex-5Ca			(5) 6AvP-4Dex-5Ca		
	k_1	k_2	n	AIC	
Higuchi	2.10	-	-	-46.6	Higuchi
Ritger-Peppas	2.00	-	0.51	-41.0	Ritger-Peppas
Peppas-Sahlin	1.83	0.0158	-	-40.0	Peppas-Sahlin
(4) 2AvP-500Dex-5Ca			(6) 6AvP-500Dex-5Ca		
	k_1	k_2	n	AIC	
Higuchi	1.95	-	-	-21.4	Higuchi
Ritger-Peppas	0.83	-	0.63	-40.6	Ritger-Peppas
Peppas-Sahlin	1.61	0.0160	-	-25.0	Peppas-Sahlin
	k_1	k_2	n	AIC	
Higuchi	1.63	-	-	-27.1	Higuchi
Ritger-Peppas	0.42	-	0.63	-37.4	Ritger-Peppas
Peppas-Sahlin	1.03	0.0157	-	-25.9	Peppas-Sahlin
	k_1	k_2	n	AIC	
Higuchi	0.90	-	-	-15.1	Higuchi
Ritger-Peppas	0.33	-	0.76	-35.3	Ritger-Peppas
Peppas-Sahlin	0.87	0.0268	-	-22.0	Peppas-Sahlin

Release Mechanisms in View of Hydrogel Characteristics. The observed release mechanisms may be explained by consideration of both the microscopic aqueous pores and the free pore volume within the segmental structure of the AvP2 network. In both the 0.20 and 0.60 wt% systems, aqueous pores with RMS radii between 8 and 13 μm have been experimentally observed by PFG-NMR. Within these pores the diffusion of 3 and 27 nm dextrans will be unhindered and thus Fickian in nature. Fickian diffusion is the dominant component within each of the AvP hydrogel systems studied, even those that fit anomalous release models, suggesting that a large portion of dextran diffusion occurs within these micron scale pores.

Calculations of the molecular weight between crosslinks (M_c) based on elastic modulus relationships suggest that nanometer scale pores exist within the AvP network, which may hinder the diffusion of dextran through segmental interactions. Examination of release profiles in terms of theoretical models reveals that a significant Case II component is involved in the diffusion of Dex4 and Dex500 (D_H , 3 and 27 nm) from 0.60 wt% hydrogels (Table IV-5), suggesting that segmental (matrix) interactions are present. The elastic modulus- M_c relationship predicts a distance of 25 nm between crosslinks, consistent with the increase in Case II diffusion observed between 3 and 27 nm dextrans for 0.60 wt% hydrogels (Table IV-5).

The reduction in dextran release rate observed between the control systems gelled by Ca^{+2} only and the same 2AvP-Dex4 system gelled upon crosslinking with SNF containing Ca^{+2} , Na^+ and K^+ ions suggests that changes in morphology occur when monovalent salts are present. Experimental evidence collected for 0.60 wt% AvP hydrogels shows that approximately 5% of the dextran population is entrapped within

crosslinked domains that cannot be disrupted by extraction of Ca^{2+} by EDTA, suggesting that microphase separated domains contribute to the elastic nature of the hydrogel and affect the release of dextran. The $[\text{Ca}^{2+}]/[\text{COO}^-]$ ratio in 0.60 wt% systems is low at physiological concentrations of Ca^{2+} , resulting in a large number of free carboxylate functional groups, and presumably a significant number of uncrosslinked chain segments. Solid state NMR experiments conducted by Jarvis *et. al.*⁷⁸ have shown that free pectin chain segments within Ca^{2+} crosslinked hydrogels exhibit mobility similar to that in solution.

In view of the experimental evidence including phase behavior, elastic moduli and PFG-NMR, it may be concluded that monovalent electrolyte addition results in chain constriction and poorer solvation creating dense AvP2 regions which limit diffusion by increasing tortuosity. Further support for this conclusion is drawn from the micrographs shown in Figure IV-30. AvP hydrogels were stained with ruthenium red in order to obtain a visual diagnostic of polymer homogeneity in the hydrogels. Similarly the fluorescence emission of FITC-dextran was used to determine the dispersion of dextran throughout the hydrogel matrix. Figure IV-30a depicts a 0.20 wt% AvP hydrogel containing FITC-dextran that was formed on crosslinking with Ca^{2+} . The bright field and fluorescence images indicate that the dispersion of AvP and dextran are both homogeneous throughout the hydrogel. In contrast, micrographs taken of AvP hydrogels formed in the presence of 0.15 M NaCl contain polymer rich domains which contain locally high concentrations of dextran (Figure IV-30b).

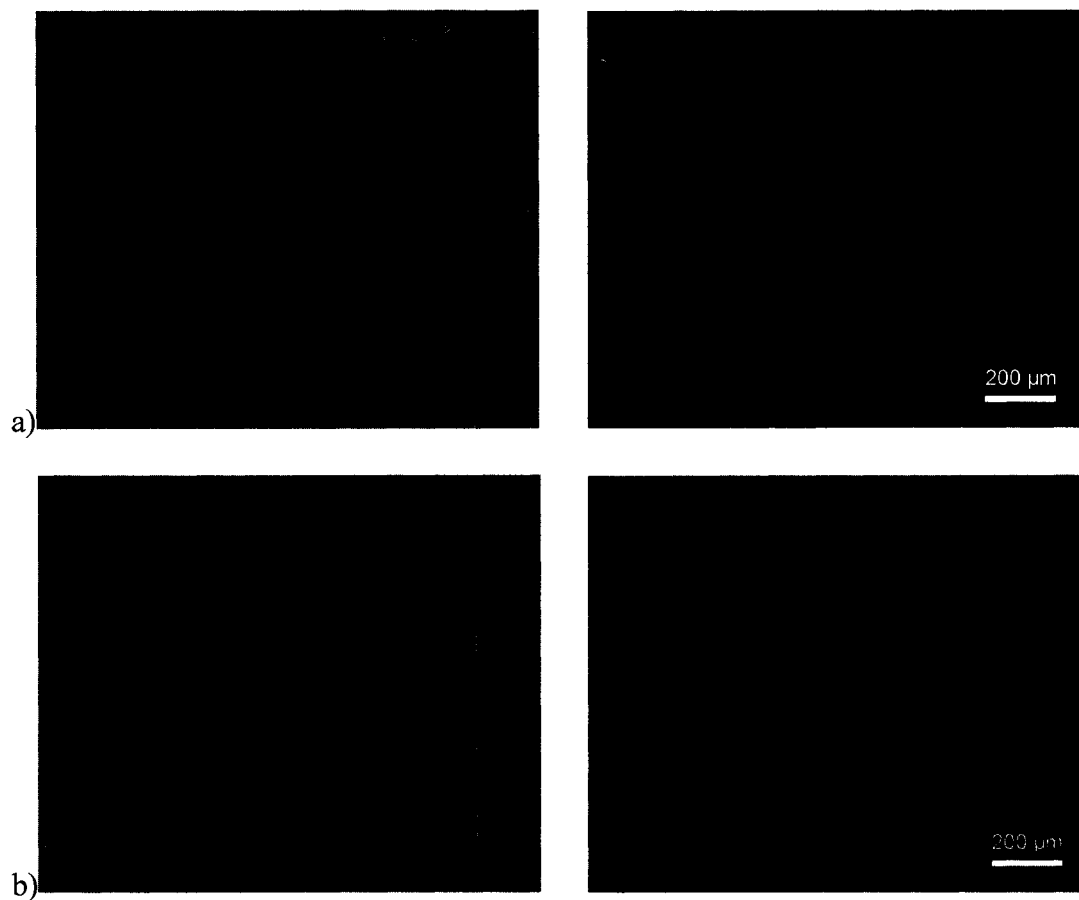


Figure IV-30. Bright field (left image) and fluorescence (right image) of a) 0.20 wt% AvP2 hydrogels containing FITC-dextran formed by crosslinking with 5 mM CaCl_2 and b) 0.20 wt% hydrogels formed after 2 h of exposure to 0.15 M NaCl. The line seen in image *a* is the sample edge, with the sample lying to the left.

CHAPTER V

CONCLUSIONS

An anionic polysaccharide AvP isolated from the *Aloe vera* plant and belonging to the class of pectins has been studied in order to relate the chemical composition and structure to solution properties. It has been shown that this high molecular weight pectin with polysaccharide composition of 95% galacturonic acid with a 3.0% degree of methylation exhibits properties including high chain stiffness, and calcium responsiveness of significant potential in *in situ* gelation. Solution studies in 0.10 M NaCl have revealed intrinsic viscosities ranging from 19.8 to 8.0 dL/g depending on MW. Subsequent calculations of persistence length yield values between 153 and 170 Å and the Mark-Houwink a value is found to range from 0.71 to 0.76, indicating an extended coil conformation in solution. Viscosity studies as a function of salt concentration allowed calculation of a stiffness parameter B of ~ 0.04 , indicating an inflexible polymer backbone. Zeta potential measurements indicate that at salt concentrations of 0.10 M, significant shielding of the polyion charge occurs, allowing for a greater degree of intra and intermolecular association. Examination of the zero shear viscosity of AvP in water and in 0.10 M NaCl reveals that intermolecular interactions are more prevalent in the latter case, as is indicated by a shift in the critical entanglement concentration (C_e). Finally, the ability of AvP to form strong gels at low polymer (0.20 wt%) and Ca^{2+} (<10 mM) concentrations has been demonstrated, indicating the potential for AvP to impart *in-situ* gelling functionality in drug delivery systems.

The *Aloe vera* polysaccharide has been shown to form hydrogels that can be easily tailored for delivery of therapeutic agents when crosslinked by calcium ions.

Hydrogel elastic modulus is independent of AvP molecular weight over the range of 200-500 kDa. However, viscoelastic properties are dependent upon the concentration of AvP2 and Ca^{2+} in solution, and are also affected by monovalent electrolyte concentrations in AvP2 solutions prior to Ca^{2+} gelation. Values of G' ranging from 20-20,000 Pa can be obtained by varying the polymer concentration, the ratio of Ca^{2+} to COO^- and ionic strength.

As evidenced by changes in the value of the Huggins constant with monovalent electrolyte addition, segmental association of AvP occurs in both a concentration and time dependent manner. Above concentrations of 0.15 M NaCl, phase separation occurs in both dilute and concentrated (near C^*) AvP solutions. The observed increase in modulus values for gels formed in the presence of monovalent electrolytes is attributed to changes in chain stiffness and solvation, as well as local segmental associations formed prior to Ca^{2+} induced gelation. A simplistic model (depicted in Figure IV-25 2) has been proposed describing these matrix changes based on viscoelastic behavior, PFG-NMR studies of water diffusion, and controlled release of fluorescein labeled dextrans of known hydrodynamic volume. The increased surface to volume ratio and tortuosity in the segmentally dense regions of the crosslinked matrices appear to be the factors contributing to the experimentally observed release behavior.

Factors such as polymer stability and hydrogel morphology are important when considering the design of protein delivery systems. Experimental evidence suggests that addition of monovalent salts to AvP formulations prior to gelation may be beneficial, increasing elastic modulus and tortuosity while reducing release rates. However, concentrations must be relatively low since high ionic strengths cause phase separation

and inhibit Ca^{2+} induced gelation. Considering these results, it is clear that salt and polymer concentrations must be judiciously chosen when formulating an *in situ* gelling therapeutic delivery system. It is recommended that an ionic strength less than 0.10 M is maintained when AvP concentrations are above 0.10 wt% in order to prevent large scale phase separation and inhibition of Ca^{2+} crosslinking. In addition to providing stability and long shelf life, a delivery formulation must also release a precise quantity of protein over a given time interval. Optimal conditions for AvP mediated release involve polymer concentrations above C_e (0.60 wt%), $[\text{Ca}^{2+}]/[\text{COO}^-]$ ratios that are less than 1, and solutions at moderate ionic strength.

CHAPTER VI

RECOMMENDATIONS FOR FUTURE RESEARCH

The study of AvP structure, solution behavior and hydrogel properties reported in this thesis provides a foundation upon which drug delivery systems may be designed and future studies can be based. The viscoelastic nature of AvP hydrogels, observed diffusion profiles and optical micrographs have been utilized to gain insight into the network characteristics of AvP hydrogels. However, supporting techniques such as cryogenic-TEM and small angle neutron scattering could be utilized to further elucidate the detailed structure of AvP networks. Additionally, studies regarding the release of model therapeutic compounds were limited the work thus far and should be expanded to include proteins of clinical interest. Examining the release of proteins will require consideration of additional factors including electrostatic interactions, and, as such, it may be beneficial to examine the release of charged model nanoparticles. For example, sulfonated polystyrene nanospheres of various diameter and surface charge ratio could be readily purchased and used to diagnose whether hydrodynamic or electrostatic effects dominate diffusion from AvP matrixes.

Studies presented in this thesis also point to potential issues concerning the stability of AvP in aqueous media at an ionic strength greater than 0.10 M. While this may not prove to be detrimental to the performance of AvP in drug delivery systems, it may be beneficial to investigate hydrophilic modification of AvP. Hydrophilic modification will certainly alleviate solubility issues and may reduce release rates by increasing the local viscosity within aqueous hydrogel domains. Recently, Banthia *et al.*¹⁸⁷ have shown that pectins may be hydrophilically modified using a grafting from

approach. Utilizing controlled radical polymerization techniques particularly, reversible addition fragmentation chain transfer (RAFT) it may be possible to easily synthesize hydrophilically modified AvP containing side chains with end group functionality amenable to bioconjugation.

APPENDIX A

SUPPLEMENTAL INFORMATION CHAPTER IV

STRUCTURAL CHARACTERIZATION AND SOLUTION PROPERTIES OF A
GALACTURONATE POLSACCHARIDE DERIVED FROM *ALOE VERA* CAPABLE
OF *IN SITU* GELATION

Size exclusion chromatography with multi angle laser light scattering.

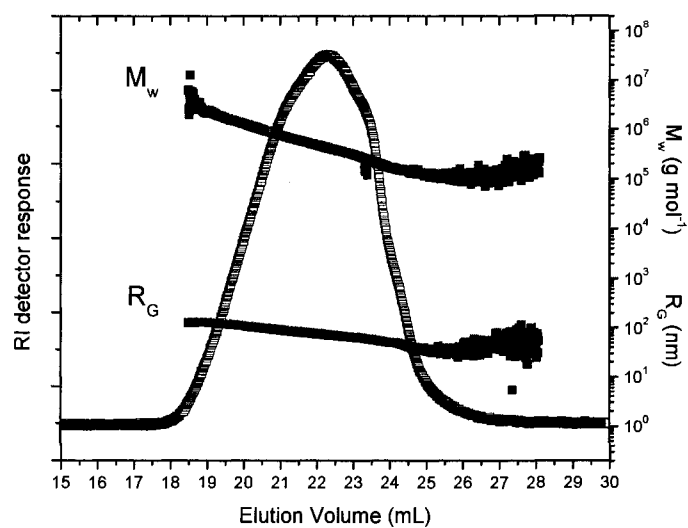


Figure A-1. SEC-MALLS trace of AvP4 including molecular weight (M_w) and radius of gyration (R_g) analysis.

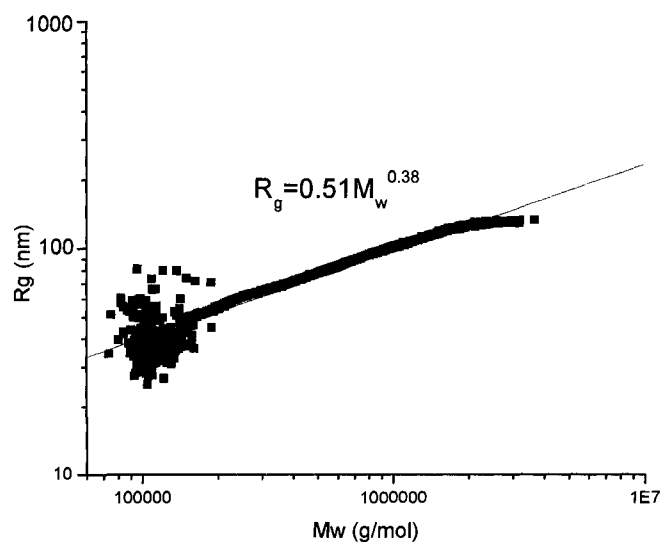


Figure A-2. SEC-MALLS trace of AvP4 depicting radius of gyration (R_g) as a function of molecular weight (M_w).

1H NMR. The degree of methylation (DM) along the galacturonic acid backbone is closely related to the sensitivity of the pectin towards gelation in the presence of divalent cations.¹¹⁴ Various methods have been applied in the determination of the DM including; titration, capillary electrophoresis, liquid chromatography coupled with mass spectrometry (LC-MS), and proton NMR. 1H NMR represents a quantitative, non-destructive technique for analyzing the DM of pectins. 1H NMR is particularly advantageous in the case where the DM of the pectin species is low and the accuracy of LC-MS techniques can be questioned.

1H NMR spectroscopy has proven to be a valuable tool in the complete structural determination and conformational assignment oligosaccharides derived from pectins. Grasdalen *et. al.*¹¹⁵⁻¹¹⁷ utilized 1H NMR to analyze the sequence of free galacturonic acid and methyl ester content in tri- and tetrameric pectin fragments. Additionally, 1H NMR may be utilized to determine the macroscopic or average DM of a pectin sample.

One of the primary methods for the determination of DM by ^1H NMR involves analysis the H-1 and H-5 protons. The H-5 proton peak is shifted downfield when the carboxylic acid on carbon 5 is converted to a methyl ester. This results in two separate peaks for H-5 protons, the one located adjacent to a carboxylic acid (COO^-) and that adjacent to a methyl ester (COOMe). Unfortunately direct resolution of the H-5 (COOMe) is not achievable because the peak location corresponds with that of the H-1 proton.¹¹⁴ However, this is dealt with utilizing the fact the number of H-1 protons equals the sum of H-5 protons adjacent to both ester and carboxylic acid groups.

$$H1 = H5_{me} + H5_{COO}$$

Where the DM is defined by the following equation;

$$DM = \frac{\int H5_{COO^-}}{\int H5_{COO^-} + \int H5_{me}}$$

Following algebraic manipulation and substitution;

$$DM = \frac{\int (H1 + H5_{me}) - \int H5_{COO^-}}{\int (H1 + H5_{me}) + \int H5_{COO^-}}$$

In a study involving a series of systematically de-esterified pectins, ^1H NMR has been found to agree with DM values determined via standard titration methods, exhibiting a correlation of 0.95 as determined by a least squares fit.¹¹⁴ All experiments were conducted at 80°C , in order to shift the HOD signal upfield and provide resolution of the H5 peak; chemical shifts were determined using the HOD peak as a reference which is known to be a function of temperature (3.385 ppm at 80°C).⁹³ Peak analysis and integration were conducted using MestReC 4.7.0 software. Fourier transform was performed on the raw data; the data was then subjected to a polynomial baseline

correction. Peaks were fit using lorentzian curves and integration widths were defined manually for each spectrum according to appearance. The spectra for each of AvP sample are provided below, and the results are summarized in Table A-1.

Table A-1. Integrals of ^1H NMR peaks and calculated values of degree of methylation (DM).

Sample	Mw (kDa)	Peak		
		H1 + H5	H5	DM
AvP1	523	1.00	0.90	5.3%
AvP2	435	1.00	0.90	5.3%
AvP3	405	1.00	0.97	1.5%
AvP4	330	1.00	0.96	2.0%
AvP5	200	1.00	0.88	6.4%

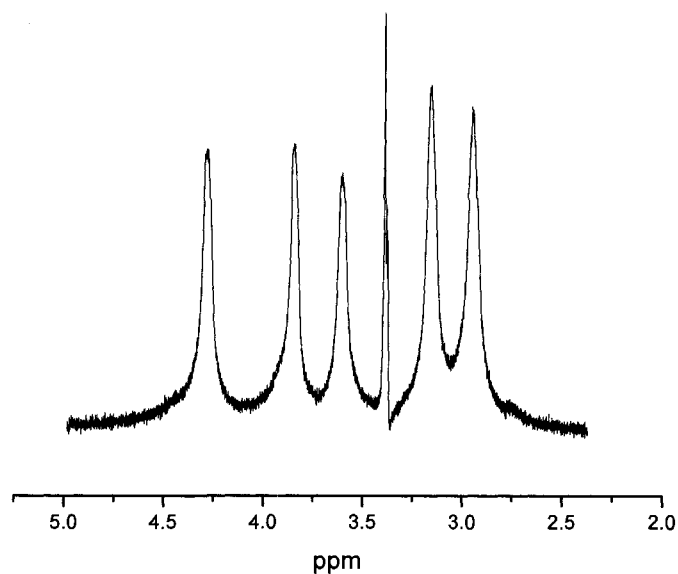


Figure A-3. ^1H NMR spectrum of AvP1, obtained using HOD suppression techniques on a 500 MHz NMR spectrometer.

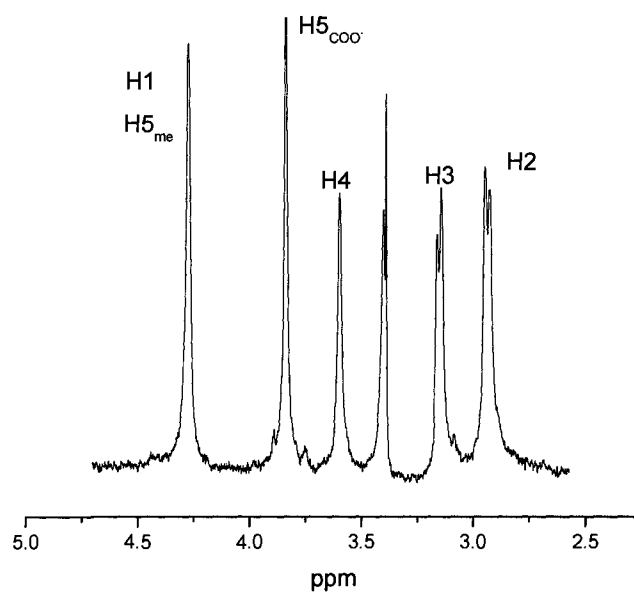


Figure A-4. ^1H NMR spectrum of AvP2, obtained using HOD suppression techniques on a 500 MHz NMR spectrometer.

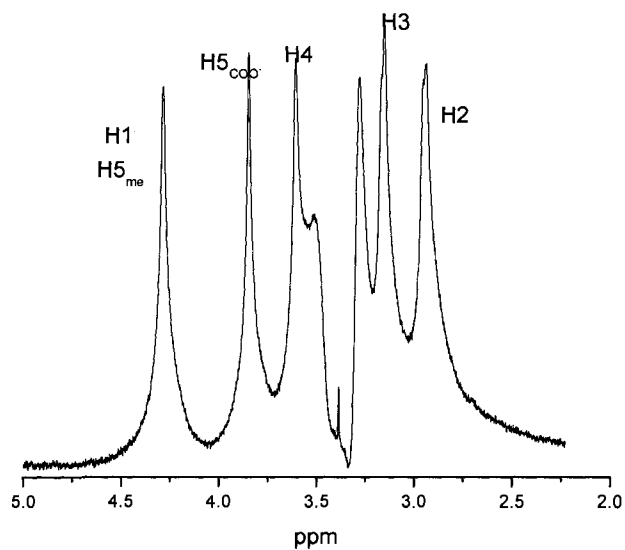


Figure A-5. ^1H NMR spectrum of AvP4, obtained using HOD suppression techniques on a 500 MHz NMR spectrometer.

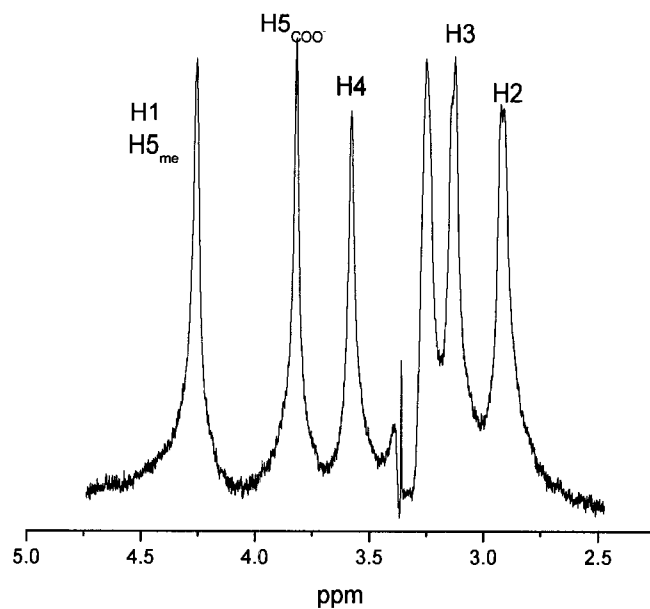


Figure A-6. ^1H NMR spectrum of AvP5, obtained using HOD suppression techniques on a 500 MHz NMR spectrometer.

Determination of intrinsic viscosity.

The following figures were constructed to determine the intrinsic viscosity values shown in Table IV-2.

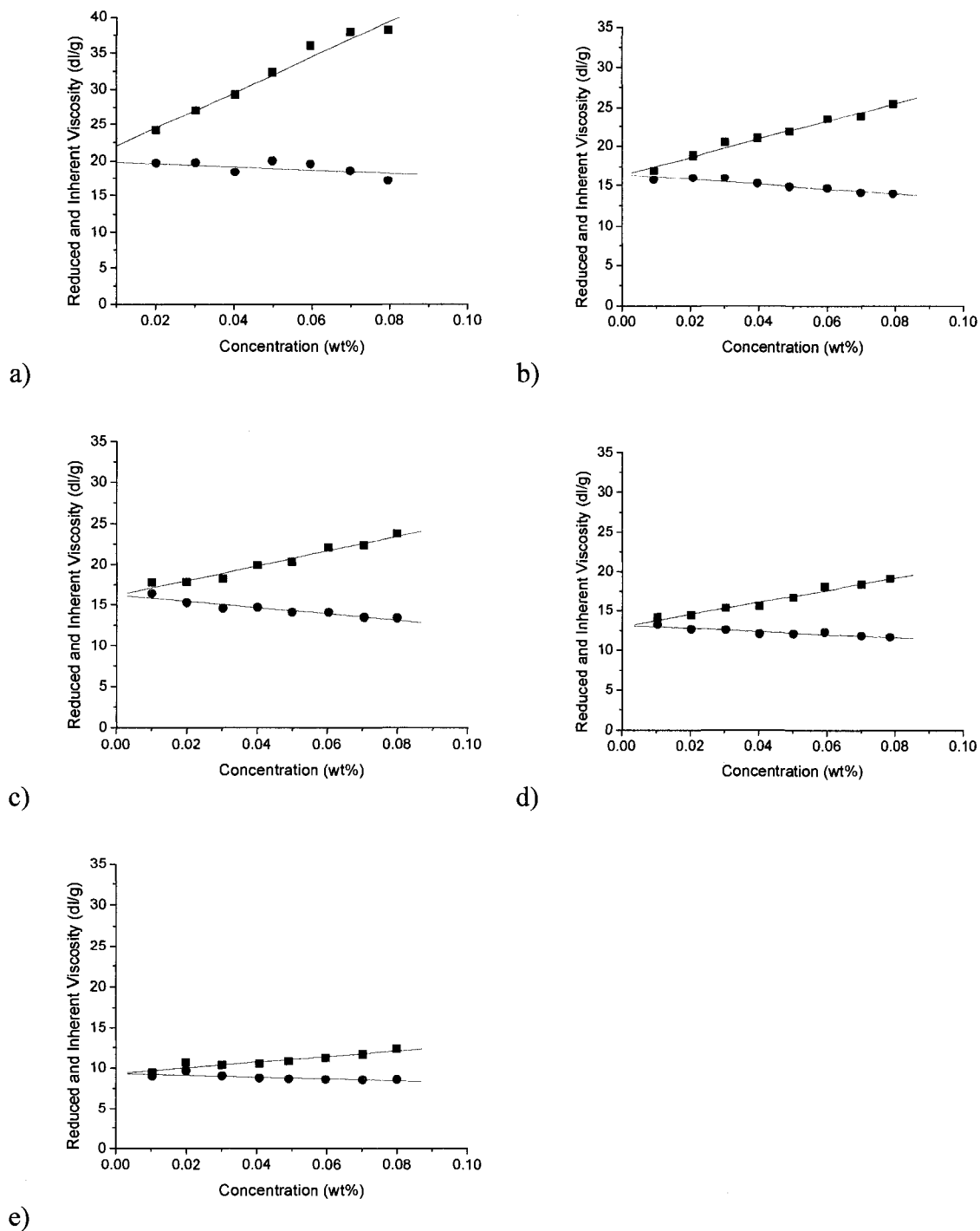


Figure A-7. Huggins (■) and Kraemer (●) plots, illustrated for a) AvP1, b) AvP2, c) AvP3, d) AvP4, e) AvP5 in 0.05 M NaCl.

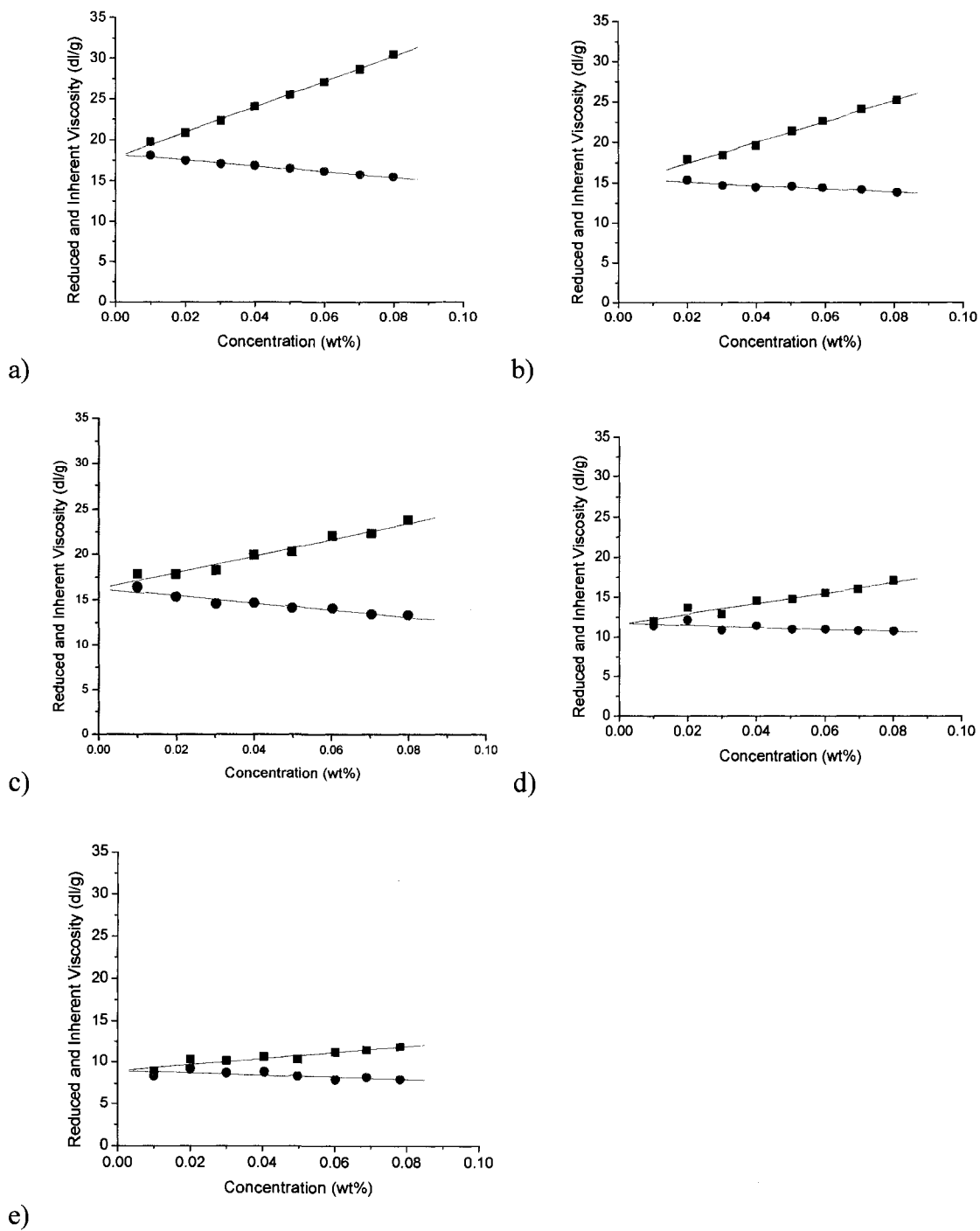


Figure A-8. Huggins (■) and Kraemer (●) plots, illustrated for a) AvP1, b) AvP2, c) AvP3, d) AvP4, e) AvP5 in 0.10 M NaCl.

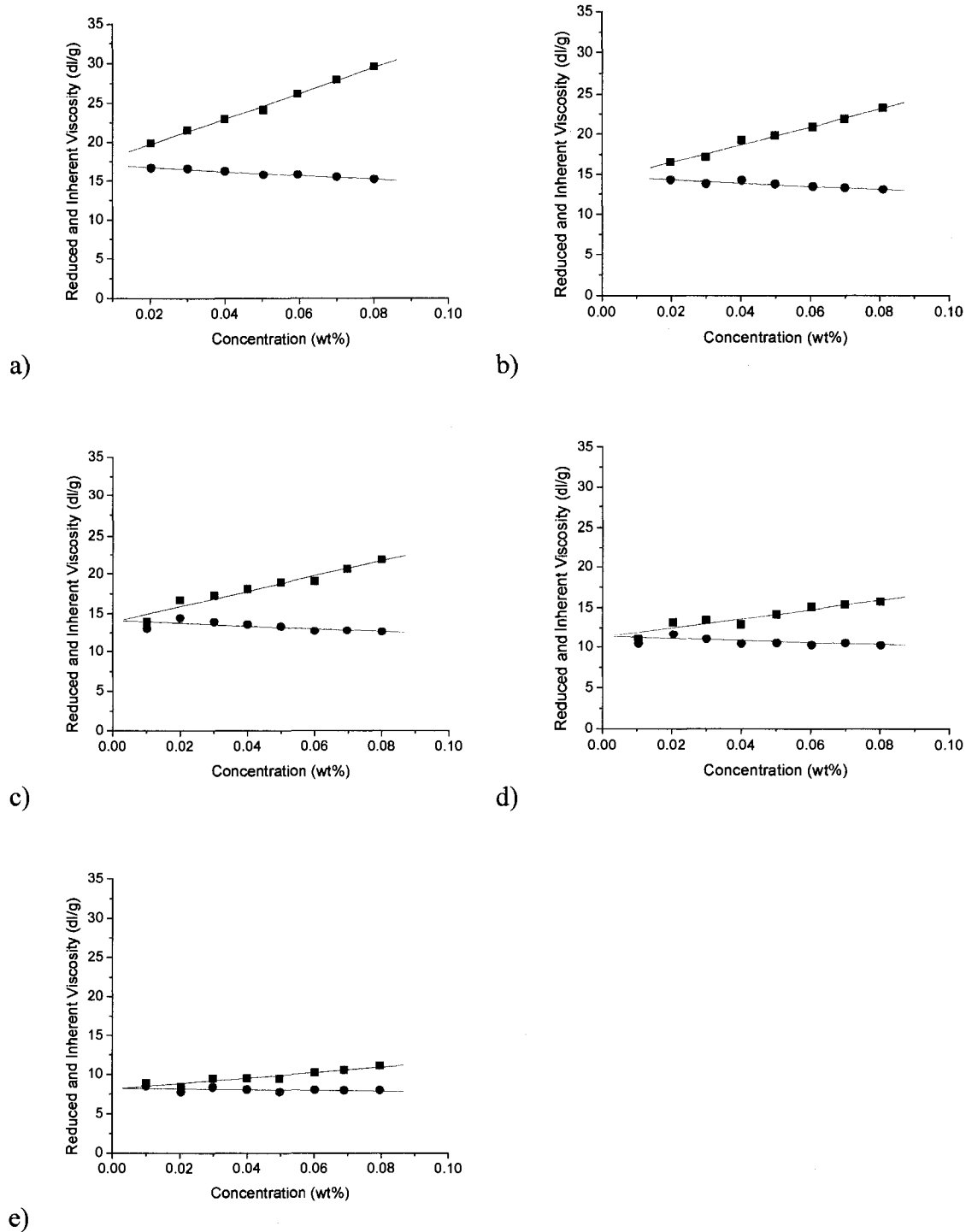


Figure A-9. Huggins (■) and Kraemer (●) plots, illustrated for a) AvP1, b) AvP2, c) AvP3, d) AvP4, e) AvP5 in 0.15 M NaCl.

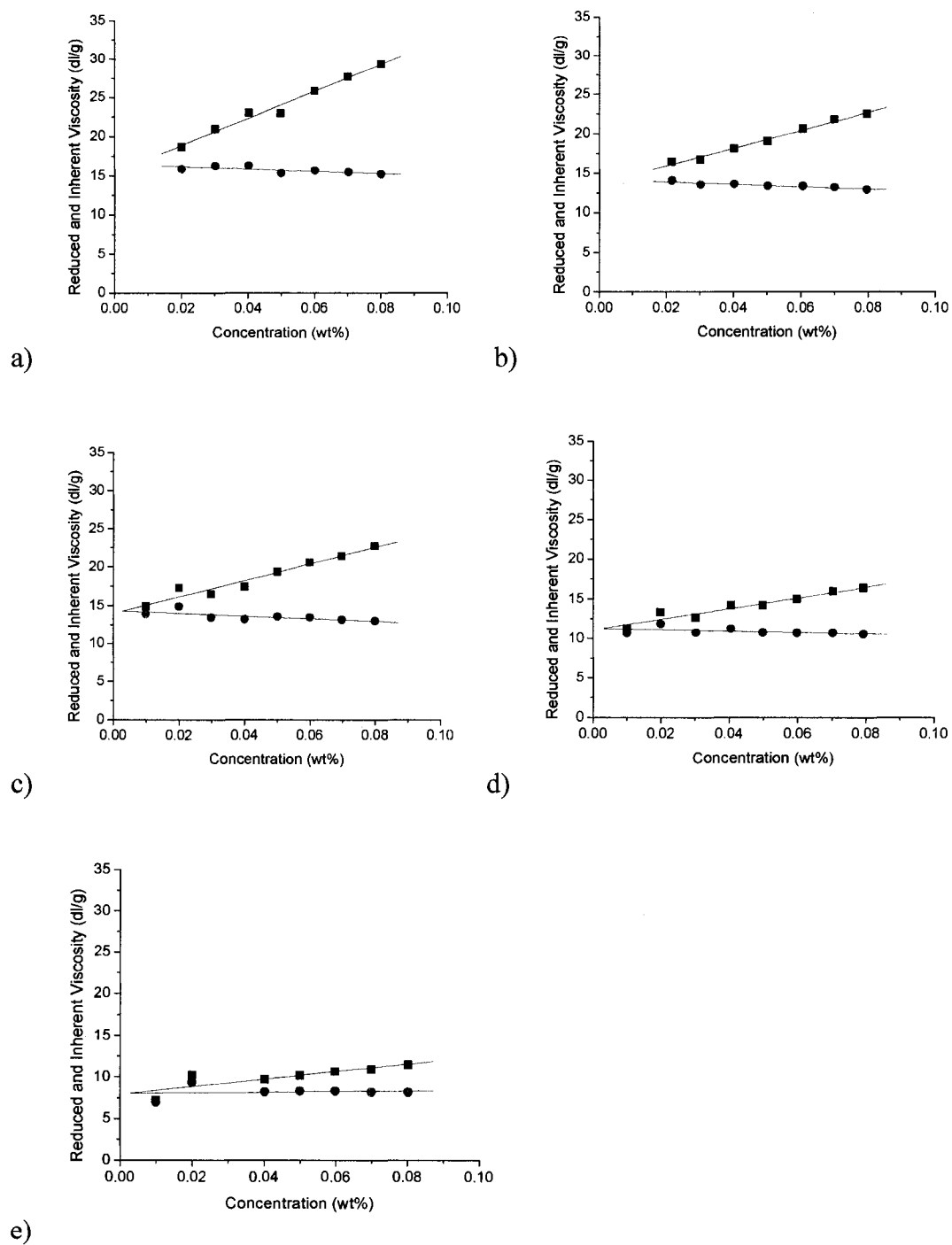


Figure A-10. Huggins (■) and Kraemer (●) plots, illustrated for a) AvP1, b) AvP2, c) AvP3, d) AvP4, e) AvP5 in 0.20 M NaCl.

Persistence length calculations. The persistence length (L_p) of AvP was calculated utilizing both the Yamakawa-Fuji¹²⁴ and Bohandecy¹²⁹ methods, as outlined in Chapter IV Section A. In order to calculate L_p , simultaneous equations must be solved in an iterative manner. Yamakawa-Fuji analysis was conducted utilizing a Mathcad program written by Dr. Roger Hester. Bohandecy analysis was conducted utilizing a Mathcad program written by Shawn McConaughy and Adam Smith. Transcripts of each program are provided on the following pages.

One interesting observation that came from the Bohandecy analysis is that the electrostatic expansion factor (α) passes through a minimum when examined as a function of the Mark-Houwink coefficient (a). The minimum α value (~ 1.03) corresponds to an a value of approximately 0.63, suggesting that electrostatic expansion is negligible when an expanded coil conformation is present.

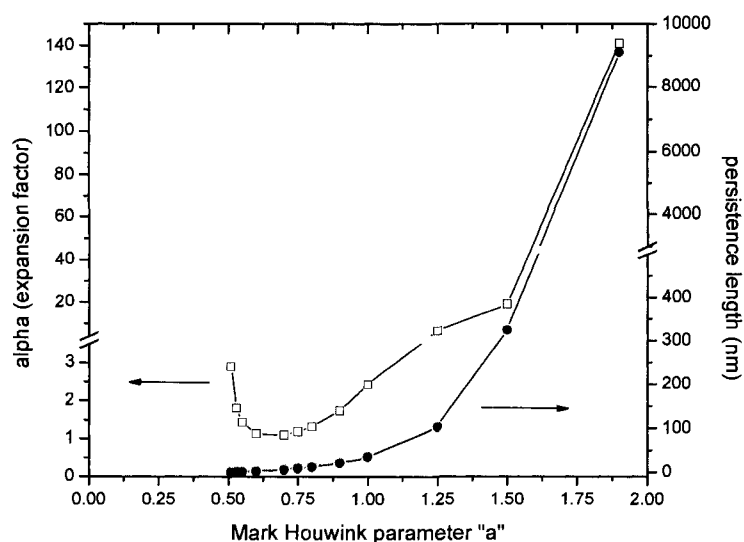


Figure AI-11. Determination of electrostatic expansion factor (α) and persistence length as a function of the Mark Houwink parameter “a”.

L_p calculation based on the Yamakawa-Fuji Mathcad program:

Mathcad file name: YamakawaFloryConstantCorrection2001Mathcad

See H. Yamakawa & M. Fujii, *Macromolecules*, 7, (1), 128-35 (1974)

For $0.10 < d < 1.0$ and $L > 2.278$ *RDH 9/25/03*

$$\Phi_0 := 2.87 \cdot \frac{10^{23}}{\text{mole}} \quad \text{Ang} := 10^{-10} \cdot \text{m} \quad dL := 100 \cdot \text{mL}$$

$$C1(d) := \left(0.120367 + 0.220714 \cdot d + 4.36037 \cdot d^2 - 6.99899 \cdot d^3 + 7.94714 \cdot d^4 \right) \dots \\ + \left(2.16769 - 12.5326 \cdot d^2 - 0.293796 \cdot d^4 \right) \cdot \ln(d)$$

$$C2(d) := \left(1.30917 + 129.550 \cdot d + 96.9912 \cdot d^2 - 435.952 \cdot d^3 \right) \dots \\ + 126.457 \cdot d^4 - \left(3.92040 - 413.189 \cdot d^2 - 4.94474 \cdot d^4 \right) \cdot \ln(d)$$

$$C3(d) := \left(161.109 - 4926.443 \cdot d - 43988.8 \cdot d^2 + 78765.85 \cdot d^3 - 29296.43 \cdot d^4 \right) \dots \\ + \left(40.1861 - 31548.53 \cdot d^2 - 38.3938 \cdot d^4 \right) \cdot \ln(d)$$

*<= Changed 4398.88
to 43988.8
to get closer
to Table values
in Yamakawa-Fuji paper.*

$$C4(d) := \left(-582.038 + 16873.42 \cdot d + 159994.7 \cdot d^2 - 273427.7 \cdot d^3 + 85028.34 \cdot d^4 \right) \dots \\ + (-1) \cdot \left(102.876 - 113150.70 \cdot d^2 - 88.8684 \cdot d^4 \right) \cdot \ln(d)$$

For $d < 0.1$ and $L > 2.278$

$$c1(d) := 3.230981 - 143.7458 \cdot d - 1906.263 \cdot d^2 + \left(2.463404 - 1422.067 \cdot d^2 \right) \cdot \ln(d)$$

$$c2(d) := -22.46149 + 1347.079 \cdot d + 19387.400 \cdot d^2 + \left(-5.318869 + 13868.57 \cdot d^2 \right) \cdot \ln(d)$$

$$c3(d) := 54.81690 - 3235.401 \cdot d - 49357.06 \cdot d^2 + \left(15.41744 - 34447.63 \cdot d^2 \right) \cdot \ln(d)$$

$$c4(d) := -32.91952 + 2306.793 \cdot d + 36732.64 \cdot d^2 + \left(-8.516339 + 25198.11 \cdot d^2 \right) \cdot \ln(d)$$

$$\text{Correction}\alpha(d, L) := \frac{1}{1 - \frac{c1(d)}{\frac{1}{L^2}} - \frac{c2(d)}{\frac{2}{L^2}} - \frac{c3(d)}{\frac{3}{L^2}} - \frac{c4(d)}{\frac{4}{L^2}}} \quad \leq \text{For } d < 0.1 \text{ and } L > 2.278$$

$$\text{Correction}\lambda(d, L) := \frac{1}{1 - \frac{C1(d)}{\frac{1}{L^2}} - \frac{C2(d)}{\frac{2}{L^2}} - \frac{C3(d)}{\frac{3}{L^2}} - \frac{C4(d)}{\frac{4}{L^2}}} \quad \leq \text{For } 0.10 < d < 1.0 \text{ and } L > 2.278$$

$$\Phi(d, L) := \Phi_0 \bullet \text{if}(d \geq 0.1, \text{CorrectionI}(d, L), \text{CorrectionZ}(d, L))$$

<= table values

$\Phi(1, 10^4) = \blacksquare$	$\Phi(1, 10^3) = \blacksquare$	$\Phi(1, 200) = \blacksquare$
3.01	3.25	3.86
$\Phi(0.8, 10^6) = \blacksquare$	$\Phi(0.8, 4000) = \blacksquare$	$\Phi(0.8, 200) = \blacksquare$
2.88	3.02	3.42
$\Phi(0.6, 10^6) = \blacksquare$	$\Phi(0.6, 4000) = \blacksquare$	$\Phi(0.6, 100) = \blacksquare$
2.88	2.97	3.23
$\Phi(0.4, 10^6) = \blacksquare$	$\Phi(0.4, 1000) = \blacksquare$	$\Phi(0.4, 100) = \blacksquare$
2.87	2.88	2.73
$\Phi(0.15, 10^6) = \blacksquare$	$\Phi(0.15, 4000) = \blacksquare$	$\Phi(0.15, 50) = \blacksquare$
2.86	2.75	2.08
$\Phi(0.1, 10^4) = \blacksquare$	$\Phi(0.1, 1000) = \blacksquare$	$\Phi(0.1, 20) = \blacksquare$
2.76	2.57	1.63

<= table values

$\Phi(0.06, 10^4) = \blacksquare$	$\Phi(0.06, 10^3) = \blacksquare$	$\Phi(0.06, 100) = \blacksquare$
2.70	2.45	1.95
$\Phi(0.03, 10^4) = \blacksquare$	$\Phi(0.03, 100) = \blacksquare$	$\Phi(0.03, 10) = \blacksquare$
2.67	1.78	0.95
$\Phi(0.01, 4000) = \blacksquare$	$\Phi(0.01, 100) = \blacksquare$	$\Phi(0.01, 10) = \blacksquare$
2.47	1.57	0.765
$\Phi(0.001, 10^6) = \blacksquare$	$\Phi(0.001, 1000) = \blacksquare$	$\Phi(0.001, 100) = \blacksquare$
2.82	1.96	1.26

$$i := 0..100$$

$$j := 0..100$$

$$dd_i := 0.1 + \frac{0.9}{100} \cdot i$$

$$LL_j := 5 + \frac{495}{100} \cdot j$$

$$MM_{i,j} := \frac{\Phi(dd_i, LL_j)}{10^{23}}$$

$$L = \frac{L_{contour}}{2 \cdot q}$$

$$d = \frac{d_{polymer}}{2 \cdot q}$$

$$\max(MM) = 3.35 \text{ mol}^{-1}$$

$$dd_{76} = 0.784$$

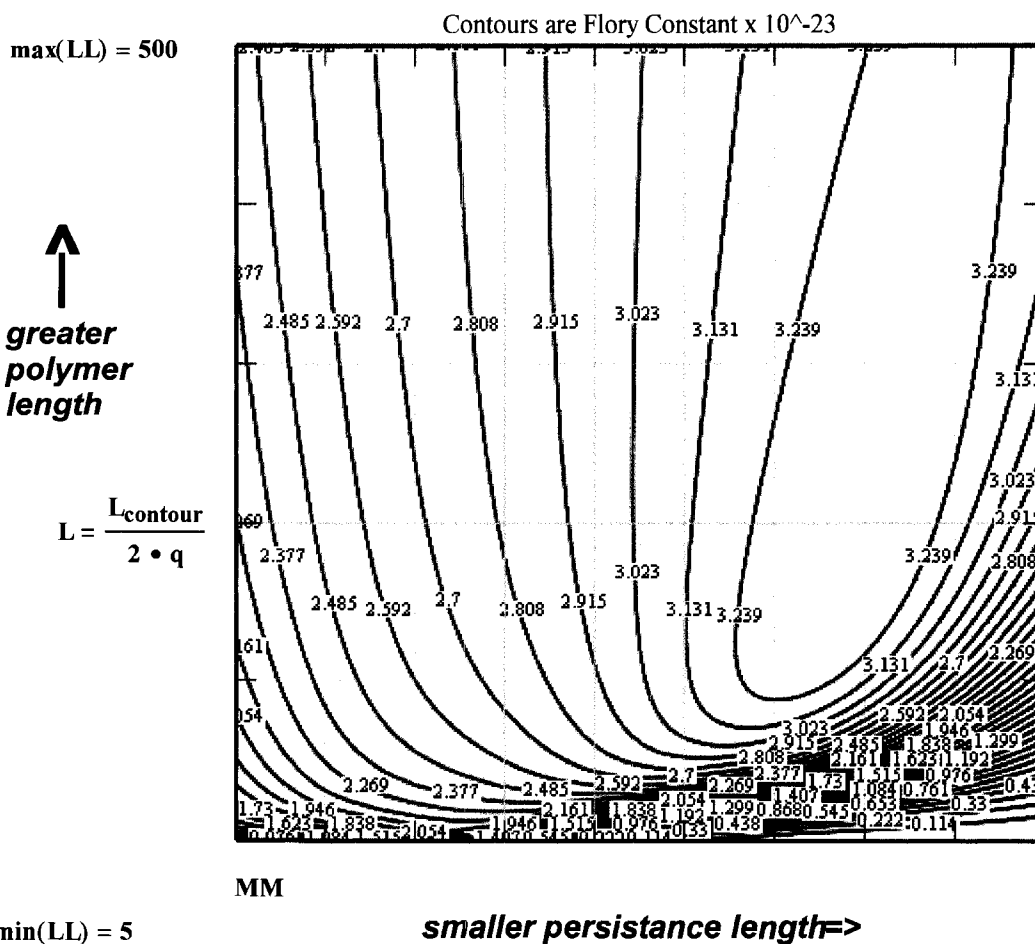
$$LL_{35} = 178.3$$

$$MM_{76,35} = 3.35 \text{ mol}^{-1}$$

$L_{contour}$ = polymer contour length

$d_{polymer}$ = polymer chain diameter

q = persistence length



$$\min(dd) = 0.10$$

$$d = \frac{d_{polymer}}{2 \cdot q}$$

$$\max(dd) = 1.00$$

q is the persistence length

```

FloryPhi(eta, Mpolymer, Mmonomer, Lmonomer, Dpolymer) :=
  Lcontour ←  $\frac{M_{\text{polymer}}}{M_{\text{monomer}}} \cdot L_{\text{monomer}}$ 
  PhiPhi_0 ←  $2.87 \cdot \frac{10^{23}}{\text{mole}}$ 
  q_0 ←  $\eta \cdot \frac{\frac{2}{3} \cdot M_{\text{monomer}}}{2 \cdot L_{\text{monomer}}} \cdot \frac{1}{(\text{PhiPhi}_0)^{\frac{2}{3}} \cdot M_{\text{polymer}}^{\frac{1}{3}}}$ 
  GG_0,0 ← PhiPhi_0 • mole
  GG_0,1 ←  $\frac{q_0}{\text{Ang}}$ 
  for i ∈ 0..100
    L_i ←  $\frac{L_{\text{contour}}}{2 \cdot q_i}$ 
    d_i ←  $\frac{D_{\text{polymer}}}{2 \cdot q_i}$ 
    PhiPhi_{i+1} ← Phi(d_i, L_i)
    GG_{i+1,0} ← PhiPhi_{i+1} • mole
    GG_{i+1,0} ← 0 if d_i ≥ 1.0
    GG_{i+1,0} ← 0 if L_i < 2.28
    q_{i+1} ←  $\eta \cdot \frac{\frac{2}{3} \cdot M_{\text{monomer}}}{2 \cdot L_{\text{monomer}}} \cdot \frac{1}{(\text{PhiPhi}_{i+1})^{\frac{2}{3}} \cdot M_{\text{polymer}}^{\frac{1}{3}}}$ 
    GG_{i+1,1} ←  $\frac{q_{i+1}}{\text{Ang}}$ 
    GG_{i+1,1} ← 0 if d_i ≥ 1.0
    GG_{i+1,1} ← 0 if L_i < 2.28
    break if d_i ≥ 1.0
    break if L_i < 2.28
    break if  $\frac{|\text{PhiPhi}_{i+1} - \text{PhiPhi}_i|}{\text{PhiPhi}_i} \leq 0.001$ 
  GG

```

Note that the final elements in the GG matrix are zero if d becomes greater than 1 or if L becomes less than 2.28

AvP1 - in 0.10 M NaCl

$$q_{\text{new}} := \text{Flory}\Phi \left(18.0 \cdot \frac{\text{dL}}{\text{gm}}, 5.23 \cdot 10^5 \cdot \frac{\text{gm}}{\text{mole}}, 198 \cdot \frac{\text{gm}}{\text{mole}}, 4.35 \cdot \text{Ang}, 7 \cdot \text{Ang} \right)^{\langle 1 \rangle} \cdot \text{Ang}$$

$$\Phi_{\text{new}} := \text{Flory}\Phi \left(18.0 \cdot \frac{\text{dL}}{\text{gm}}, 5.23 \cdot 10^5 \cdot \frac{\text{gm}}{\text{mole}}, 198 \cdot \frac{\text{gm}}{\text{mole}}, 4.35 \cdot \text{Ang}, 7 \cdot \text{Ang} \right)^{\langle 0 \rangle} \cdot \frac{1}{\text{mole}}$$

$$q_{\text{new}} = \blacksquare \text{Ang} \qquad \frac{\Phi_{\text{new}}}{10^{23}} = \blacksquare$$

AvP2 - in 0.10 M NaCl

$$q_{\text{new}} := \text{Flory}\Phi \left(15.2 \cdot \frac{\text{dL}}{\text{gm}}, 4.35 \cdot 10^5 \cdot \frac{\text{gm}}{\text{mole}}, 198 \cdot \frac{\text{gm}}{\text{mole}}, 4.35 \cdot \text{Ang}, 7 \cdot \text{Ang} \right)^{\langle 1 \rangle} \cdot \text{Ang}$$

$$\Phi_{\text{new}} := \text{Flory}\Phi \left(15.2 \cdot \frac{\text{dL}}{\text{gm}}, 4.35 \cdot 10^5 \cdot \frac{\text{gm}}{\text{mole}}, 198 \cdot \frac{\text{gm}}{\text{mole}}, 4.35 \cdot \text{Ang}, 7 \cdot \text{Ang} \right)^{\langle 0 \rangle} \cdot \frac{1}{\text{mole}}$$

$$q_{\text{new}} = \blacksquare \text{Ang} \qquad \frac{\Phi_{\text{new}}}{10^{23}} = \blacksquare$$

AvP3 - in 0.10 M NaCl

$$q_{\text{new}} := \text{Flory}\Phi \left(15.0 \cdot \frac{\text{dL}}{\text{gm}}, 4.05 \cdot 10^5 \cdot \frac{\text{gm}}{\text{mole}}, 198 \cdot \frac{\text{gm}}{\text{mole}}, 4.35 \cdot \text{Ang}, 7 \cdot \text{Ang} \right)^{\langle 1 \rangle} \cdot \text{Ang}$$

$$\Phi_{\text{new}} := \text{Flory}\Phi \left(15.0 \cdot \frac{\text{dL}}{\text{gm}}, 4.05 \cdot 10^5 \cdot \frac{\text{gm}}{\text{mole}}, 198 \cdot \frac{\text{gm}}{\text{mole}}, 4.35 \cdot \text{Ang}, 7 \cdot \text{Ang} \right)^{\langle 0 \rangle} \cdot \frac{1}{\text{mole}}$$

$$q_{\text{new}} = \begin{pmatrix} 92.64 \\ 137.54 \\ 152.68 \\ 157.30 \\ 158.68 \\ 159.09 \\ 159.21 \\ 159.25 \end{pmatrix} \text{Ang} \quad \frac{\Phi_{\text{new}}}{10^{23}} = \begin{pmatrix} 2.87 \\ 1.59 \\ 1.36 \\ 1.30 \\ 1.28 \\ 1.28 \\ 1.27 \\ 1.27 \end{pmatrix} \text{mol}^{-1}$$

AvP4 - in 0.10 M NaCl

$$q_{\text{new}} := \text{Flory}\Phi \left(11.6 \cdot \frac{\text{dL}}{\text{gm}}, 3.30 \cdot 10^5 \cdot \frac{\text{gm}}{\text{mole}}, 198 \cdot \frac{\text{gm}}{\text{mole}}, 4.35 \cdot \text{Ang}, 7 \cdot \text{Ang} \right)^{\langle 1 \rangle} \cdot \text{Ang}$$

$$\Phi_{\text{new}} := \text{Flory}\Phi \left(11.6 \cdot \frac{\text{dL}}{\text{gm}}, 3.30 \cdot 10^5 \cdot \frac{\text{gm}}{\text{mole}}, 198 \cdot \frac{\text{gm}}{\text{mole}}, 4.35 \cdot \text{Ang}, 7 \cdot \text{Ang} \right)^{\langle 0 \rangle} \cdot \frac{1}{\text{mole}}$$

$$q_{\text{new}} = \begin{pmatrix} 83.57 \\ 124.45 \\ 138.69 \\ 143.19 \\ 144.57 \\ 144.99 \\ 145.12 \\ 145.16 \end{pmatrix} \text{Ang} \quad \frac{\Phi_{\text{new}}}{10^{23}} = \begin{pmatrix} 2.87 \\ 1.58 \\ 1.34 \\ 1.28 \\ 1.26 \\ 1.26 \\ 1.25 \\ 1.25 \end{pmatrix} \text{mol}^{-1}$$

AvP5 - in 0.10 M NaCl

$$q_{\text{new}} := \text{Flory}\Phi \left(9.0 \cdot \frac{\text{dL}}{\text{gm}}, 2.0 \cdot 10^5 \cdot \frac{\text{gm}}{\text{mole}}, 198 \cdot \frac{\text{gm}}{\text{mole}}, 4.35 \cdot \text{Ang}, 7 \cdot \text{Ang} \right)^{\langle 1 \rangle} \cdot \text{Ang}$$

$$\Phi_{\text{new}} := \text{Flory}\Phi \left(9.0 \cdot \frac{\text{dL}}{\text{gm}}, 2.0 \cdot 10^5 \cdot \frac{\text{gm}}{\text{mole}}, 198 \cdot \frac{\text{gm}}{\text{mole}}, 4.35 \cdot \text{Ang}, 7 \cdot \text{Ang} \right)^{\langle 0 \rangle} \cdot \frac{1}{\text{mole}}$$

$$q_{\text{new}} = \begin{pmatrix} 83.38 \\ 134.27 \\ 156.39 \\ 165.25 \\ 168.71 \\ 170.05 \\ 170.57 \\ 170.77 \\ 170.84 \end{pmatrix} \text{Ang} \quad \frac{\Phi_{\text{new}}}{10^{23}} = \begin{pmatrix} 2.87 \\ 1.40 \\ 1.12 \\ 1.03 \\ 1.00 \\ 0.99 \\ 0.98 \\ 0.98 \\ 0.98 \end{pmatrix} \text{mol}^{-1}$$

L_p calculations based on the Bohandeky calculations.

Using equations 6 - 11 Biomacromolecules, vol 4, no 6, 1805 (Mendichi *et. al.*), which is the Bohandeky method utilizing the Tsaki approximation for d (hydrodynamic diameter), additionally considering the expansion factor α which accounts for excluded volume.

Solving for q and α based on η and M data for AvP in 0.15 M NaCl

$$nm := 10^{-9} \text{ m} \quad N_A := \frac{6.02 \cdot 10^{23}}{\text{mol}}$$

$\alpha := 1.073$ as determined by sepearte analysis where M_L is known

$$v := .71 \frac{\text{cm}^3}{\text{gm}}$$

v for pectic acid (food hydrocolloids 1998, 12, 167)

$$M := \begin{pmatrix} 100000 \\ 200000 \\ 300000 \\ 400000 \\ 500000 \end{pmatrix} \frac{\text{gm}}{\text{mol}}$$

$$\eta(M) := 0.074 \cdot \left(\frac{M}{\frac{\text{gm}}{\text{mol}}} \right)^{.76} \frac{\text{cm}^3}{\text{gm}}$$

Mark-Houwink relationship for AvP in 0.15 M NaCl

Provided with;

$$\lambda^{-1} = 2q \quad d_r = \frac{d}{\lambda^{-1}}$$

Substituting into equation (9) from Mendichi

$$d_r(q, M_L) := \left[\frac{\left[\frac{(4 \cdot v \cdot M_L)}{\pi \cdot N_A} \right]^{\frac{1}{2}}}{2 \cdot q} \right]$$

Equations for A_0 and B_0 are from reference #28 (Bohdanecky) eqs 8 & 9

$$A_0(q, M_L) := .46 - .53 \log(d_r(q, M_L)) \quad A_0 = \blacksquare$$

$$B_0(q, M_L) := 1.00 - .0367 \log(d_r(q, M_L)) \quad B_0 = \blacksquare$$

Substituting A_0 and B_0 into equations (7) and (8)

$$A_\eta(q, M_L) := \left(\frac{2.86 \cdot 10^{23}}{\text{mol}} \right)^{\frac{-1}{3}} \cdot A_0(q, M_L) \cdot M_L \quad (7) \quad A_\eta = \text{function}$$

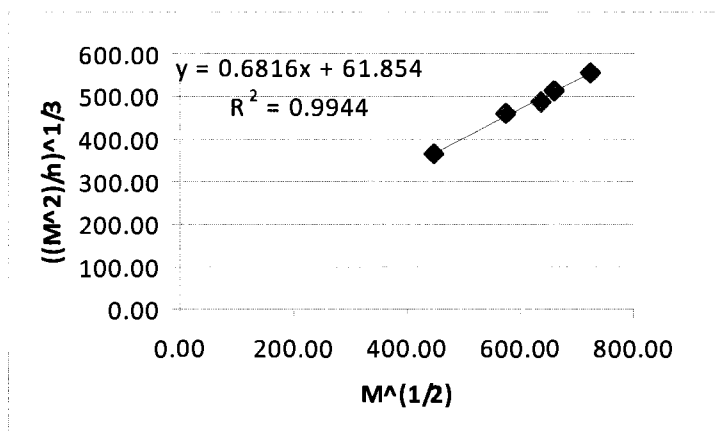
$$B_\eta(q, M_L) := \left(\frac{2.86 \cdot 10^{23}}{\text{mol}} \right)^{\frac{-1}{3}} \cdot B_0(q, M_L) \cdot \left(\frac{2q}{M_L} \right)^{\frac{-1}{2}} \quad (8) \quad B_\eta = \text{function}$$

Provided with;

$$\eta = \eta_0 \cdot \alpha_\eta^3 \quad (10)$$

$$\alpha_\eta^3 = \alpha_s^{2.43} \quad (11)$$

Molecular Weight (g/mol)	Intrinsic Viscosity (ml/g)	x	y
		$M^{(1/2)}$	$(M^2/h)^{(1/3)}$
523000	1591.47	723.19	555.99
435000	1399.62	659.55	513.24
405000	1416.23	636.40	487.44
330000	1119.99	574.46	459.84
200000	820.23	447.21	365.35



where the slope = $(B_\eta)/(\alpha^{2.43/3})$
and the intercept = $(A_\eta)/(\alpha^{2.43/3})$

$$\text{int} := \begin{pmatrix} 81.33 \\ 69.95 \\ 80.47 \\ 61.85 \end{pmatrix} \cdot \frac{\text{gm}}{\text{mol}^3 \cdot \text{cm}}$$

$$\text{slp} := \begin{pmatrix} 0.606 \\ 0.648 \\ 0.645 \\ 0.682 \end{pmatrix} \cdot \frac{\frac{1}{\text{gm}^2}}{\text{mol}^6 \cdot \text{cm}}$$

Substituting the combination of (11) and (10) into equation (6)

guess

$$M_L := 400 \frac{\text{gm}}{\text{nm}\cdot\text{mol}} \quad q := 8 \text{ nm} \quad i := 0..3$$

Given

$$\text{int}_i = \frac{\left(\frac{2.86 \cdot 10^{23}}{\text{mol}}\right)^{\frac{-1}{3}} \cdot \left[.46 - .53 \cdot \log \left[\frac{\left[\frac{(4 \cdot v \cdot M_L)^{\frac{1}{2}}}{\pi \cdot N_A} \right]^2}{2 \cdot q} \right] \right]^{\alpha \cdot .81}}{\alpha \cdot .81} \cdot (M_L)$$

$$\text{slp}_i = \frac{\left(\frac{2.86 \cdot 10^{23}}{\text{mol}}\right)^{\frac{-1}{3}} \cdot \left[1.00 - .0367 \cdot \log \left[\frac{\left[\frac{(4 \cdot v \cdot M_L)^{\frac{1}{2}}}{\pi \cdot N_A} \right]^2}{2 \cdot q} \right] \right]^{\alpha \cdot .81} \cdot \left(\frac{2 \cdot q}{M_L}\right)^{\frac{-1}{2}}}{\alpha \cdot .81}$$

$$\begin{pmatrix} M_{L_i} \\ q_i \end{pmatrix} := \text{Find}(M_L, q)$$

$M_{L_i} =$

446.051
397.834
451.344
362.224

$\frac{\text{gm}}{\text{nm}\cdot\text{mol}}$

$q_i =$

13.924
10.797
12.391
8.833

nm

Solution viscosity as a function of shear rate. The solution viscosity of AvP3 was determined as a function of shear rate and used in combination with the viscosities determined in the dilute concentration regime to create a plot of zero shear viscosity vs. polymer concentration (Figure IV-9). Shown below are the viscosity vs. shear rate profiles of AvP3 dissolved in aqueous solution and 0.10 M NaCl.

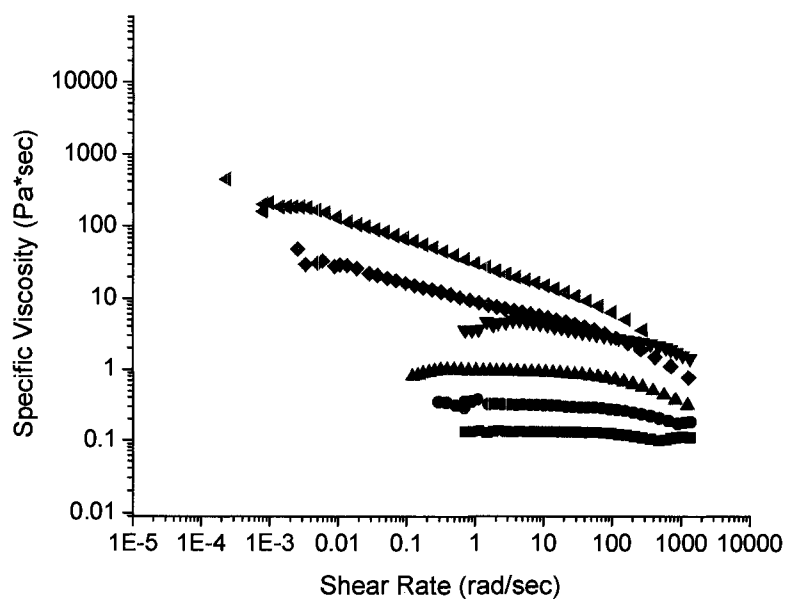


Figure A-12. Specific viscosity (Pa*sec) as a function of shear rate (rad/sec) for 0.25 (■), 0.50 (●), 0.75 (▲), 1.0 (▼), 1.25 (◆), 1.5 (◄), 1.8 (◃) wt% AvP3 samples dissolved in aqueous solutions.

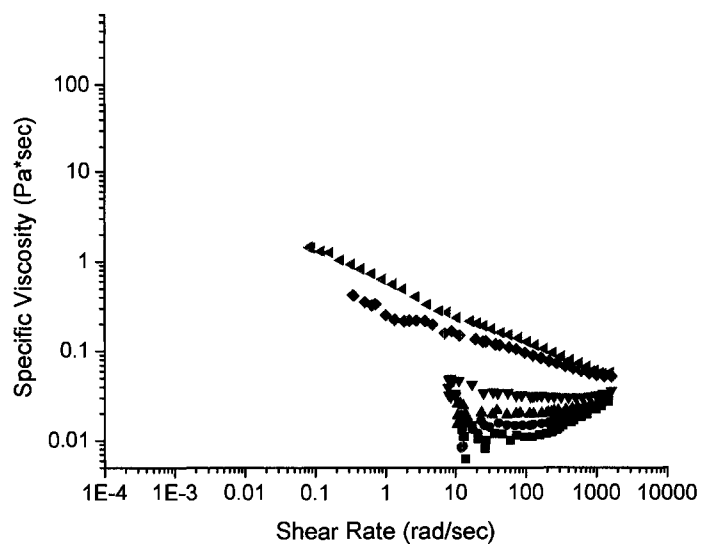


Figure A-13. Specific viscosity (Pa*sec) as a function of shear rate (rad/sec) for 0.15 (■), 0.25 (●), 0.30 (▲), 0.40 (▼), 0.50 (◆), 0.75 (◄), 0.90 () wt% AvP3 samples dissolved in 0.10 M NaCl.

In addition, dynamic oscillatory rheology was conducted on concentrated AvP aqueous solutions.

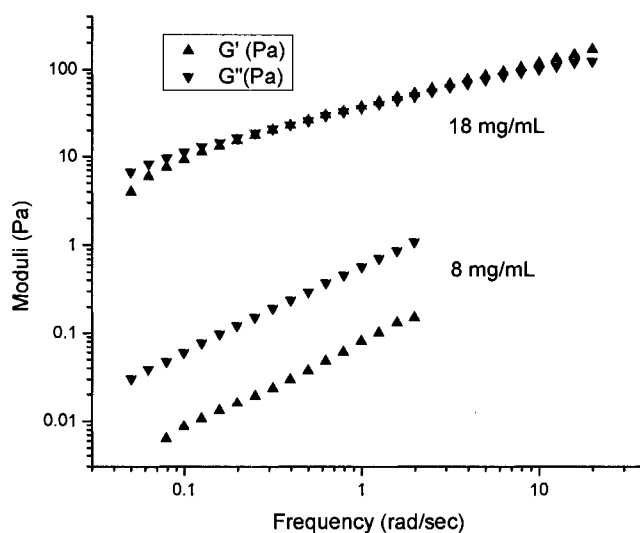


Figure A-14. Elastic and viscous modulus (Pa) as a function of frequency for aqueous AvP solutions. Dynamic oscillatory rheology was conducted at an applied stress of 5 Pa.

Fluorescence emission of 1,8-ANS.

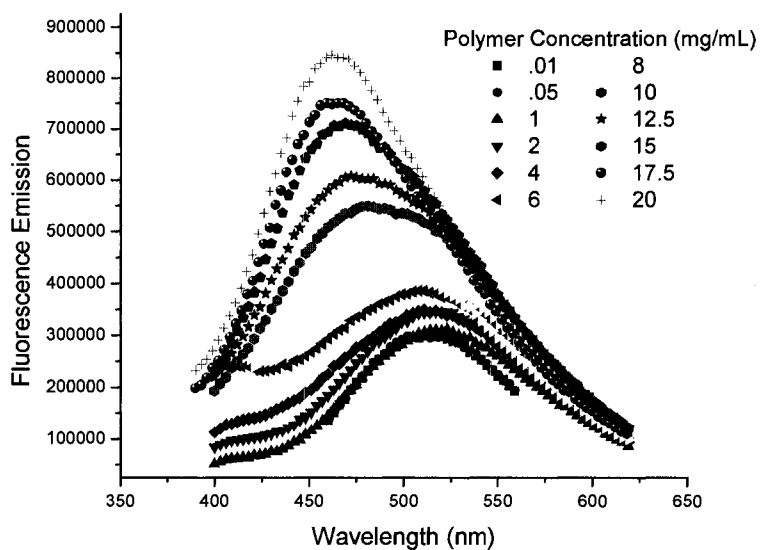


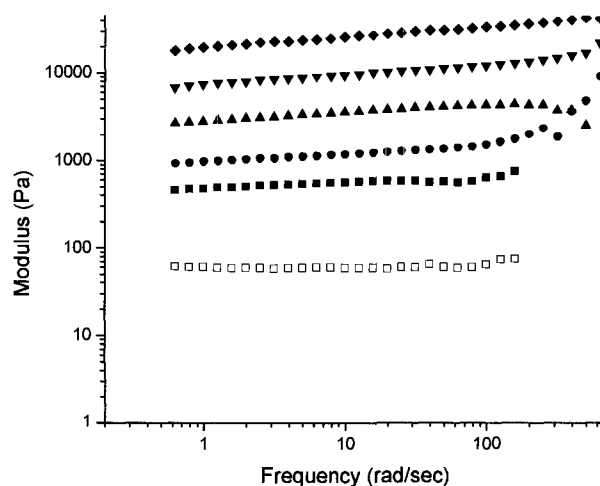
Figure A-15. Fluorescence emission of 1,8-ANS as seen in the inset of Figure IV-10.

APPENDIX B

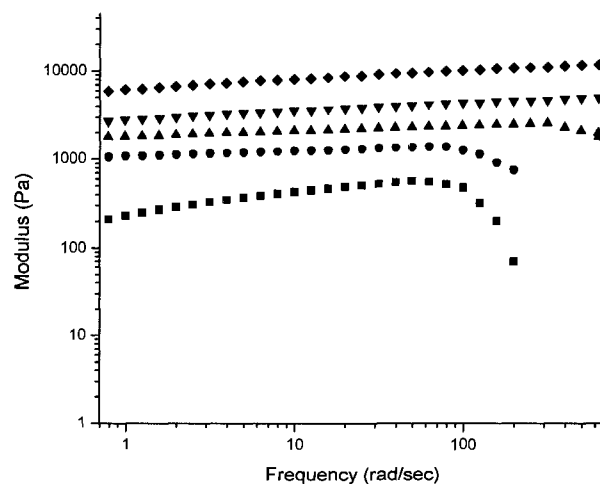
SUPPLEMENTAL INFORMATION CHAPTER IV

TAILORING THE NETWORK PROPERTIES OF Ca^{2+} CROSSLINKED *ALOE VERA* POLYSACCHARIDE HYDROGELS FOR *IN SITU* RELEASE OF THERAPEUTIC AGENTS

Oscillatory Rheology. The following figures were constructed to show the data used to create Figure IV-16.



a)



b)

Figure B-1. Elastic (open symbols) and viscous (closed symbols) moduli as a function of frequency for AvP2 gels at equilibrium conditions (a) 35 and (b) 15 mM CaCl_2 . Polymer concentrations of 0.10 (■), 0.20 (●), 0.40 (▲), 0.60 (▼), and 0.80 (◆) wt% were utilized for gel formation.

Phase Behavior. Provided below is the turbidity data used to construct Figures IV-20a & b.

Table B-1. Absorbance of AvP at 2 and 24 h over a range of polymer (0-2 mg/mL) and NaCl (0-0.20) concentrations.

Salt Concentration (M)	Polymer Concentration (mg/mL)									
	0	0.182	0.364	0.545	0.727	0.909	1.091	1.273	1.818	2
0	0.1344	0.1156	0.1297	0.2841	0.1072	0.1089	0.1429	0.2197	0.1071	0.0608
0.0286	0.1510	0.1026	0.1137	0.1361	0.1140	0.1155	0.1252	0.1503	0.0693	0.0761
0.0571	0.0996	0.0784	0.1309	0.1176	0.1888	0.1160	0.0985	0.0926	0.0784	0.0809
0.0857	0.1113	0.0792	0.0788	0.0874	0.1638	0.1315	0.1015	0.1622	0.1432	0.1366
0.1143	0.1021	0.1636	0.1137	0.1779	0.1281	0.1223	0.1126	0.1556	0.2178	0.1172
0.1429	0.0777	0.1643	0.1493	0.1074	0.0854	0.2428	0.1705	0.3293	0.1882	0.1961
0.1714	0.1193	0.1266	0.1410	0.1108	0.0916	0.2074	0.2030	0.3253	0.4927	0.4517
0.2000	0.1342	0.1403	0.1076	0.2423	0.1437	0.3588	0.3768	0.4325	0.5060	0.4607

Salt Concentration (M)	Polymer Concentration (mg/mL)									
	0	0.182	0.364	0.545	0.727	0.909	1.091	1.273	1.818	2
0	0.1595	0.1307	0.1549	0.3358	0.1286	0.1121	0.1371	0.2704	0.1222	0.0692
0.0286	0.2066	0.1751	0.1308	0.1423	0.1209	0.1792	0.1354	0.1670	0.0808	0.0818
0.0571	0.1301	0.1145	0.1489	0.1220	0.2204	0.1410	0.1073	0.1041	0.0878	0.0844
0.0857	0.1607	0.0912	0.1079	0.1075	0.2209	0.1583	0.1149	0.1909	0.1678	0.3682
0.1143	0.2556	0.1967	0.2158	0.1815	0.2020	0.2481	0.2516	0.3108	0.4375	0.3212
0.1429	0.0988	0.2020	0.2430	0.2147	0.2009	0.4239	0.2977	0.3886	0.4303	0.5891
0.1714	0.2675	0.1518	0.2404	0.2283	0.2286	0.3080	0.3376	0.3732	0.7455	0.9300
0.2000	0.1701	0.2437	0.1875	0.3157	0.2852	0.3381	0.3745	0.4032	1.6939	1.5944

Rubber Elasticity Theory. The characterization of crosslinked networks has long been a subject of interest. Pioneering work conducted by Flory,¹⁶⁷ Treloar,¹⁶⁹ and Ferry¹⁶⁸ sought to describe the relationship between macroscopic mechanical properties and the fundamental physics of lightly crosslinked elastomeric materials, specifically vulcanized rubbers. However, as suggested by Treloar,¹⁶⁹ the swelling phenomenon of rubbers markedly differs from that of biopolymer systems where the enthalpic interactions between water and polymer are significant. Recognizing the limitations of rubber elasticity theory, Ross-Murphy, Clark, and others sought to develop a model that would more accurately describe the gelation of hydrophilic systems.^{164, 165}

The resulting theory for biopolymer network formation, termed cascade theory, provides a relationship between gel shear modulus (G) and factors such as polymer concentration, molecular weight, degree of crosslinking, and temperature, based on the assumption that the binding energy of all crosslink sites is equivalent. Gel shear modulus can be calculated by Eq B-1.

$$G = \frac{Nf\alpha(1-\nu)^2(1-\beta)}{2} aRT \quad (\text{B-1})$$

N is the number of moles of polymer per unit volume initially present (equal to C/M_w , where C is concentration), f is the functionality of the individual polymer molecule in terms of total number of potential crosslinking sites, α is the fraction of these sites which have reacted at any stage in gel formation and is equal to the product of NfK , where K is the equilibrium constant for crosslinking and is defined by single values of entropy and enthalpy, ν is a function created to account for the probability of a functional site becoming extinct through a reaction that does not contribute to the elastically active

network, and β is a function which has been formulated to make the numerator of Equ. B-1 equal the average number of elastically active junctions per polymer molecule, when divided by N . The remaining aRT term in Equ. B-1 is the average contribution per mole of elastically active chains to the free energy increase exhibited upon strain and is based upon rubber elasticity theory.

The a term represents the mobility and functionality of the crosslinks and is not included in traditional equations for rubber elasticity because it is often assumed to be unity for elastomeric rubbers which have tetra-functional crosslinks (4 branches originate from 1 crosslink).¹⁸⁸ However, evidence suggests that this assumption is not accurate for biopolymer systems, as a may be a function of polymer concentration.¹⁶²

Cascade theory has been shown to work well for biopolymer systems such as gelatin¹⁶³ and galactomannan¹⁶⁰ where large enthalpic interactions are responsible for gelation. However, its application to pectins has been limited based on a number of restraints, specifically the high correlation between the adjustable parameters f and a , the apparent low enthalpy of crosslinking present in pectin systems and the possibility that pectins do not contain a well defined number of equivalent crosslink sites.¹⁷⁰ Thus, researchers have sought to develop alternative models that describe pectin gelation. Rao *et. al.*⁶² determine a structure development factor (dG'/dt) by monitoring the evolution of G' as a function of temperature. Using information from the structure development factor and rubber elasticity theory, kinetic descriptions of network formation were proposed.¹⁷¹ In contradiction to the cascade theory, Durand *et. al.*^{150, 170} developed a model for low methoxy pectin (LMP) gelation based upon the assumption that the concentration of binding sites (N_c) decreases exponentially with bond energy as described by:

$$N_c = Ae^{-BT} \quad (\text{B-2})$$

At the gel temperature (T_g) the value of N_c is given by $N_c^* = Ae^{-BT_g}$. Following the rationale of the Durand *et. al.*, ν the molar concentration of elastically active network chains (from rubber elasticity theory, written with the formalism $G = \nu RT$) is a universal function of N_c / N_c^* and is defined by:

$$\nu = 2N_c - \frac{C}{M_n} \quad (\text{B-3})$$

C is polymer concentration and M_n is number average molar mass of the pectin chain. Utilizing rubber elasticity theory the following expression which relates G to ν is obtained:

$$G = \frac{C}{M_n} e^{(-B(T-T_g)-1)} (aRT) \quad (\text{B-4})$$

Both the cascade theory and the theory presented by Durand *et. al.* seek to provide a comprehensive model for Ca^{2+} mediated pectin gelation, which is certainly desirable. However, both theories are ultimately based on rubber elasticity, with separate pre-factors being applied to account for non-linearity in empirical modulus data. As such, the elastic modulus data presented herein will be discussed in terms of traditional rubber elasticity theory.

Theories derived for rubber elastomers are based upon changes in polymer entropy induced during strain, and hence require that the elastic constant G be purely entropic in origin. Based upon this reasoning and a number of other assumptions the following expression for G and M_c the average molecular weight between crosslinks is derived.¹⁶⁷⁻¹⁶⁹

$$G = \frac{\rho RT}{M_c} \quad (\text{B-5})$$

In Eq. B-5, ρ is the material density, R the gas constant, and T the absolute temperature. Numerous corrections to this expression have been made in attempt to account for network imperfections such as loose chain ends, intramolecular loop formation, and entrapment of entanglements. Additionally, the case of a solvent swollen rubber was examined, for which it has been determined that the process of swelling is largely entropic in nature.¹⁶⁹ The amount of entropy gained by the system can be related directly to solvent volume fraction v_1 and applied to Equ. B-5 in terms of polymer volume fraction v_2 .

$$G = \frac{\rho RT}{M_c} v_2^{1/3} \quad (\text{B-6})$$

Considering the limitations discussed above, the application of rubber elasticity theory is limited. However, equation B-6 is of fundamental importance and is often used in attempts to describe crosslinked hydrogel networks. The application of theory can still be useful for determining the relative molecular weight between crosslinks (M_c) and gaining insight into the functionality of the crosslinks (a).

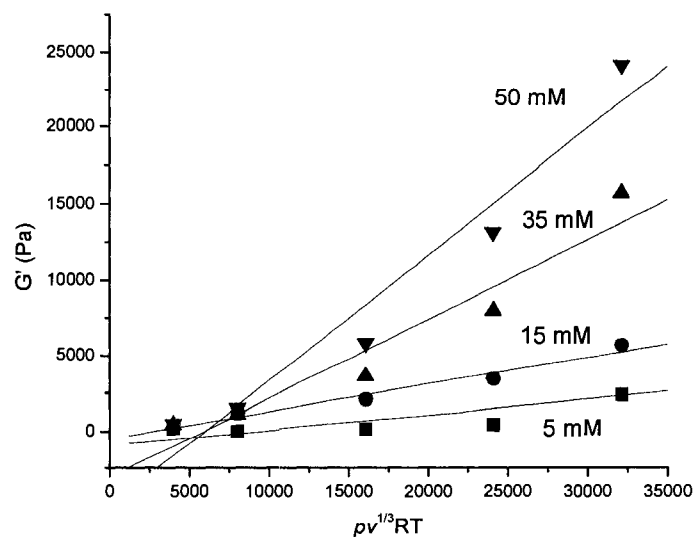


Figure B-2. Elastic modulus (Pa) of AvP hydrogels formed at calcium concentrations of 5.0 (■), 15 (●), 35 (▲), 50 (▼) mM with corresponding fits based on rubber elasticity theory. Inset is scaled to focus on the series of hydrogels crosslinked by 5.0 (■).

In Figure B-2, data is plotted according to Equ. B-6 where the slope of the regression line equals a/M_c . The data will first be discussed assuming that the crosslinks are tetrafunctional and $a=1$.

The slope of the regression line was used to calculate M_c values of 10000, 6000, 2000 and 1200 g/mol. As CaCl_2 concentration was increased from 5 to 50 mM the value of M_c decreased. Qualitatively these numbers are reasonable; they depict an increase in the number of intermolecular crosslinks as the Ca^{2+} concentration in the system increases. An approximate distance between crosslinks can be calculated from these M_c values, the M_w of the monomer unit (174 g/mol) and the reported length of a GalA unit as determined by x-ray diffraction (4.35 Å).⁵⁷ M_c values of 10,000 and 1200 g/mol yield a crosslink spacing of approximately 25 and 3 nm, respectively.

However, as seen in Figure B-1, the data obtained at high crosslink density ($[\text{Ca}^{2+}] > 15\text{mM}$) is non-linear suggesting that M_c is not constant as a function of polymer concentration. Non-linearity is particularly evident for the series of data taken at 35 and 50 mM CaCl_2 , where an increase in slope is observed as polymer concentration increases. An increase in slope suggests the formation of a greater number of intermolecular crosslinks and a decrease in M_c . The observed decrease in M_c as polymer concentration increases is reasonable when one considers that the probability of forming intermolecular junctions increases as the volume fraction of polymer in the system increases.

One must also consider that the slope of the regression line is dependent upon a , and that the functionality of a crosslink in pectin hydrogel systems is not necessarily well defined. Clark *et. al.*¹⁶² have suggested that a may be a function of polymer concentration, where a becomes larger at higher polymer concentrations due to an increase in crosslink functionality. Recent simulations by Perez *et. al.*⁸¹ suggest that this may be the case. Using interaction energy calculations and chain pairing procedures, it was shown that pectins do not undergo “egg box” dimerization in the same manner as alginates; instead, undergoing a two stage process where strong dimer associations are first formed, followed by weaker inter-dimer associations. If this is indeed occurring, an increase in a can be expected as the junctions within a macroscopic gel would no longer be tetravalent.

APPENDIX C

UNPUBLISHED RESULTS

Specific viscosity of AvP solutions containing NaCl. AvP displays typical polyelectrolyte behavior, exhibiting a decrease in specific viscosity as the solution ionic strength is increased from 0 to 0.20 M. Of note is the shear thinning behavior observed for the sample dissolved in water, which dissipates as the ionic strength of the system is increased.

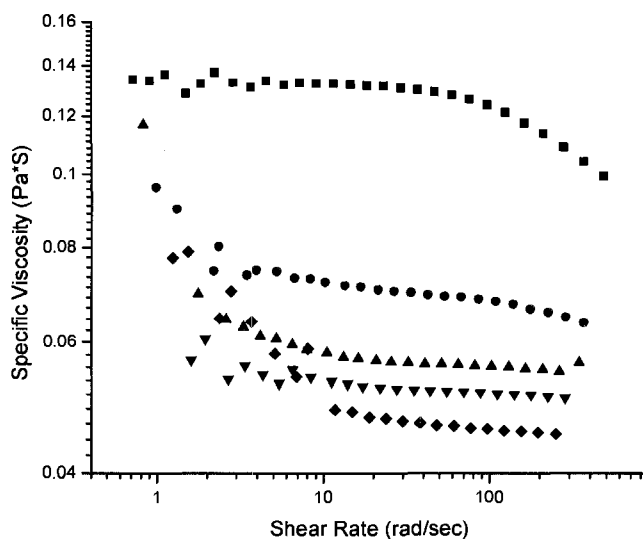


Figure C-1. Specific viscosity (Pa*S) of AvP3 (0.25 wt%) dissolved in water (■), 0.05 (●), 0.10 (▲), 0.15 (▼) and 0.20 (◆) mM NaCl as a function of shear rate.

Scattering intensity as a function of time for specific ionic strength/temperature combinations. Due to the screening of electrostatic repulsions at ionic strengths above 0.10 M, AvP undergoes phase separation over time as discussed in Chapter IV Section B, forming colloidal dispersions at appropriate ionic strengths and polymer concentrations. Observations of AvP solution behavior indicated that these dispersions have the ability to

form either reversible gels or irreversible crystal like structures. While extensive studies were not conducted on the subject, this unique solution behavior is of importance and has potential applicability to commercial applications involving refrigeration of AvP-containing drug delivery systems.

Colloidal association processes have been shown to be regulated by the energetics of the system. The solution conditions necessary to form either gels or crystals from colloidal systems remains poorly understood.¹⁸⁹ Equilibrium thermodynamics can be used to describe the occurrence of crystals,¹⁹⁰ while gelation is a kinetic transition which has been described in terms of a percolation threshold,^{191, 192} and more recently through a mode coupling approach. As discussed by Zukoski and Dixit,¹⁸⁹ the competition between crystal and gel formation is controlled by relative rates of particle aggregation and dissociation. These two processes are influenced by the strength of attraction between particles and the thermal energy of the system.

Solution studies on hard-sphere colloidal systems comprised of surface modified silica particles have demonstrated that depleting or increasing attraction between particles results in formation of either gels or crystals.^{193, 194} Recent studies on globular protein suspensions revealed that crystals formed at high strengths of attraction while gels were observed at low strengths of attraction.¹⁹⁵ Herein, we have examined the phase behavior of a soft-colloid system, comprised of the *Aloe vera* polysaccharide (AvP), in which the interparticle strength of attraction is directly tunable via changes in solution ionic strength.

In Figure C-2, an increase in scattering intensity is noted for the AvP sample (0.05 wt%) dissolved in 0.20 M NaCl held at 25°C. However, upon increasing the temperature

to 50°C or decreasing the ionic strength to 0.10 M, the scattering intensity remains constant over time. The increase in scattering intensity at a combination of 25°C/0.20 M is directly correlated to a moderate increase in turbidity and formation of microphase separated domains as discussed in Chapter IV Section B. As seen in Figure C-2, microphase separation can be prevented by increasing the energy present in the system (increasing temperature to 50 °C) or by decreasing the attractive nature of AvP (decreasing electrostatic screening by lowering ionic strength).

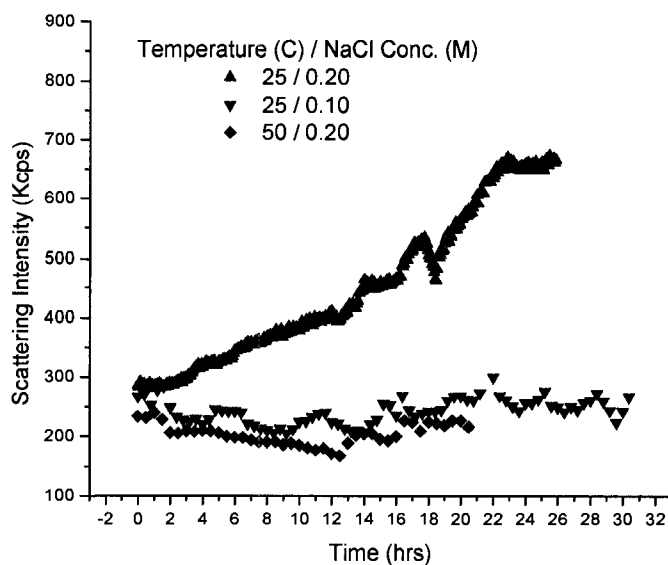


Figure C-2. Time dependent scattering intensity (Kcps) of AvP3 (0.50 wt%) dissolved at specified temperature/ionic strength combination 25°C/0.20 M (▲), 25°C/0.10 M (▼) and 15°C/0.20 M (◆) NaCl.

When 0.20 M AvP solutions are held at lower temperatures (15-10°C), large increases in scattering intensities are observed (Figure C-3). Interestingly, the observed increase in scattering intensity occurs over a very discrete time interval (12-14 h) for samples held at 15°C. When held at 10°C immediate transitions are noted. Increases in scattering intensity correspond to large decreases in the diffusion coefficients as determined by dynamic light scattering and indicate gel formation. Observations of colloidal suspensions at a fixed volume fraction have revealed that a small increase in particle attraction results in a dramatic drop in long-time self diffusivity.¹⁹⁶ This is similar to the increased association present in AvP solutions at high ionic strengths. In the case of 0.50 wt% AvP dissolved in 0.20 M, a reduction in temperature from 15° to 10°C results in a system where the strength of particle association is not overcome by the ΔS^*T thermodynamic component.

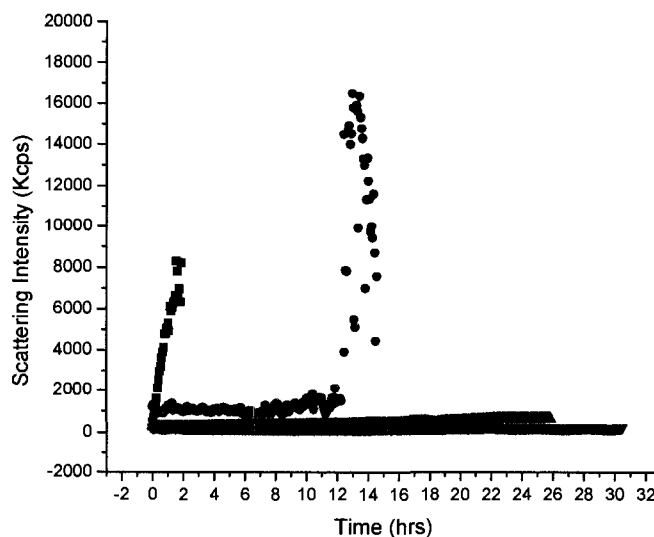


Figure C-3. Time dependent scattering intensity (Kcps) of AvP3 (0.50 wt%) dissolved at specified temperature/ionic strength conditions 10°C/0.20 M (■), 15°C/0.20 M (●), 25°C/0.20 M (▲), 25°C/0.10 M (▼) and 15°C/0.20 M (◆) NaCl.

In order to further study the nature of AvP networks formed at combinations of low temperature and high ionic strength, dynamic oscillatory rheology was conducted. Due to the weak nature of the networks, dynamic rheology could not be conducted at the low polymer concentrations utilized in the light scattering experiments. Experiments were conducted at 0.20 wt% with the Rheometrics SR5000 utilizing a 45 mm cone and plate geometry (Figure C-4). This experiment had undesirable signal to noise ratios and may be more successful utilizing the ARES-G2 rheometer and more sensitive geometries. Nonetheless, a clear increase in G' is noted as temperature decreases when AvP is dissolved in 0.15 M NaCl. The increase in G' is more evident when higher concentrations of AvP are employed (Figure C-5).

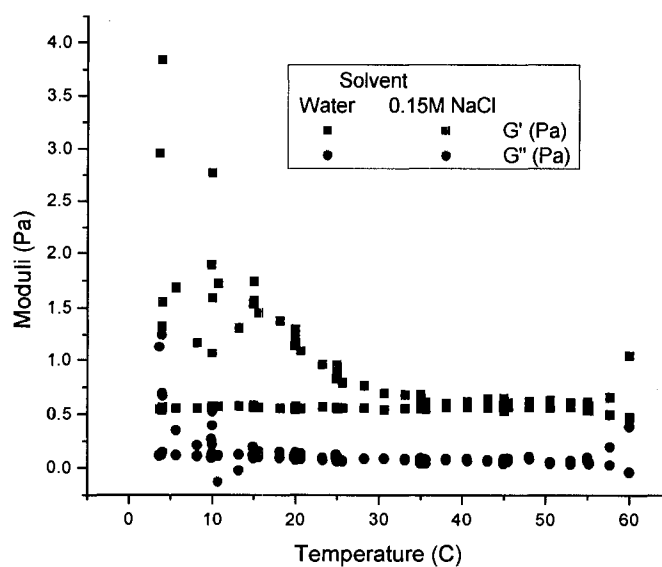


Figure C-4. Dynamic oscillatory rheology of AvP3 (0.20wt%) conducted as a function of temperature ($^{\circ}\text{C}$) at a frequency of 6.2 rad/sec and a stress of 0.5 Pa.

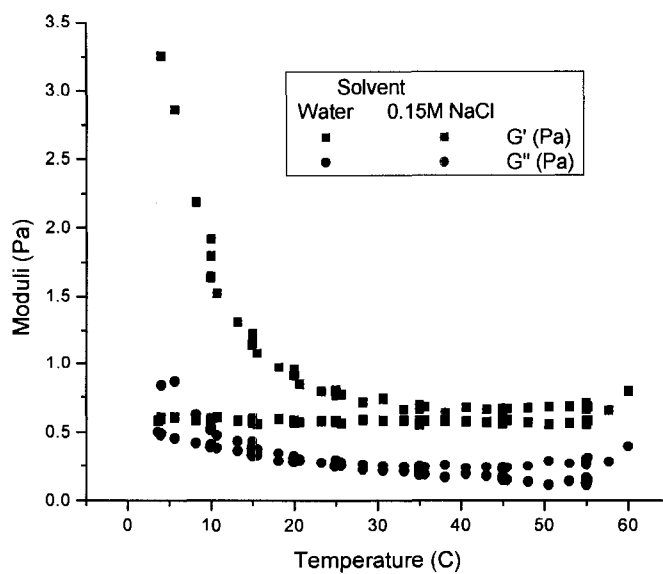


Figure C-5. Dynamic oscillatory rheology of AvP3 (0.50wt%) conducted as a function of temperature ($^{\circ}\text{C}$) at a frequency of 6.2 rad/sec and a stress of 0.5 Pa.

Further studies over a larger set of temperature/ionic strength combinations and at additional polymer concentrations are recommended to gain further insight into the formation of soft, colloidal AvP gels.

REFERENCES

1. Hoffman, A. S., *Advanced Drug Delivery Reviews* **2002**, 43, 3-12.
2. Qiu, Y.; Park, K., *Advanced Drug Delivery Reviews* **2001**, 53, 321-329.
3. Gupta, P.; Vermani, K.; Grag, S., *Drug Discovery Today* **2002**, 7, 569-579.
4. Ruel-Gariepy, E.; Leroux, J. C., *European Journal of Pharmaceuticals and Biopharmaceuticals* **2004**, 58, 409-426.
5. Oh, J. K.; Drumright, R.; Siegwart, D. J.; Matyjaszewski, K., *Progress in Polymer Science* **2008**, 33, (4), 448-477.
6. He, C.; Kim, S. W.; Lee, D. S., *Journal of Controlled Release* **2008**, 127, (3), 189-207.
7. McCormick, C. L.; Bock, J.; Schultz, D. N., Water Soluble Polymer. In *Encyclopedia of Polymer Science and Engineering*, Second ed.; Mark-Bilkales-Overberger-Menges, Ed. John Wiley & Sons, Inc.: 1989; Vol. 17, pp 730-784.
8. Li, W.-C.; Yu, D.-G.; Yang, M.-C., *Colloids and Surfaces B: Biointerfaces* **2005**, 44, 143-151.
9. Bajpai, A. K.; Giri, A., *Carbohydrate Polymers* **2003**, 53, 271.
10. Wach, R. A.; Mitomo, H., *Journal of Applied Polymer Science* **2001**, 81, (12), 3030-3037.
11. Gao, Y.; Xiao, C., *Journal of Applied Polymer Science* **2008**, 107, 1568-1572.
12. Perioli, L.; Ambrogi, V.; Venezia, L.; Pagano, C.; Ricci, M.; Rossi, C., *Colloids and Surfaces B: Biointerfaces* **2008**, 66, 141-145.
13. Illum, L., *European Journal of Pharmaceutical Sciences* **2000**, 11, (1), 1-18.
14. Illum, L., *Drug Discovery Today* **2002**, 7, (23), 1184-1189.
15. Illum, L., *Journal of Controlled Release* **2003**, 87, (1-3), 187-198.
16. Illum, L.; Jabbal-Gill, I.; Hinchcliffe, M.; Fischer, A. N.; Davis, S. S., *Advanced Drug Delivery Reviews* **2001**, 51, 81-96.
17. Illum, L., *Journal of Aerosol Medicine: Deposition, Clearance, and Effects in the Lung* **2007**, 19, (1), 92-99.
18. Read, R. C.; Naylor, S. C.; Illum, L.; Jennings, R., *Vaccine* **2005**, 23, (35), 4367-4374.
19. Prabakaran, M., *Journal of Biomaterials Applications* **2008**, 23, (1), 5-36.
20. Tomihata, K.; Ikada, Y., *Journal of Polymer Science, Part A* **1997**, 35, 3553-3559.
21. Vercruyse, K. P.; Marecak, D. M.; Marecek, G. D. P., G.D., *Bioconjugate Chemistry* **1997**, 8, 686-694.
22. Shu, X. Z.; Liu, Y.; Luo, Y.; Roberts, M. C.; Prestwich, G. D., *Biomacromolecules* **2002**, 3, 1304-1311.
23. Whistler, R. L., *Industrial Gums*. Academic Press: New York, 1973.
24. Kamath, K. R.; Park, K., *Polymer Gels and Networks* **1995**, 3, 243-254.
25. Franssen, O.; Vos, O. P.; Hennink, W. E., *Journal of Controlled Release* **1997**, 48, 107-114.
26. Hennink, W. E.; Franssen, O.; Dijk-Wolthuis, W. N. E.; Tasma, H., *Journal of Controlled Release* **1997**, 60, 211-221.
27. Cadee, J. A.; De Groot, C. J.; Jiskoot, W.; Den Otter, W.; Hennink, W. E., *Journal of Controlled Release* **1999**, 78, 1-13.

28. De Gest, B. G.; Stubbe, B. G.; Jonas, A. M.; Thienen, T. V.; Hinrichs, W. L. J.; Demeester, J.; De Smedt, S. C., *Biomacromolecules* **2006**, *7*, 373-379.
29. Steinbuchel, A., *Biopolymers Volume 6: Polysaccharides II*. Wiley-VCH: 2002.
30. Lee, I.; Akiyoshi, K., *Biomaterials* **2004**, *25*, 2911-2918.
31. Akiyoshi, K.; Kang, E. C.; Kuromada, S.; Sunamoto, J., *Macromolecules* **2000**, *33*, 3244-3249.
32. Nishikawa, T.; Akiyoshi, K.; Sunamoto, J., *Journal of the American Chemical Society* **1996**, *118*, 6110-6115.
33. Nishikawa, T.; Akiyoshi, K.; Sunamoto, J., *Macromolecules* **1994**, *27*, 7654-7659.
34. Akiyoshi, K.; Kobayashi, S.; Shichibe, S.; Mix, D.; Baudys, M.; Kim, S. W.; Sunamoto, J., *Journal of Controlled Release* **1998**, *54*, 313-320.
35. Dumitriu, S.; Chornet, E., *Advanced Drug Delivery Reviews* **1998**, *31*, 223-246.
36. Bertram, U.; Bodmeier, R., *European Journal of Pharmaceutical Sciences* **2006**, *27*, 62-71.
37. Rozier, A.; Mazuel, C.; Grove, J.; Plazonnet, B., *International Journal of Biological Macromolecules* **1997**, *153*, 191-198.
38. Jansson, B.; Haegerstrom, H.; Fransen, N.; Edsman, K.; Bjoerk, E., *European Journal of Pharmaceuticals and Biopharmaceuticals* **2005**, *59*, 557-564.
39. Rees, D. A.; Steele, I. W.; Williamson, F. B., *Journal of Polymer Science, Part C* **1969**, *28*, 261.
40. Rees, D. A., *Journal of Chemical Society, B* **1969**, 217.
41. Liu, J.; Lin, S.; Li, L.; Liu, E., *International Journal of Pharmaceutics* **2005**, *298*, 117-125.
42. Garcia, A. M.; Ghaly, E. S., *Journal of Controlled Release* **1996**, *40*, 179-186.
43. Haug, A.; Smidrod, O., *Acta. Chem. Scand.* **1965**, *19*, 1221-1226.
44. Haug, A.; Smidrod, O., *Acta Chem. Scand.* **1970**, *24*, 843-854.
45. Grant, G. T.; Morris, E. R.; Rees, D. A.; Smith, P.; Thom, J. C., *FEBS Lett.* **1973**, *32*, 195-198.
46. Steginsky, C. A.; Beale, J. M.; Floss, H. G.; Mayer, R. M., *Carbohydrate Research* **1992**, *225*, 11-26.
47. Braccini, I.; Rodriguez-Carvajal, M. A.; Perez, S., *Biomacromolecules* **2005**, *6*, 1322-1328.
48. Thibault, J.-F.; Rinaudo, M., *Biopolymers* **1985**, *24*, 2131-2143.
49. Ralet, M.-C.; Dronnet, V.; Buchholt, H. C.; Thibault, J.-F., *Carbohydrate Research* **2001**, *336*, 117-125.
50. Thibault, J.-F.; Rinaudo, M., *Biopolymers* **1986**, *25*, 455-468.
51. Oosterveld, A.; Beldman, M. J. F.; Leeuwen, S.; Voragen, A. G. J., *Carbohydrate Polymers* **2000**, *43*, 249-256.
52. Schmelter, T.; Wientjes, R.; Vreeker, R.; Klaffke, W., *Carbohydrate Polymers* **2002**, *47*, 99-108.
53. Gilsenan, P. M.; Richardson, R. K.; Morris, E. R., *Carbohydrate Polymers* **2000**, *41*, 339-349.
54. Donato, L.; Garnier, C.; Novales, B.; Doublier, J. L., *Food Hydrocolloids* **2005**, *19*, (3), 549-556.

55. Donato, L.; Garnier, C.; Novales, B.; Durand, S.; Doublier, J. L., *Biomacromolecules* **2005**, 6, (1), 374-385.
56. Cardoso, S. M.; Coimbra, M. A.; Lopes da Silva, J. A., *Food Hydrocolloids* **2003**, 17, 801-807.
57. Garnier, C.; Axelos, M. A. V.; Thibault, J.-F., *Carbohydrate Research* **1993**, 240, 219-232.
58. Morris, E. R.; Powell, D. A.; Gidley, M. J.; Rees, D. A., *Journal of Molecular Biology* **1982**, 155, 507-516.
59. Powell, D. A.; Morris, E. R.; Gidley, M. J.; Rees, D. A., *Journal of Molecular Biology* **1982**, 155, 517-531.
60. Oakenfull, D.; Scott, A., *Journal of Food Science* **1984**, 49, 1093-1098.
61. Lofgren, C.; Guillotin, S.; Evenbratt, H.; Schols, H.; Hermansson, A.-M., *Biomacromolecules* **2005**, 6, 646-652.
62. Grosso, C. R. F.; Rao, M. A., *Food Hydrocolloids* **1998**, 12, 357-363.
63. Grosso, C. R. F.; Bobbio, P. A.; Airoidi, C., *Carbohydrate Polymers* **2000**, 41, 421-424.
64. Fu, J.-T.; Rao, M. A., *Food Hydrocolloids* **1999**, 13, 371-380.
65. Lofgren, C.; Hermansson, A.-M., *Food Hydrocolloids* **2007**, 21, 480-486.
66. Picout, D. R.; Richardson, R. K.; Rolin, C.; Abeysekera, R. M.; Morris, E. R., *Carbohydrate Polymers* **2000**, 43, 113-122.
67. Picout, D. R.; Richardson, R. K.; Rolin, C.; Abeysekera, R. M.; Morris, E. R., *Carbohydrate Polymers* **2000**, 43, 123-131.
68. Giannouli, P.; Richardson, R. K.; Morris, E. R., *Carbohydrate Polymers* **2004**, 55, 366-377.
69. Giannouli, P.; Richardson, R. K.; Morris, E. R., *Carbohydrate Polymers* **2004**, 55, 343-356.
70. Giannouli, P.; Richardson, R. K.; Morris, E. R., *Carbohydrate Polymers* **2004**, 55, 357-365.
71. Rees, D. A., *Carbohydrate Polymers* **1982**, 2, 254-263.
72. Gidley, M. J.; Morris, E. R.; Murray, E. J.; Powell, D. A.; Rees, D. A., *International Journal of Biological Macromolecules* **1980**, 2, 332-334.
73. Davis, M. A. F.; Gidley, M. J.; Morris, E. R.; Powell, D. A.; Rees, D. A., *International Journal of Biological Macromolecules* **1980**, 2, 330-332.
74. Malovikova, A.; Rinaudo, M.; Milas, M., *Biopolymers* **1994**, 34, 1059-1064.
75. Gidley, M. J.; Morris, E. R.; Murray, E. J.; Powell, D. A.; Rees, D. A., *Chemical Communication* **1979**, 990-991.
76. Dobies, M.; Kozak, M.; Jurga, S., *Solid State Nuclear Magnetic Resonance* **2004**, 25, 188-193.
77. Wellner, N.; Kacurakova, M.; Malovikova, A.; Wilson, R. H.; Belton, P. S., *Carbohydrate Research* **1998**, 308, 123-131.
78. Jarvis, M. C.; Apperley, D. C., *Carbohydrate Research* **1995**, 275, 131-145.
79. Newman, J. K. ²³Na NMR Studies of Ion-Binding to Anionic Homopolyelectrolytes and Conformational Changes in Hydrophobically-Modified Polyelectrolytes. University of Southern Mississippi, 1993.
80. Fang, Y.; Al-Assaf, S.; Phillips, G. O.; Nishinari, K.; Funami, T.; Williams, P. A., *Carbohydrate Polymers* **2008**, 72, 334-341.

81. Braccini, I.; Rodriguez-Carvajal, M. A.; Perez, S., *Biomacromolecules* **2005**, *8*, 1322-1328.
82. Voragen, A. G. J.; Pilnik, W.; Thibault, J.-F.; Axelos, M. A. V.; Renard, C. M. G. C., *Food Polysaccharides and Their Applications* Marcel Dekker: New York, 1995.
83. Phillips, G. O.; Williams, M. A. K., *Handbook of Hydrocolloids*. Woodhead Publishing Ltd.: Cambridge, 2000.
84. Liu, L.; Fishman, M.; Hicks, K., *Cellulose* **2007**, *14*, (1), 15-24.
85. Leader, B.; Baca, Q. J.; Golan, D. E., *Nature Reviews Drug Discovery* **2008**, *7*, (1), 21-39.
86. Chen, J.; Jo, S.; Park, K., *Carbohydrate Polymers* **1995**, *28*, 69-76.
87. Hoare, T. R.; Kohane, D. S., *Polymer* **2008**, *49*, (8), 1993-2007.
88. Gombotz, W. R.; Wee, S. F., *Advanced Drug Delivery Reviews* **1998**, *31*, 267-285.
89. Liu, L.; Fishman, M. L.; Kost, J.; Hicks, K. B., *Biomaterials* **2003**, *24*, 3333-3343.
90. Tabata, Y.; Ikada, Y., *Advanced Drug Delivery Reviews* **1998**, *31*, 287-301.
91. Van Tomme, S. R.; Storm, G.; Hennink, W. E., *International Journal of Pharmaceutics* **2008**, *355*, (1-2), 1-18.
92. Smallcombe, S. H.; Patt, S. L.; Keifer, P. A., *Journal of Magnetic Resonance Series A* **1995**, 295.
93. Hoffman, R. E.; Davis, D. B., *Magnetic Resonance Chemistry* **1988**, *26*, 523-525.
94. Serra, L.; Domenech, J.; Peppas, N. A., *Biomaterials* **2006**, *27*, 5440-5451.
95. Blanchette, J.; Kavimandan, N.; Peppas, N. A., *Biomedecine & Pharmacotherapy* **2004**, *58*, (3), 142-151.
96. Treanor, J. J.; Campbell, J. D.; Zangwill, K. M.; Rowe, T.; Wolff, M., *New England Journal of Medicine* **2006**, *354*, 1434-1351.
97. Soane, R. J.; Frier, M.; Perkins, A. C.; Jones, N. S.; Davis, S. S.; Illum, L., *International Journal of Pharmaceutics* **1999**, *178*, 55-65.
98. Liao, Y.-H.; Jones, N. S.; Forbes, B.; Martin, G.; Brown, M., *Drug Delivery* **2005**, *12*, 327-342.
99. Fishman, M. L.; Pfeffer, P. E.; Barford, R. A.; Doner, L. W., *Journal of Agricultural Food Chemistry* **1984**, *32*, 372.
100. Axelos, M. A. V.; Thibault, J.-F., *International Journal of Biological Macromolecules* **1990**, *13*, 77-82.
101. Axelos, M. A. V.; Thibault, J.-F.; Lefebvre, J., *International Journal of Biological Macromolecules* **1989**, 11.
102. Harding, S. E.; Berth, G.; Ball, A.; Mitchell, J. R.; Garcia de la Torre, J., *Carbohydrate Polymers* **1991**, *16*, 1-15.
103. Hourdet, D.; Muller, G., *Carbohydrate Polymers* **1987**, *7*, 301-312.
104. Hourdet, D.; Muller, G., *Carbohydrate Polymers* **1991**, *16*, 113-135.
105. Hourdet, D.; Muller, G., *Carbohydrate Polymers* **1991**, *16*, 409-432.
106. Morris, G. A.; Foster, T. J.; Harding, S. E., *Food Hydrocolloids* **2000**, *14*, 227-235.
107. Yoo, S.-H.; Fishman, M. L.; Hotchkiss, A. T.; Lee, H. G., *Food Hydrocolloids* **2006**, *20*, 62-67.

108. Corredig, M.; Kerr, W.; Wicker, L., *Food Hydrocolloids* **2000**, 14, 41-47.
109. Deckers, H. A.; Olieman, C.; Rombouts, F. M.; Pilnik, W., *Carbohydrate Polymers* **1986**, 6, 361-378.
110. Braccini, I.; Perez, S., *Biomacromolecules* **2001**, 2, 1089-1096.
111. Garnier, C.; Axelos, M. A. V.; Thibault, J.-F., *Carbohydrate Research* **1994**, 256, 71-81.
112. Vold, I. M. N.; Kristiansen, K. A.; Christensen, B. E., *Biomacromolecules* **2006**, 7.
113. Guillotin, S. E.; Bakx, E. J.; Boulenguer, P.; Scols, H. A.; Voragen, A. G. J., *Food Hydrocolloids* **2007**, 21, 444-451.
114. Rosenbohm, C.; Lundt, I.; Christensen, T. M. I. E.; Young, N. W. G., *Carbohydrate Research* **2003**, 338, 637-649.
115. Grasdalen, H.; Anderson, A. K.; Larsen, B., *Carbohydrate Research* **1996**, 289, 105-114.
116. Anderson, K. H.; Larsen, B.; Grasdalen, H., *Carbohydrate Research* **1995**, 273, 93-98.
117. Grasdalen, H.; Bakoy, O. E.; Larsen, B., *Carbohydrate Research* **1988**, 184, 183-191.
118. Freed, K. F.; Edwards, S. F., *Journal of Chemistry and Physics* **1975**, 62, (4032-4035).
119. Cheng, Y.; Brown, K. M.; Prud'homme, R. K., *Biomacromolecules* **2002**, 3, 456-461.
120. Pelletier, S.; Hubert, P.; Lapique, F.; Payan, E.; Dellacherie, E., *Carbohydrate Polymers* **2000**, 43, 343-349.
121. Lochhead, R. Y., *Cosmetics & Toiletries Magazine* **2006**, 121, 73-81.
122. Ezell, G. R.; Gorman, I.; Lokitz, B.; Ayers, N.; McCormick, C. L., *Journal of Polymer Science Part A: Polymer Chemistry* **2006**, 44, 3125-3139.
123. Yamakawa, H., *Modern Theory of Polymer Solutions*. Harper and Row: New York, 1971.
124. Yamakawa, H.; Fujii, M., *Macromolecules* **1974**, 7, 128-135.
125. Cros, S.; Garnier, C.; Axelos, M. A. V.; Imberty, A.; Perez, S., *Biopolymers* **1996**, 39, 339-352.
126. Plashchina, I. G.; Semenova, M. G.; Braudo, E. E.; Tolstoguzov, V. B., *Carbohydrate Polymers* **1985**, 5, 159-179.
127. Higashimura, M.; Mulder-Bosman, B. W.; Reich, R.; Iwasaki, T.; Robijn, G. W., *Biopolymers* **2000**, 54, 143-158.
128. Avaltroni, F.; Seijo, M.; Ulrich, S.; Stoll, S.; Wilkonson, K. J., *Biomacromolecules* **2007**, 8, 106-112.
129. Bohandeky, M., *Macromolecules* **1983**, 16, 1483-1492.
130. Mendichi, R.; Soltes, L.; Schieron, A. G., *Biomacromolecules* **2003**, 4, 1805-1810.
131. Abramonic, H.; Klofutar, C., *Food Hydrocolloids* **1998**, 12, 167-173.
132. Noto, R.; Martorana, V.; Bulone, D.; San Biagio, P. L., *Biomacromolecules* **2005**, 6, 2555-2562.
133. Boutherin, B.; Mazeau, K.; Tvaroska, I., *Carbohydrate Polymers* **1997**, 32, 255-266.

134. Elias, H.-G., *Macromolecules 1 Structure and Properties*. Plenum Press: New York, 1977.
135. Morawetz, H., *Macromolecules in Solution*. John Wiley and Sons, Inc.: New York, 1975.
136. Teraoka, I., *Polymer Solutions An Introduction to Physical Properties*. John Wiley and Sons, Inc.: New York, 2002.
137. Smidrod, O.; Haug, A., *Biopolymers* **1971**, 10, 1213-1227.
138. Koelmans, H.; Overbeek, J., *Discussions of the Faraday Society* **1954**, 18, 52-63.
139. Dorbrynin, A. V.; Colby, R. H.; Rubinstein, M., *Macromolecules* **1995**, 28, 1859-1871.
140. Kujawa, P.; Audibert-Hayet, A.; Selb, J.; Candau, F., *Macromolecules* **2006**, 39, 384-392.
141. Regalado, E. J.; Selb, J.; Candau, F., *Macromolecules* **1999**, 32, 8580-8588.
142. Abdala, A. A.; Wu, W.; Olesen, K. R.; Jenkins, R. D.; Tonelli, A. E.; Khan, S. A., *Journal of Rheology* **2004**, 48, 543-549.
143. Hazra, P.; Chakrabarty, D.; Chakraborty, A.; Sarkar, N., *Biochemical Biophysical Research Communications* **2003**, 314, 543-549.
144. Bertsch, M.; Mayburd, A. L.; Kassner, R. J., *Analytical Biochemistry* **2003**, 313, 187-195.
145. Kujawa, P.; Watanabe, H.; Tanaka, F.; F.M., W., *European Physics Journal E - Soft Matter* **2005**, 17, 129-137.
146. Fishman, M. L.; Cooke, P.; Coffin, D. R., *Biomacromolecules* **2006**, 5, 334-341.
147. Fishman, M. L.; Cooke, P.; Levaj, B.; Gillespie, G. T.; Sondey, S. M.; Scorza, R., *Archives of Biochemical Biophysics* **1992**, 294, 253-260.
148. Lofgren, C.; Guillotin, S.; Hermansson, A.-M., *Biomacromolecules* **2006**, 7, 114-121.
149. Strom, A.; Ribelles, P.; Lundin, I.; Norton, I.; Morris, E. R.; Williams, M. A. K., *Biomacromolecules* **2007**, 8, 2668-2674.
150. Capel, F.; Nicolai, T.; Durand, D., *Biomacromolecules* **2005**, 6, 2954-2960.
151. Siew, C. K.; Williams, P. A., *Biomacromolecules* **2005**, 6, 963-969.
152. Davis, M. A. F.; Gidley, M. J.; Morris, E. R.; Powell, D. A.; Rees, D. A., *International Journal of Biological Macromolecules* **1980**, 2, 330-332.
153. Kubo, W.; Itoh, K.; Miyazaki, S., *Drug Development and Industrial Pharmacy* **2005**, 31, 819-825.
154. Pillay, V.; Fassihi, R., *Journal of Controlled Release* **1999**, 59, 243-256.
155. Lorin, M. I.; Gaerlan, P. F.; Mandel, I. D., *Journal of Laboratory Clinical Medicine* **1972**, 80, (2), 275-281.
156. Folk, B. P.; Zierler, K. L.; Lilienthal, J. L., *American Journal of Physiology* **1948**, 153, 381-385.
157. McConaughy, S. D.; Stroud, P. A.; Boudreaux, B.; Hester, R. D.; McCormick, C. L., *Biomacromolecules* **2008**, 9, 472-480.
158. Cardoso, S. M.; Coimbra, M. A.; J.A., L. d. S., *Carbohydrate Polymers* **2003**, 52, 125-133.
159. Clark, A. H., *Polymer Gels and Networks* **1993**, 1, 139-158.
160. Richardson, P. H.; Clark, A. H.; Russell, A. L.; Norton, I. T., *Macromolecules* **1999**, 32, 1519-1527.

161. Richardson, P. H.; Norton, I. T., *Macromolecules* **1998**, 31, 1575-1583.
162. Durand, D.; Bertrand, C.; Clark, A. H.; Lips, A., *International Journal of Biological Macromolecules* **1990**, 12, 14-18.
163. Clark, A. H.; Evans, K. T.; Farrer, D. B., *International Journal of Biological Macromolecules* **1994**, 16, (3), 125-130.
164. Clark, A. H.; Ross-Murphy, R. K., *Advances in Polymer Science* **1987**, 83, 57-192.
165. Clark, A. H.; Ross-Murphy, R. K., *British Polymer Journal* **1985**, 17, 164-168.
166. Tsukeshiba, H.; Huang, M.; Na, Y. H.; Kurokawa, T.; Kuwabara, R.; Tanaka, Y.; Furukawa, H.; Osada, Y.; Gong, J. P., *Journal of Physical Chemistry B*. **2005**, 109, (34), 16304-16309.
167. Flory, P. J., *Principles of Polymer Chemistry*. Cornell University Press: Ithica, 1953.
168. Ferry, J. D., *Viscoelastic Properties of Polymers*. John Wiley & Sons, Inc.: New York, 1980.
169. Treloar, L. R. G., *The Physics of Rubber Elasticity*. Third Edition ed.; Oxford University Press: Oxford, 1975.
170. Lootens, D.; Capel, F.; Durand, D.; Nicolai, T.; Boulenguer, P.; Langendorff, V., *Food Hydrocolloids* **2003**, 17, 237-244.
171. Fu, J.-T.; Rao, M. A., *Food Hydrocolloids* **2001**, 15, 93-100.
172. Tolstoguzov, V. B., *Food Hydrocolloids* **2003**, 17, (1), 1-23.
173. Price, W. S., *Concepts in Magnetic Resonance* **1997**, 9, 299-336.
174. Sen, P. N., *Concepts in Magnetic Resonance Part A* **2004**, 23A, (1), 1-21.
175. Latour, L. L.; Mitra, P. P.; Klienberg, R. L.; Sotak, C. H., *Journal of Magnetic Resonance A* **1993**, 101, 342.
176. Mair, R. W.; Sen, P. N.; Hurlimann, M. D.; Patz, S.; Cory, D. G.; Walsworth, R. L., *Journal of Magnetic Resonance A* **2002**, 156, 202.
177. Candela, D.; Wong, P. Z., *Physical Review Letters* **2003**, 90, 039601-039602.
178. Ohtsuka, A.; Watanabe, T., *Carbohydrate Polymers* **1996**, 30, (2-3), 135-140.
179. Iskakov, R. M.; Kikuchi, A.; Okano, T., *Journal of Controlled Release* **2002**, 80, 57-68.
180. Kikuchi, A.; Kawabuchi, M.; Watanabe, A.; Sugihara, M.; Sakurai, Y.; Okano, T., *Journal of Controlled Release* **1999**, 58, 21-28.
181. Peppas, N. A.; Sahlin, J. J., *International Journal of Pharmaceutics* **1989**, 57, 169-172.
182. Ritger, P. L.; Peppas, N. A., *Journal of Controlled Release* **1987**, 5, 23-36.
183. Ritger, P. L.; Peppas, N. A., *Journal of Controlled Release* **1987**, 5, 37-42.
184. Pillay, V.; Fassihi, R., *Journal of Controlled Release* **1999**, 59, 229-242.
185. Higuchi, T., *Journal of Pharmaceutical Sciences* **1963**, 52, 1145-1148.
186. Ensore, D. J.; Hopfenberg, H. B.; Stannett, V. T., *Polymer* **1977**, 18, 793-800.
187. Prashant, B. S.; Mishra, R.; Pal, K.; Banthia, A., *Journal of Material Science: Materials in Medicine* **2008**, 19, 2247-2253.
188. Mark, J. E.; Erman, B., *Rubberlike Elasticity a Molecular Primer*. John Wiley and Sons: New York, 1988.
189. Drixit, N. M.; Zukoski, C. F., *Physical Review E* **2003**, 67, 061501.

190. Russell, W. B.; Saville, D. A.; Schowalter, W. R., *Colloidal Dispersions*. Cambridge University Press: Cambridge, 1989.
191. Grant, M. C.; Russell, W. B., *Physical Review E* **1993**, 47, 2606.
192. Noro, M. G.; Kern, N.; Frenkel, D., *Europhysics Letters* **1999**, 48, 332.
193. Ramakrishnan, S.; Fuchs, M.; Schweizer, K. S.; Zukoski, C. F., *Journal of Chemical Physics* **2002**, 116, (5), 2201.
194. Shah, S. A.; Chen, Y. L.; Schweizer, K. S.; Zukoski, C. F., *Journal of Chemical Physics* **2003**, 118, (7), 3350-3361.
195. Kulkarni, A. M.; Dixit, N. M.; Zukoski, C. F., *Faraday Discussions* **2003**, 123, 37-50.
196. Gopalakrishnan, V.; Zukoski, C. F., *Industrial Engineering Chemical Research* **2006**, 45, 6906-6914.